
Selective Sequestration of Heavy Metals and Radionuclide from Water by Layered Metal Chalcophosphate

A thesis submitted in Partial Fulfillment of the Degree of

MASTER OF SCIENCE

as a part of

Integrated Ph.D. Programme (Chemical Science)

By

Ekashmi Rathore



New Chemistry Unit

Jawaharlal Nehru Centre for Advanced Scientific Research

(A deemed University)

Bangalore, India

(March 2017)

*Dedicated to my beloved parents
and Biswas's Group*

Declaration

I hereby declare that this thesis entitled “*Selective Sequestration of Heavy Metals and Radionuclide from Water by Layered Metal Chalcophosphate*” is an authentic record of research work that has been carried out by me at Solid State Chemistry Laboratory, New Chemistry Unit, Jawaharlal Nehru Centre for Advanced Scientific Research, Bangalore, India under supervision of Dr. Kanishka Biswas. This work has not been submitted elsewhere for the award of any degree or diploma. Whenever contributions of others are required, every effort is made to indicate it clearly, with due reference to the literature, and acknowledgement of collaborative research and discussions.

Date:
Bangalore, India

Ekashmi Rathore



Dr. Kanishka Biswas
Faculty Fellow, Ramanujan Fellow
New Chemistry Unit
Jawaharlal Nehru Centre for
Advanced Scientific Research
Bangalore, India -560064

Email :kanishka@jncasr.ac.in
Phone: +91-80-22082678 (office)
+91-9902063469(mobile)
FAX : +91-80-2208-2627
Web: <http://www.jncasr.ac.in/kanishka/>

Certificate

Certified that the work described in this thesis titled “*Selective Sequestration of Heavy Metals and Radionuclide from Water by Layered Metal Chalcophosphate*” has been carried out by Ms. Ekashmi Rathore at Solid State Chemistry Laboratory, New Chemistry Unit, Jawaharlal Nehru Centre for Advanced Scientific Research, Bangalore, India under my supervision and that it has not been submitted elsewhere for the award of any degree or diploma.

Date:
Bangalore, India

Dr. Kanishka Biswas
(Research Supervisor)

Acknowledgements

Completion of my M.S. thesis necessitated a lot of guidance and support from many people. I take this opportunity to mention a few of them. However, my sincere thanks extend to everyone who has played a role in making this dream a reality.

Firstly, I would like to thank my research supervisor, Dr. Kanishka Biswas for suggesting me a research problem and guiding me throughout. He has been a constant source of inspiration for me to build up new ideas and carry out experiments. I greatly admire his enthusiasm towards science. His enthusiasm makes a mark upon the young heart, urging them to perform as best as one could. I express my hearty gratitude to him for giving me an opportunity to work under his guidance. I also wish to thank him for correcting me with patience and for forgiving my flaw.

I would like to thank Prof. C. N. R. Rao, FRS, the chairman of New Chemistry Unit (NCU) for his generous support and encouragement throughout my stay in JNCASR. The zeal with which he practices science and his way of looking into a problem with a scientific eye has been a source of inspiration for me. His presence has given me immense inspiration to indulge in active research. I also thank him for providing the infrastructure and facilities to carry out my research work.

I would like to thank Dr. Ramananda Chakrabarti and his students, Anupam and Rahul from Centre for Earth Sciences, Indian Institute of Science, Bangalore for helping me in ICP-MS measurements. I have learnt a lot whenever I had meeting with them or discussion with them. I am grateful to Dr. Mrinmoy De and his student Subrata for helping me in Zeta-Potential measurements.

I thank my lab mates Dr. Provas, Satya Narayan, Manoj, Ananya, Subhajit, Manisha, Dr. Suresh, Moinak, Sushmita and Arka for their cheerful company and help in various occasions. I got the opportunity to learn a lot about research and many instruments from them. Their discussion on past experience, valuable inputs about research life and experiments helped me immensely.

I would like to thank JNCASR for providing me all the facilities.

I would like to express my sincere thanks to Dr. Sebastian C. Peter and Dr. M. Eswaramoorthy for giving me the opportunity to do semester and summer projects in their laboratory. I would like to thank Dr. Amritroop, Dheeraj and Saurav for fruitful discussions.

I am thankful to all faculty members of New Chemistry Unit and Chemistry & Physics Material Science Unit of JNCASR for their courses.

Constant assistance and a friendly nature of the technical staff helped me doing my experiments smoothly. Here, I would like to acknowledge Mrs. Selvi (FESEM), Mr. Anil (XRD), Mr. Vasu (ICP-OES) for their technical help. I am thankful to all the academic, administrative, technical, security, complab and health center staffs for making our campus life smooth and easy.

I express my deep gratitude to all my high school and undergraduate teachers for training me to be disciplined, the basics of science and for growing my interest in research field.

I have benefited a lot from my senior Ph.D. and Int. Ph.D. students. Their help and advice made my academic and non-academic life a memorable and comfortable one here at JNC. I am thankful to all of them. A special thanks to Shikha, Sruthi, Chaitali, Pavitra and Srimayee for all the moments I spent with them. I would like to thank Manjeet, Ankit, Sonu, Nikita and Uma for supporting me any time I required.

Simple words of thanks are never enough to convey feelings to my Guruji and family members who have supported me and placed their trust and faith in all activities. Their love, edurance and utmost patience are the backbone of my future. I am grateful to you all for whatever you gave me.

Preface

Environmental pollution with heavy metal ions and radioactive species is an important issue. As the anthropogenic release of heavy metals and radioactive discharge into the environment is becoming a global epidemic, there is a need to develop efficient materials to remove heavy metals and radioactive species from waste water. Although clay, layered double hydroxides, alkali-intercalated metal sulfides like Li_xMoS_2 , KMS-1, KMS-2, KTS-1, etc. have been studied to capture heavy metals like Pb^{2+} , Cd^{2+} , Hg^{2+} , Ni^{2+} , Co^{2+} and radioactive species like Sr^{2+} , Cs^+ , UO_2^{2+} but they suffer from pH instability, low capacity, low distribution coefficients, inability to distinguish between other cations like Na^+ , Mg^{2+} , K^+ , Ca^{2+} , etc and inability to capture them from low ppb level contamination. The thesis entitled “*Selective Sequestration of Heavy Metals and Radionuclide from Water by Layered Metal Chalcophosphate*” demonstrates the efficient and selective removal of Pb^{2+} , Cd^{2+} and Cs^+ from water by using layered metal chalcophosphate. The thesis has been divided into three chapters.

Chapter I of this thesis begins with a brief introduction to intercalation and ion-exchange chemistry in layered inorganic solids and its useful approaches to solve environmental pollution related issues. Herein, I have discussed various state of art inorganic layered material and their intercalation and ion-exchange properties with the present understanding and latest development. Then, I have discussed about the motivation of the present work.

Chapter II discusses about the detailed Pb^{2+} and Cd^{2+} adsorption and ion-exchange kinetics of layered metal chalcophosphate, $\text{K}_{0.48}\text{Mn}_{0.76}\text{PS}_3\cdot\text{H}_2\text{O}$ (K-MPS-1). K-MPS-1 is capable of efficient removal of Pb^{2+} and Cd^{2+} (>99 %) from very dilute concentration (1-1000 ppb) selectively even in presence of other monovalent and divalent cations such as Na^+ , Ca^{2+} , Mg^{2+} . It can operate within a broad pH range of 2-12 effectively with high distribution co-efficient (K_d^{Pb}) of 5.36×10^5 mL/g.

Chapter III discusses a detailed Cs^+ ion-exchange investigation of K-MPS-1. The sorption of Cs^+ by K-MPS-1 follows Langmuir adsorption model with a high capacity of 333.1 ± 17 mg/g (at pH ~7) and distribution coefficients in order of $\sim 10^4$ mL/g. K-MPS-1 exhibits high

cesium uptake under broad pH range and also even in the presence of complex solutions containing excess Na^+ , Ca^{2+} , Mg^{2+} ions.

Contents

Declaration	III
Certificate	V
Acknowledgements	VII
Preface	IX
Contents	XI
Chapter 1 A brief introduction to intercalation and ion-exchange reactions	1
1.1 Layered inorganic solids and intercalation chemistry	1
1.1.1 Mechanism of intercalation reactions	3
1.1.2 Insulating 2D host lattices for intercalation	3
1.1.2.1 Clay minerals.....	3
1.1.2.2 Layered double hydroxides (LDH).....	4
1.1.2.3 Tetravalent acid phosphates.....	5
1.1.2.4 Layered oxides.....	6
1.1.3 Redox active 2D host lattices for intercalation	7
1.1.3.1. Graphite	7
1.1.3.2 Transition metal dichalcogenides (TMDs)	8
1.1.3.3 Transition metal oxyhalides.....	8
1.1.3.4 Alkali metal intercalated nitride halides MNX (M = Zr, Hf; X = Cl, Br, I).....	9
1.1.3.5 Layered transition metal oxides.....	9
1.1.3.6 Lithium transition metal phosphates.....	10
1.2 Ion-exchange reactions	10
1.2.1 Mechanism of ion-exchange reactions.....	11

1.2.2 Ion-exchange reactions of layered inorganic solids	12
1.2.2.1 Alkali –ion intercalated metal disulfides	12
1.2.2.2 KMS materials	13
1.2.2.3 LHMS material	13
1.2.2.4 Materials based on the $\text{Sn}_3\text{S}_7^{2-}$ net	13
1.2.2.5 KTS materials	14
1.2.2.6 Layered sulfides with trivalent metal ions in their framework	15
1.2.2.7 Polysulfide and MoS_4^{2-} intercalated layered double hydroxides	16
1.3. Metal chalcophosphates	16
1.3.1 Molecular intercalations	17
1.3.2. Intercalations of organometallic molecules	17
1.3.3 Cationic substitution-intercalation	18
1.3.4. Ion-exchange in MPS_3	18
1.4 Motivation of the thesis	19
References	21

Chapter 2 Layered Metal Chalcophosphate, $\text{K}_{0.48}\text{Mn}_{0.76}\text{PS}_3 \cdot \text{H}_2\text{O}$, for Efficient Selective and ppb level Sequestration of Pb and Cd from Water

Summary	29
2.1 Introduction	31
2.2 Experimental section	32
2.2.1 Reagents	32
2.2.2 Synthesis	32
2.2.3 Powder X-ray diffraction.	32
2.2.4 Band gap measurement.	33
2.2.5 Fourier transform infrared spectroscopy	33

2.2.6 Raman spectroscopy.....	33
2.2.7 Thermogravimetric analysis.....	33
2.2.8 Fourier transform infrared spectroscopy.....	33
2.2.9 Field emission scanning electron microscopy and energy dispersive spectroscopy analysis.....	33
2.2.10 X-ray photoelectron spectroscopy.....	33
2.2.11 Zeta potential measurement.....	33
2.2.12 ICP-AES.....	33
2.2.13 ICP-MS.....	34
2.2.14. Pb ²⁺ and Cd ²⁺ sorption and ion-exchange kinetics.....	34
2.3 Results and discussion.....	34
2.3.1 Sythesis and Characterization.....	34
2.3.2 Mechanism of lead capture by K-MPS-1.....	40
2.3.3 Sorption studies.....	42
2.3.4 Kinetics studies.....	45
2.3.5 Competitive ion-exchange and selectivity studies.....	48
2.2.6 pH studies.....	50
2.3.7 Low concentration (ppb level) Pb capture and capture of Pb from Bangalore Lake.....	50
2.4 Cd sequestration by K-MPS-1.....	52
2.5 Conclusions.....	54
References.....	56
Chapter 3 Reversible and efficient sequestration of Cs from water by layered metal chalcophosphate, K-MPS-1.....	61
Summary.....	63
3.1 Introduction.....	65

3.2 Experimental section.....	66
3.2.1 Reagents.	66
3.2.2 Synthesis.....	67
3.2.3 Characterizations.....	67
3.2.4 Cs ⁺ sorption and ion-exchange kinetics.	68
3.3 Results and discussion	68
3.3.1 Characterization of Cs-MPS-1	68
3.3.2 Cs ⁺ sorption studies	72
3.3.3 Kinetics studies	78
3.3.4 pH and competitive ion-exchange studies.....	79
3.3.5 Low concentration (ppb level) Cs ⁺ capture.....	80
3.4. Conclusions.....	80
References.....	81
List of publications	85
Biography.....	87

Chapter 1

A Brief Introduction to Intercalation and Ion-exchange Reactions

A Brief Introduction to Intercalation and Ion-exchange Reactions

1.1 Layered inorganic solids and intercalation chemistry

Bulk layered materials have been studied extensively in the past several decades because of their unique structural features, and physical and chemical properties.^[1] Materials with layered structures remain an extensively investigated subject in current chemistry and physics due to their interesting properties. The rich family of layered materials consists of single-element crystals, such as graphite, phosphorus, arsenic, antimony and bismuth, silicates, hydroxides, transition metal chalcogenides and many oxides.^[2,3] The valuable properties of layered inorganic solids and the possibility of modification by various post-synthesis treatments have attracted a lot of attention for many years. Layered materials typically exhibit strong in-plane covalent bonding and weak out-of-plane van der Waals interactions through the interlayer gap.^[4] They exhibit a wide range of electronic band structures from insulators, semiconductors, metals, superconductors to topological insulators.^[4] Hence, layered phases present new physical and chemical properties that are not commonly encountered in three-dimensional materials.^[5-7] Many of these properties are strongly related to nature and extent of interactions between the layers, hence reflects the type of behavior which falls between two and three dimensional systems.^[8] Research into the basic science of layered solids has intensified in the last decade due to a number of emerging applications in catalysis, adsorption, photovoltaics and medicine.^[9] Most of the promising technological applications, however, deal with intercalation compounds of layered inorganic solids. These intercalated materials have various applications, for instance as catalysts, sorbents, ion-exchange, electrochromic displays, electrodes for secondary batteries (Li-ion batteries) and components for fuel cells.^[8]

Intercalation is a solid state reaction which involves the chemical or thermal reversible inclusion or insertion of a guest species (ion or molecule) into a layered inorganic solid host. The structure of the host remains unchanged or is only slightly altered in the guest-host complex (intercalate). The reaction does not involve diffusive rearrangement of host and therefore is considered to be a topotactic reaction.^[8] A wide variety of intercalated structures can form including ordered vacancy compound because of the specificity of the interactions between the guest atoms and host lattice. Table 1.1 describes insulating host lattices and redox-active host lattices. The reversible ion-electron transfer reaction is described as



where A is an alkali metal and x is the molar intercalation fraction.

Table 1.1 Two-dimensional host lattices for intercalation.

Insulating host lattices	Redox-active host lattices
Clays and layered silicates Kaolinite $\text{Al}_2\text{Si}_2\text{O}_5(\text{OH})_4$	Graphite Dichalcogenides MX_2 (M = Ti, Zr, Hf, V, Nb, Ta, Mo, W; X = S, Se, Te)
Hectorite $\text{Na}_x(\text{Mg}_{3-x}\text{Li}_x)\text{Si}_4\text{O}_{10}(\text{OH})_2 \cdot m\text{H}_2\text{O}$	Metal phosphorus trichalcogenides MPX_3 (M = Mg, V, Mn, Fe, Co, Ni, Zn, Cd, In; X = S, Se)
Montmorillonite $\text{Na}_x(\text{Al}_{2-x}\text{Mg}_x)\text{Si}_4\text{O}_{10}(\text{OH})_2 \cdot m\text{H}_2\text{O}$	Metal oxyhalides MOX (M = Ti, V, Cr, Fe; X = Cl, Br)
Niobates and tantalates $\text{K}[\text{Ca}_2\text{Na}_{n-3}\text{Nb}_n\text{O}_{3n+1}]$, $3 \leq n \leq 7$; $\text{K}_2\text{Ti}_4\text{O}_9$, KTiNbO_3	Metal Nitride Halides MNX (M = Zr, Hf; X = Cl, Br, I)
Hydrous oxides $\text{A}_x\text{UO}_2\text{XO}_4 \cdot m\text{H}_2\text{O}$	Ternary chalcogenides AMX_2 (A = Group 1; M = Ti, V, Cr, Mn, Fe, Co, Ni; X = O, S)
Layered double hydroxides $\text{LiAl}_2(\text{OH})_6\text{OH} \cdot 2\text{H}_2\text{O}$, $\text{Zn}_2\text{Cr}(\text{OH})_6\text{Cl} \cdot 2\text{H}_2\text{O}$	
Acid phosphates M $(\text{HPO}_4)_2 \cdot \text{H}_2\text{O}$; M = Ti, Zr, Hf, Ce, Sn	MOXO_4 (M = V, Nb, Ta, Mo; X = P, As)
$\text{Ni}(\text{CN})_2$	MoO_3 ; V_2O_5

1.1.1 Mechanism of intercalation reactions

During intercalation two main effects take place. One is a change of preferential crystallographic parameters without destruction of the original structure and other is the charge transfer which can affect the electronic properties of host strongly. It is believed that the driving force for intercalation reaction comes from the tendency for charge transfer. The charge transfer takes place from the guest to the host layered compound's conduction band, thus electron-donating species can act generally as guest. The host spans the range of electronic conductivity from insulators such as MoO_3 , clays, zeolites through semiconductors such as graphite and transition metal dichalcogenides to metallic nature such as LaNi_5 .^[5,6]

Both kinetics and thermodynamics play crucial role in the formation of these intercalated compounds. During a reaction, expansion of host lattice takes place due to nucleation of a new phase which is followed by diffusion of guest species into host lattice. Staging helps to minimize the energy required for expansion. Staging phenomenon is observed only in layered compounds. When an odd number of stages are found, it appears that in going from one stage to other an entire layer of guest should exit and re-intercalate (Figure 1.1). Lower guest concentration leads to higher stages.^[6,10]

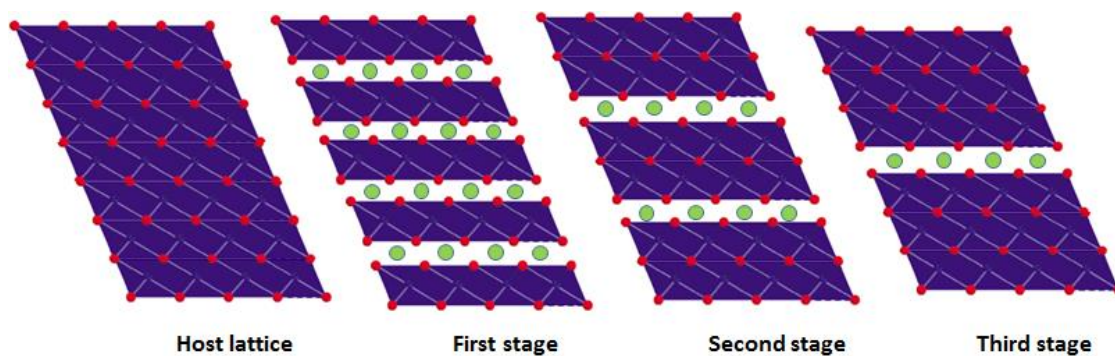


Figure 1.1 Schematic representation of different staging in intercalation compounds. Guest molecules are green spheres.

1.1.2 Insulating 2D host lattices for intercalation

1.1.2.1 Clay minerals

The sheet silicate or clay minerals constitute the largest group in insulating 2D host lattices for intercalation. Clay minerals have structures comprising complex layers made by condensing two types of sub layers. In one type, silicon is tetrahedrally coordinated, $\text{Si}_2\text{O}_3(\text{OH})_2$, and in the other aluminum is octahedral, $\text{Al}(\text{OH})_6$. The sub layers are connected to produce two different structure types that are illustrated by kaolinite, which has the ideal

composition $\text{Al}_2\text{Si}_2\text{O}_5(\text{OH})_4$ and contains one octahedral and one tetrahedral layer (1:1), and pyrophyllite, $\text{Al}_2(\text{Si}_4\text{O}_{10})(\text{OH})_2$, which has one octahedral and two tetrahedral layers (2:1) (see Figure 1.2). Compounds are also known in which three Mg^{2+} cations replace two Al^{3+} cations to give serpentine, $\text{Mg}_3\text{Si}_2\text{O}_5(\text{OH})_4$, or talc, $\text{Mg}_3(\text{Si}_4\text{O}_{10})(\text{OH})_2$. Kaolinite forms intercalation compounds with urea, formamide, acetamide and hydrazine via hydrogen bonding.^[11–13] Exceptional mechanical properties have been reported for clay-polymer intercalated nanocomposites formed between organo-cation exchanged montmorillonites and nylon-6.^[14–16] Inorganic pillared clays have also been studied by inserting poly-oxocation like $[\text{Al}_{13}\text{O}_4(\text{OH})_{24}\cdot 12\text{H}_2\text{O}]^{7+}$ into the inter-lamellar space to separate the layers and form stable pillared clay.^[17]

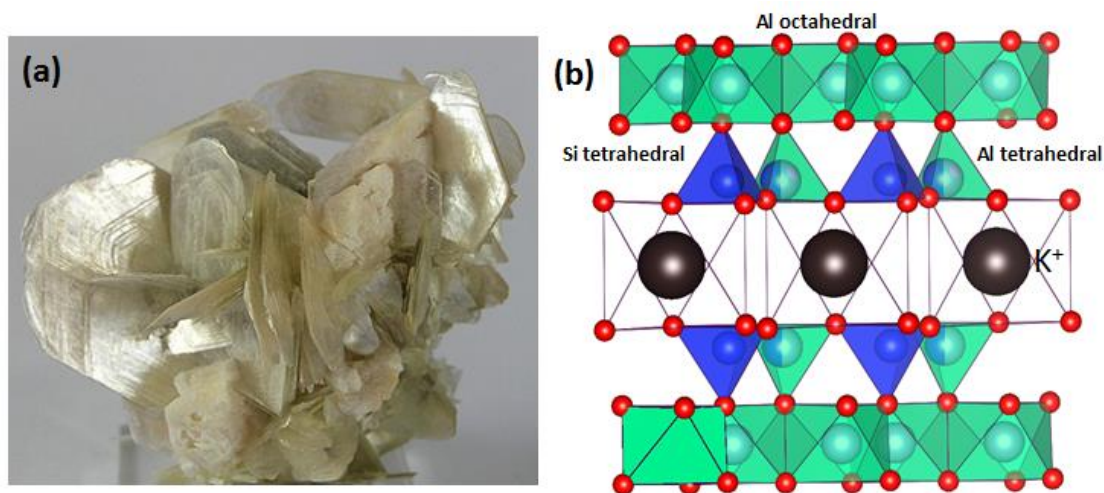


Figure 1.2 (a) Muscovite ($\text{KAl}_2(\text{Si}_3\text{AlO}_{10})(\text{OH})_2$) and (b) Structure of Muscovite, where red and black are oxygen and potassium. Potassium is intercalated between the layers of pyrophyllite ($\text{Al}_2(\text{Si}_4\text{O}_{10})(\text{OH})_2$).

1.1.2.2 Layered double hydroxides (LDH)

The layered double hydroxides are derived by partial substitution of a trivalent cation for a divalent cation in a hydroxide with the $\text{Mg}(\text{OH})_2$ brucite structure. Substitution results by the formula $\text{M}_{1-x}\text{M}'_x(\text{OH})_2\cdot\text{A}_{x/n}\cdot m\text{H}_2\text{O}$, where A is the solvated interlayer anion, $\text{M}^{2+} = \text{Mg}, \text{Zn}, \text{Fe},$ or Co and $\text{M}'^{3+} = \text{Cr}, \text{Al}, \text{Mn},$ or Fe . The natural mineral hydrotalcite, $\text{Mg}_6\text{Al}_2(\text{OH})_{16}\text{CO}_3\cdot 4\text{H}_2\text{O}$ is a best-known example with carbonate as guest species (see Figure 1.3).^[18,19] The specific interlayer anion is determined by synthesis method, but it can easily be exchanged after the compound is formed. LDHs can intercalate organic anions like n-alkanols, n-alkylamines, aliphatic carboxylates.^[20] LDHs have been used as anion exchangers, basic catalysts and catalyst precursors.

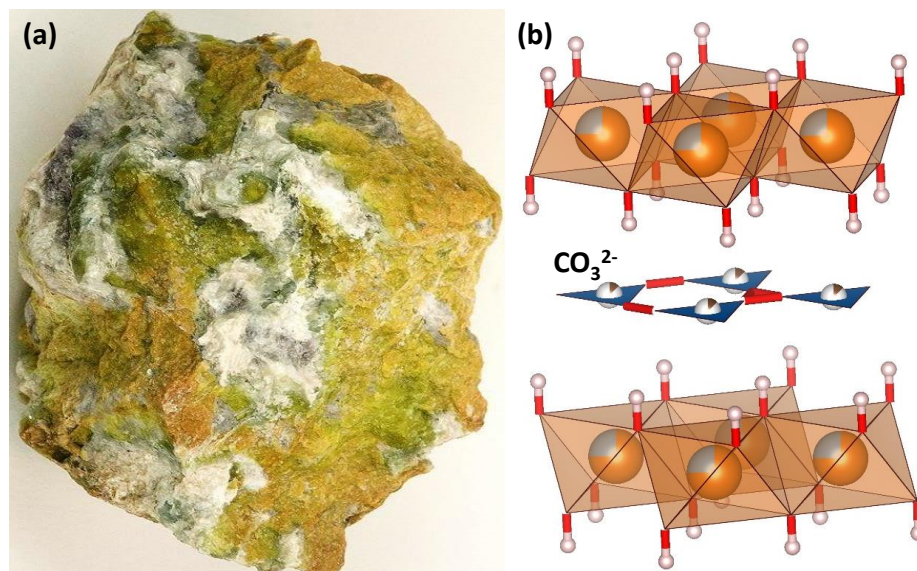


Figure 1.3 (a) Hydrotalcite($\text{Mg}_6\text{Al}_2(\text{OH})_{16}\text{CO}_3 \cdot 4\text{H}_2\text{O}$) with serpentine($\text{Mg}_3(\text{Si}_4\text{O}_{10})(\text{OH})_2$) and b) The structure of Hydrotalcite. Carbonate is intercalated between the layers of substituted trivalent Al^{3+} $\text{Mg}(\text{OH})_2$.

1.1.2.3 Tetravalent acid phosphates

The acid phosphates, $\text{M}^{4+} (\text{HXO}_4)_2 \cdot n\text{H}_2\text{O}$ ($\text{X} = \text{P}, \text{As}$) have been studied as ion exchangers where organic ion-exchange resins cannot be used due to selectivity, stability in acid solutions, thermal stability and resistance to radiations. Clearfield and Smith determined the structure of $\alpha\text{-Zr}(\text{HPO}_4)_2 \cdot \text{H}_2\text{O}$ ($\alpha\text{-ZrP}$), where each layer contains zirconium atoms octahedrally coordinated by oxygen atoms and bridged by phosphate groups (Figure 1.4).^[21]

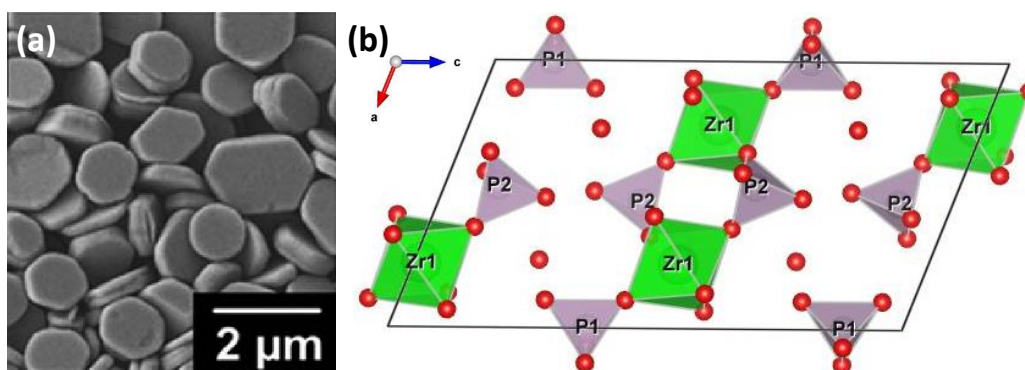


Figure 1.4 (a) SEM micrograph of $\alpha\text{-ZrP}$ crystals and (b) Crystal structure of $\alpha\text{-ZrP}$. A. F. Mejia, A. Diaz, S. Pullela, Y.W. Chang, M Simonetty, C. Carpenter, J D. Batteas, M. S. Mannan, A. Clearfield, Z Cheng, *Soft Matter*, **2012**, 8, 10245 © Royal Society of Chemistry.

The intercalation chemistry of $\alpha\text{-Zr}(\text{HPO}_4)_2 \cdot \text{H}_2\text{O}$ includes ion-exchange reactions, acid–base reactions, and layer derivatization. The protons of the P–OH groups can be partially or completely replaced with counterions by exchange reactions.^[22]

1.1.2.4 Layered oxides

Many high-temperature ternary oxides are known that have structures made up of layers of transition metal–oxygen atom octahedra separated by large alkali metal cations or layers of composition $\text{Bi}_2\text{O}_2^{2+}$. These layered oxides often can undergo ion-exchange reactions in molten salts and sometimes in aqueous solutions. Proton exchanged layered oxides of Ti and Nb, $\text{H}_2\text{Ti}_4\text{O}_9$ and HTiNbO_5 respectively, undergo intercalation with strong bases such as primary amines due to their Bronsted acid nature.^[23,24]

A second class of layered oxides have structures related to the three-dimensional perovskite lattice and include the Aurivillius phases,^[25,26] the Ruddlesden–Popper phases^[27,28] and the Dion–Jacobson phases.^[29,30]

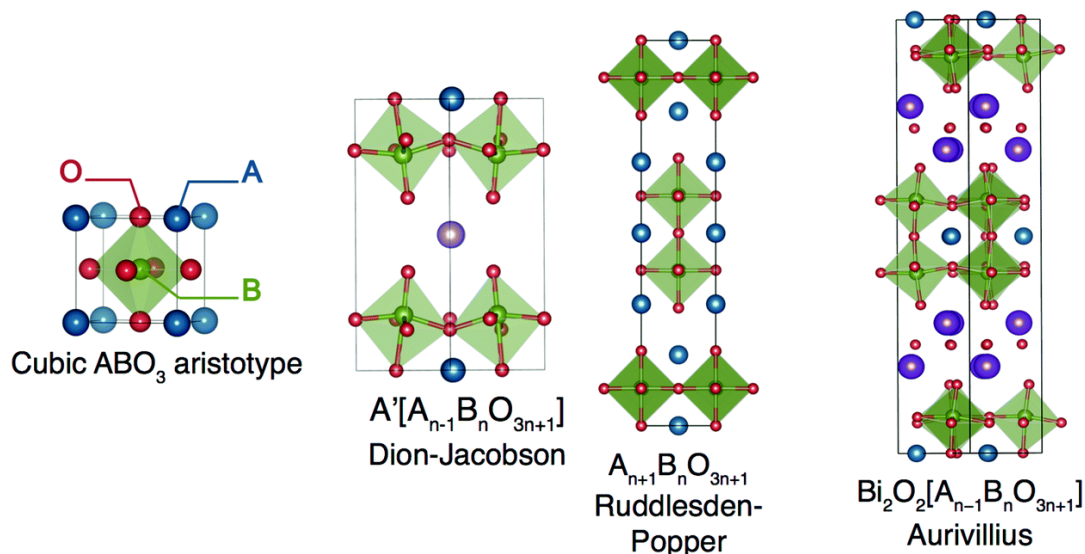


Figure 1.5 Class of layered perovskite derived from the cubic ABO_3 aristotype. N. A. Benedek, J. M. Rondinelli, H. Djani, P. Ghosez, P. Lightfoot, *Dalton Trans.*, **2015**, 44, 10543 © Royal Society of Chemistry.

The general composition can be written $\text{A}'_a[\text{A}_{n-1}\text{B}_n\text{O}_{3n+1}]$, where A is an alkaline or rare earth metal, and B is niobium or titanium. In the Aurivillius phases $\text{A}'_a = \text{Bi}_2\text{O}_2^{2+}$, whereas A' is an alkali metal cation in the ion-exchangeable Ruddlesden–Popper ($a = 2$) and Dion–Jacobson ($a = 1$) phases. The relationships between the three structure types is shown in Figure 1.5. Dion–Jacobson phase, $\text{RbLaNb}_2\text{O}_7$ undergoes reductive intercalation of Rb^0 to form Ruddlesden–Popper phase $\text{Rb}_2\text{LaNb}_2\text{O}_7$.^[31]

Ruddlesden-Popper phases like $K_2La_2Ti_3O_{10}$, $K_2CaNaTa_3O_{10}$, $K_2SrTa_2O_7$, $Na_2Ca_2Ta_3O_{10}$, $Li_2Ca_2Ta_3O_{10}$ and $Li_2LaTa_2O_7$ with interlayer alkali metal cations have been synthesized.^[32–34] Reductive intercalation reaction between Aurivillius phase $Bi_4Ti_3O_{12}$ and *n*-butyllithium leads to the formation of $Li_2Bi_4Ti_3O_{12}$.^[35] The protonated Ruddlesden-Popper compounds do not intercalate organic bases but $H_2SrNaNb_3O_{10}$, $H_2CaNaTa_3O_{10}$ and $H_2Ca_2Ta_2TiO_{10}$ are exceptions, intercalates *n*-butyl amine, *n*-octylamine and alkylamine.^[36]

1.1.3 Redox active 2D host lattices for intercalation

1.1.3.1 Graphite

The first intercalated, graphite sulphate, was reported by Schaufautl in 1841.^[37] Graphite is well-known host which intercalates a variety of guest molecules which can be electron donors or acceptors. Alkali and alkaline earth metals, act as donors, results in cation-size dependent expansion of the separation between the adjacent carbon planes.^[6] The stoichiometry MC_8 is observed for $M=K, Rb$ and Cs and MC_6 for smaller ions $M=Li^+, Sr^{2+}, Ba^{2+}, Eu^{2+}, Yb^{3+}$ and Ca^{2+} .^[5] Figure 1.6 shows the general layer arrangements and stoichiometries of intercalation compounds.

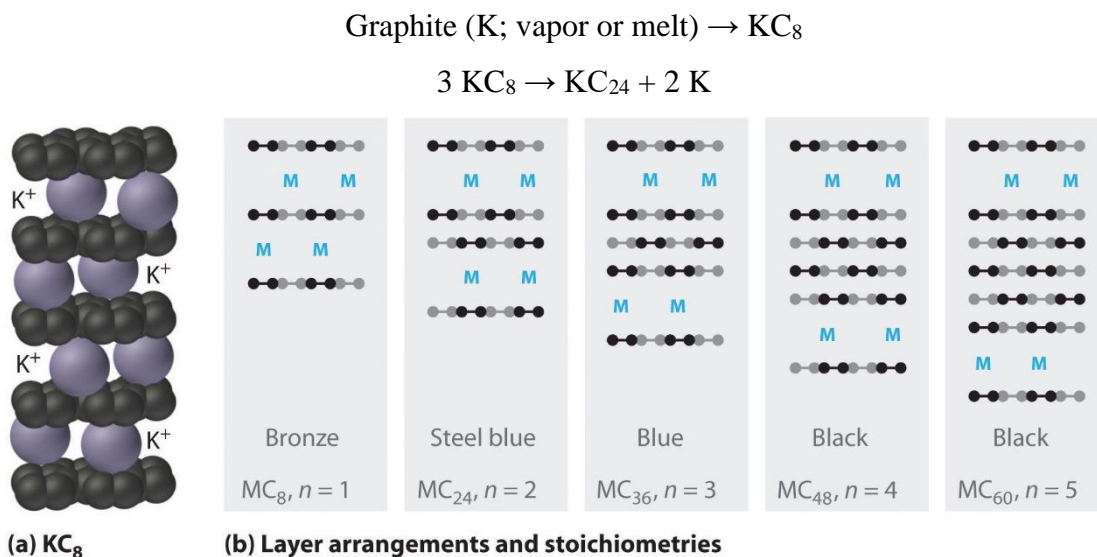
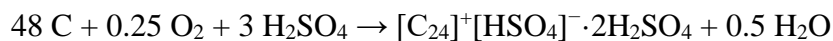
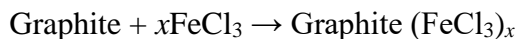


Figure 1.6 (a) Layers of K^+ ions are inserted between every pair of carbon layers, giving $n=1$ and (b) The stoichiometry and color of intercalation compounds depend on the number of layers of carbon atoms (n) between each layer of intercalated metal atoms.

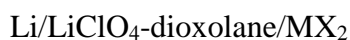
Graphite acts as electron donor when the intercalated guest species are electron acceptors such as $HSO_4, NO_3, CrO_2Cl_2, CrO_3, Br_2$ and metal halides like $MoF_6, FeCl_3$.^[5]





1.1.3.2 Transition metal dichalcogenides (TMDs)

In intercalation reaction of transition metal dichalcogenides, guest species are inserted into the octahedral, tetrahedral, or trigonal prismatic sites between the chalcogenide layers. Alkali metal intercalation in TMDs is carried out electrochemically by using TMDs as a cathode and the alkali metal as anode in presence of non-aqueous solution of the alkali metal salt as the electrolyte.^[38–40]



Direct alkali metal intercalation in TMDs ($A_x\text{MX}_2$, $M=\text{V, Nb, Ta}$) is achieved by heating elements in sealed tubes around 1070K which forms hydrated phases, $A_x(\text{H}_2\text{O})_y\text{MX}_2$ similar to layered oxides which are illustrated in Figure 1.7.^[6,40] Mg^{2+} is known to sandwich between TiS_2 using organometallic reagents. Lewis base type molecules such as ammonia, amines, amides, pyridine, organometallic cations such as cobaltocene, chromocene have also been known to intercalate in TMDs.^[41,42]

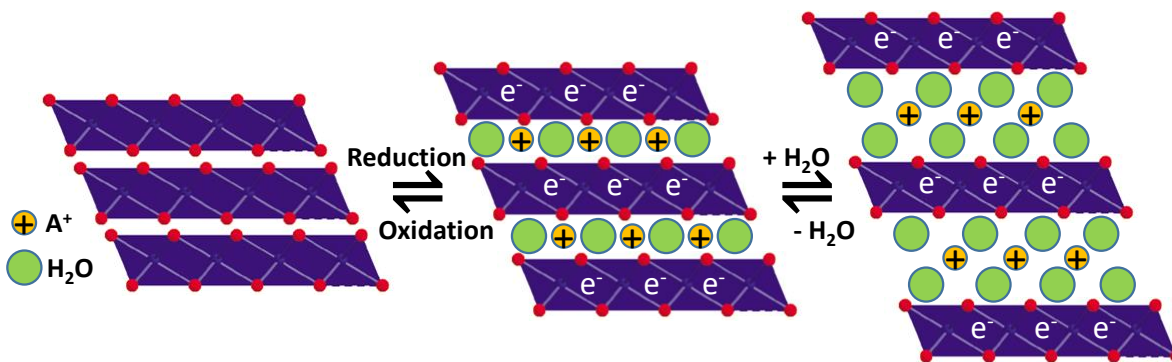
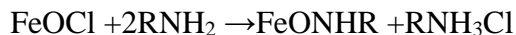


Figure 1.7 Schematic illustration of hydrated phase formation by redox intercalation in aqueous electrolyte: (a) host lattice MX_2 and (b) monolayer hydrate $A_x^+(\text{H}_2\text{O})_y[\text{MX}_2]^{x-}$ and (c) bilayer hydrate.

1.1.3.3 Transition metal oxyhalides

FeOCl shows similar redox intercalation chemistry with inorganic, organic and organometallic guest cations like TMDs.^[8] Interlayer spacing of alkali metal system $\text{M}_{0.14}(\text{H}_2\text{O})_y\text{FeOCl}$ ($M = \text{Li, Na, K, Cs}$) are dependent on the water activity. For example, the interlayer spacing in the potassium compound changes from 11.47 to 22.84 Å when the contacting liquid is changed from 3 M KCl solution to pure water. This behavior is in marked

contrast to that of the dichalcogenides, where the spacings primarily reflect cation hydration effects. The behavior of FeOCl indicates much stronger interactions between solvating water molecules with either the chloride layers or with partially hydrolyzed layers in which some Cl⁻ has been replaced by OH⁻. The oxidizing nature of FeOCl helps to intercalate organic molecules like tetrathiofulvalene (TTF), tetrathionaphthalene (TTN), tetrathiotetracene (TTT), pyridine, amines and organometallic compounds like ferrocene by direct reaction.^[43]



1.1.3.4 Alkali metal intercalated nitride halides MNX (M = Zr, Hf; X = Cl, Br, I)

In MNX, MN double layers are sandwiched between close-packed layers of chlorine and the interlayer spacing has one octahedral and one tetrahedral vacant site per 2MNX formula unit^[44]. Figure 1.8 shows the structure of β -ZrNCl where ZrN double layers are sandwiched between close-packed layers of chlorine ions. β -ZrNCl is known to form alkali metal intercalated compounds by using n-butyllithium and alkali metal naphthalide solutions. Reductive intercalation compound of β -ZrNCl with cobaltocene where metallocene is oriented with the molecular axis parallel to the layers.^[44] Intercalated compounds of β -ZrNCl, β -HfNCl, α -ZrNBr, α -ZrNI, TiNCl have shown superconductivity.^[45]

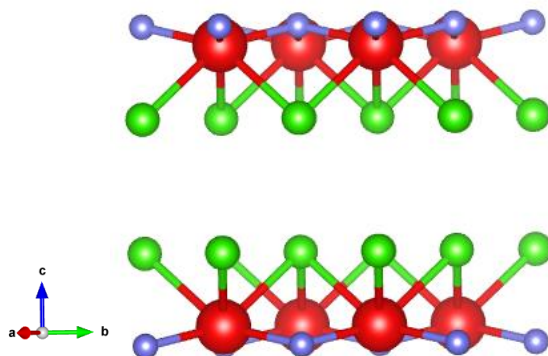


Figure 1.8 The structure of β -ZrNCl. ZrN double layers are sandwiched between close-packed layers of chlorine ions where Zr, red; N, blue and Cl, green.

1.1.3.5 Layered transition metal oxides

Glemser and co-workers have shown that MoO₃ undergo intercalation with hydrogen to form series of H_xMoO₃. Cation intercalated compounds with general formula A_x⁺(H₂O)_y[MoO₃]_x⁻ (A = Na, K, Rb, Cs, NH₄, etc.) are formed by the reduction in neutral aqueous electrolytes.^[46] V₂O₅ is known to form Li and hydrogen intercalated compound as

$\text{Li}_x\text{V}_2\text{O}_5$ and $\text{H}_x\text{V}_2\text{O}_5$ ^[47] and ammonium, alkylammonium, ferrocenium, and cobaltocenium cations intercalated compounds.^[48] α -VOPO₄ intercalates H₂O, chain alcohols, pyridine and 4,4'-bipyridine.^[49] Guest species including I₂, Br₂, IBr, HgI₂, and AgI have been intercalated into Bi-2212 (Bi₂Sr₂CaCu₂O₈).^[50,51] Intercalation chemistry of AMO₂ (A = Li, Na; M = V, Cr, Mn, Fe, Co, Ni) involves oxidation of host lattice either electrochemically or with chemical reagents such as iodine or bromine. Figure 1.9 shows the multistep soft chemistry procedure for deintercalation and intercalation using chemical reagents. The intercalation and deintercalation chemistry of LiMO₂ (M=Ni, Co) phases are the fundamentals for the working of lithium-ion batteries.^[52,53]

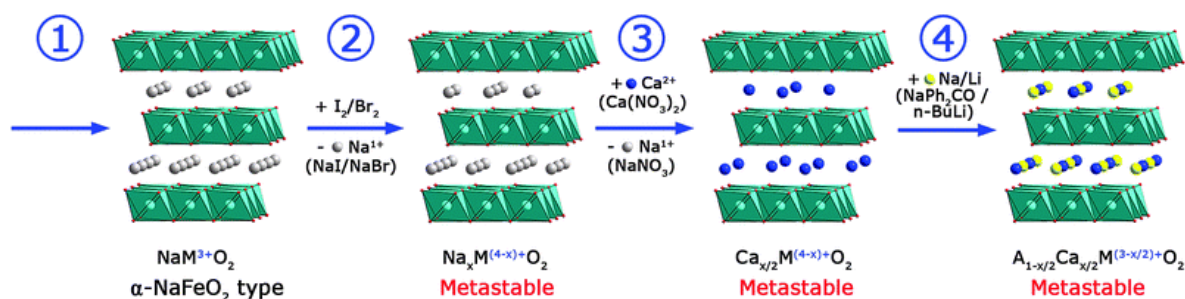


Figure 1.9 The multistep soft chemistry procedure: (1) synthesis of NaMO_2 (M = 3d metal), (2) Na-ion deintercalation from the structure, (3) aliovalent Ca^{2+} for Na^{1+} exchange, and (4) Li^{1+} or Na^{1+} intercalation into the previously produced vacancies. C. K. Blakely, S. R. Bruno, V. V. Poltavets, *Chem. Commun.*, **2014**, 50, 2797 © Royal Society of Chemistry.

1.1.3.6 Lithium transition metal phosphates

The structure of lithium transition metal phosphates, LiMPO_4 ; (M=Fe, Ni, Co, Mn) comprises a network of MO_6 octahedral connected to PO_4 tetrahedral. Li^+ forms one-dimensional chain in the structure which runs parallel to planes of corner-shared MO_6 octahedral that is separated by connecting sheets of phosphate tetrahedral.^[54] The $\text{Li}_3\text{M}_2(\text{PO}_4)_3$ (M=Fe, V) phases adopt the rhombohedral framework similar to NASICON ($\text{Na}_{1+x}\text{Zr}_2\text{Si}_x\text{P}_{3-x}\text{O}_{12}$) and a modified compact monoclinic structure.^[55]

1.2 Ion-exchange reactions

Ion-exchange is a chemical reaction in which intercalated ions of a compound with open-network or layered structure are exchanged with different ions contained in a medium with which it is in contact. Certain inorganic materials can react with ionic solutions to selectively remove one ionic component and replace it with other ions from the solution, with the end

result being new materials. Ion-exchangers are insoluble solid materials with exchangeable cations or anions. When ion-exchanger is in contact with an electrolyte solution, stoichiometrically equivalent amount of other ions of same sign can be exchanged.^[56]



The ion-exchange process, based on topotactic reactions, can result in a material crystallographically analogous to the parent phase but with a new chemical composition.

1.2.1 Mechanism of ion-exchange reactions

Ion-exchange is an adsorption phenomenon where the mechanism of adsorption is electrostatic. Electrostatic forces hold ions to charged functional groups on the surface of the ion-exchanger. The adsorbed ions replace ions that are on the surface of ion-exchanger on a 1:1 charge basis. England *et al.* revealed that ion-exchange occurs even when the diffusion coefficients are as small as $\sim 10\text{-}12 \text{ cm}^2/\text{s}$.^[57] Figure 1.10 explains the general mechanism of ion exchange reactions. Ion-exchange occurs at considerable rates in stoichiometric solid topochemically which enables the synthesis of metastable phases that are inaccessible by high-temperature reactions.^[58]

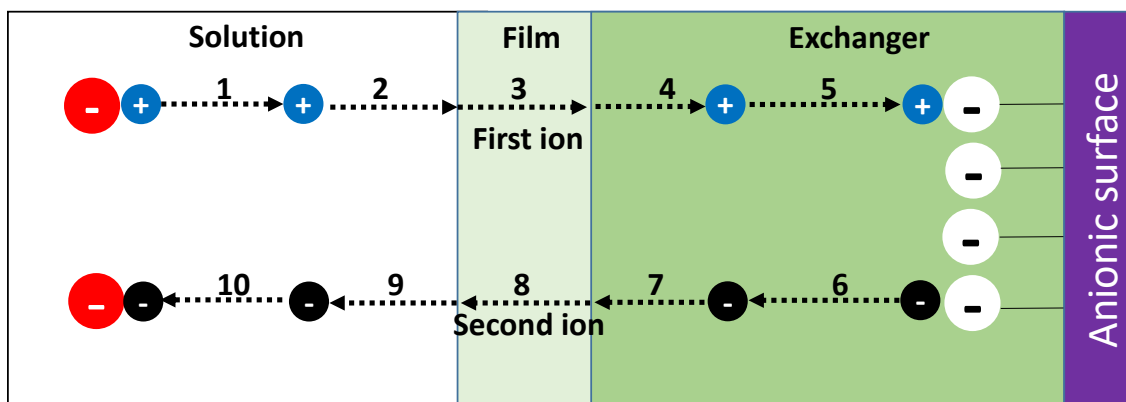


Figure 1.10 Mechanism of the ion-exchange process. (1) dissociation of the dissolved complexes containing first ion; (2) diffusion of the first ion from solution towards the inter-phase film; (3) diffusion of the first ion through the inter-phase film; (4) diffusion of the first ion inside the material phase; (5) association between the first ion and functional group; (6) dissociation of the associates between the second ion and functional group; (7) diffusion of the second ion inside the material phase towards the surface; (8) diffusion of the second ion through the inter-phase film; (9) diffusion and random distribution of the second ion in the solution; (10) formation of the second ion complexes in the solution.

1.2.2 Ion-exchange reactions of layered inorganic solids

Inorganic layered solids can react with ionic solutions to selectively remove one ionic component and replace it with other ions from the solution. For example, the ion-exchange reaction of $\text{Na}_2\text{Si}_2\text{O}_5$ with molten AgNO_3 produces a sheet silicate structure type $\text{Ag}_2\text{Si}_2\text{O}_5$.^[6] The α - NaCrO_2 type framework of α - LiFeO_2 changes to delafossite ($\text{A}^+\text{B}^{3+}\text{O}_2$; $\text{A}=\text{Ag}$, Cu , $\text{B}=\text{Fe}$, Ni , etc) when it is converted to CuFeO_2 by exchange with molten CuCl to provide linear anion coordination for Cu^+ .^[9,58]

Metal sulfides with layered anionic structure and intercalated cations constitute the well-studied class of ion-exchange reactions. They show excellent and selective ion-exchange property due to facile diffusion of the cations as they are able to access the internal surface of the metal sulfides and form strong bonds between the incorporated metals ions and S^{2-} ligands.^[59]

1.2.2.1 Alkali –ion intercalated metal disulfides

In 1979, R. Schöllhorn *et al.* reported alkali-ion intercalated metal disulfides, specifically hydrated layered Sn sulfide phases $\text{A}_x(\text{H}_2\text{O})_y[\text{SnS}_2]^{x-}$ ($\text{A}^+=\text{K}^+$, Rb^+ , Cs^+) which show facile ion-exchange properties for a series of inorganic cations, such as Li^+ , Na^+ , Mg^{2+} , Ca^{2+} , Ni^{2+} etc.^[60,61]

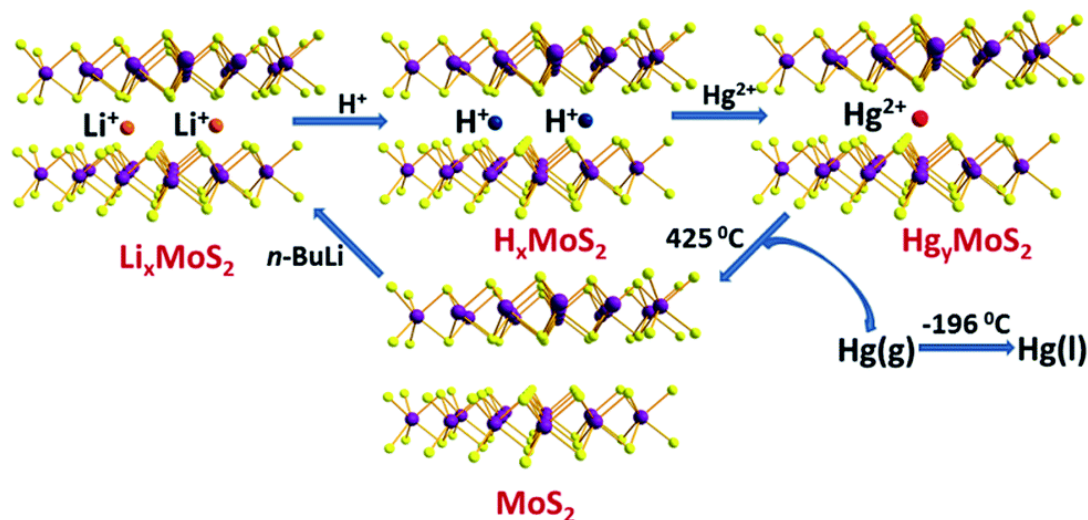


Figure 1.11 Suggested mechanism of Hg^{2+} absorption/desorption for the Li_xMoS_2 material. Mo, purple; S, yellow. M. G. Kanatzidis, *Chem. Sci.*, **2016**, 7, 4804 © Royal Society of Chemistry.

In 1999, A.E. Gash *et al.* showed that Li_xMoS_2 ($0.25 \leq x \leq 1.9$) binds to Hg^{2+} , Zn^{2+} , Pb^{2+} and Cd^{2+} in acidic conditions in order $\text{Hg}^{2+} > \text{Pb}^{2+} > \text{Cd}^{2+} > \text{Zn}^{2+}$.^[62] The mechanism for Hg^{2+} binding

is shown Figure.1.11 where the second step is favorable due to the higher affinity of the soft basic MoS_2^{x-} for soft acid Hg^{2+} in comparison to hard hydronium ions.

1.2.2.2 KMS materials

$\text{K}_{2x}\text{M}_x\text{Sn}_{3-x}\text{S}_6$ (KMS) compounds, reported by M. G. Kanatzidis and coworkers are derivatives of SnS_2 with partial substitution of Sn^{4+} by M^{2+} ($\text{M} = \text{Mn}^{2+}$ or Mg^{2+}) ions.^[62–67] These materials have general formula $\text{K}_{2x}\text{M}_x\text{Sn}_{3-x}\text{S}_6$ ($\text{M} = \text{Mn}^{2+}$, KMS-1; $\text{M} = \text{Mg}^{2+}$, KMS-2; $x = 0.5-1$), where interlayer spacing is filled with K^+ ions can be exchanged with radioactive Cs^+ , Sr^{2+} , Ni^{2+} and UO_2^{2+} and cations like Rb^+ , Hg^{2+} , Pb^{2+} , Cd^{2+} , Ag^+ , Hg^{2+} and Cu^{2+} . The Figure 1.12 describes the representation of ion-exchange in KMS-1 by Rb^+ and Cs^+ .

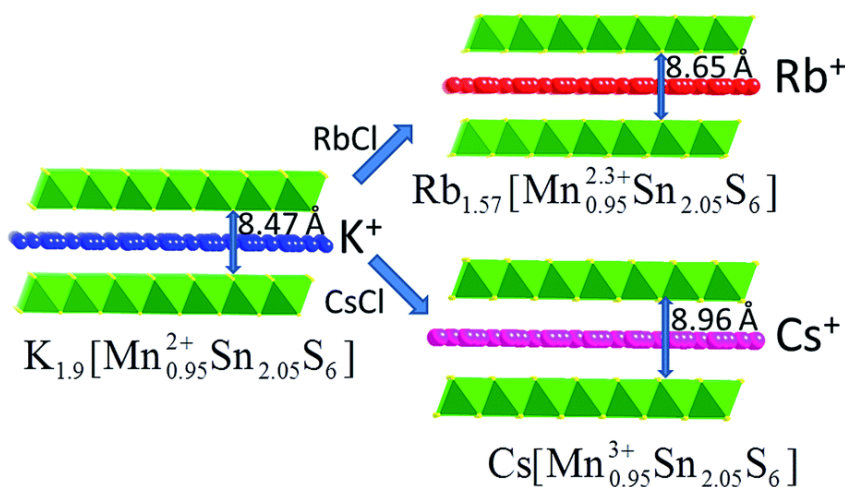


Figure 1.12 Representations of the crystal structures of KMS-1 and its Rb^+ and Cs^+ -exchanged analogs and the interlayer spacing. M. G. Kanatzidis, *Chem. Sci.*, **2016**, 7, 4804 © Royal Society of Chemistry.

1.2.2.3 LHMS material

When KMS-1 is treated with strongly acidic solutions, hydronium ions replace potassium ions and forms layered hydrogen metal sulfide compound (LHMS-1) with general formula $\text{H}_{2x}\text{Mn}_x\text{Sn}_{3-x}\text{S}_6$ ($x = 0.11-0.25$).^[65] LHMS-1 has achieved almost 100% Hg^{2+} removal under extremely acidic solutions which can be useful for removing Hg^{2+} from acid wastewater.

1.2.2.4 Materials based on the $\text{Sn}_3\text{S}_7^{2-}$ net

J. B. Praise and coworkers reported the first compound based on $\text{Sn}_3\text{S}_7^{2-}$, $(\text{TMA})_2(\text{Sn}_3\text{S}_7) \cdot \text{H}_2\text{O}$ ($\text{TMA}^+ = \text{tetramethylammonium ion}$).^[68] Figure 1.13 shows microporous

framework consisting of edge-sharing Sn_3S_4 semi cubes connected by twelve SnS_5 trigonal bipyramids, where TMA^+ and guest water species present between the layers can be exchanged with Ag^+ . Recently, FJSM-SnS, $(\text{Me}_2\text{NH}_2)_{4/3}(\text{Me}_3\text{NH})_{2/3}\text{Sn}_3\text{S}_7 \cdot 1.25\text{H}_2\text{O}$ reported by X. H. Qi *et. al.* has proven to be effective ion-exchanger for Cs^+ and Sr^{2+} .^[69]

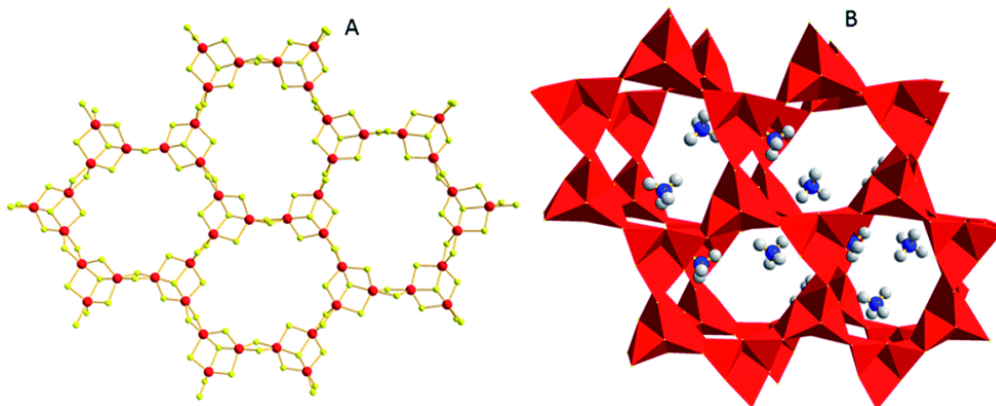


Figure 1.13 (A) The structure of $(\text{TMA})_2(\text{Sn}_3\text{S}_7) \cdot \text{H}_2\text{O}$ (Sn, red; S, yellow). (B) The arrangement of two adjacent layers (with a polyhedral representation) and the TMA^+ cations (C, grey; N, blue) located in the interlayer space (guest water molecules were omitted for clarity). M. G. Kanatzidis, *Chem. Sci.*, **2016**, 7, 4804 © Royal Society of Chemistry.

1.2.2.5 KTS materials

Tin sulfide layered material, $\text{K}_2\text{Sn}_4\text{S}_9$ (KTS-1) consists of $\text{Sn}_4\text{S}_9^{2-}$ cluster connected through S^{2-} bridges to form the layered structure perforated with large holes and the interlayer space is filled with highly disordered cations (see figure 1.14).^[70] K^+ ion of KTS-1 has been exchanged with Cs^+ and heavy metal ions like Hg^{2+} , Pb^{2+} and Cd^{2+} . KTS-3 ($\text{K}_{2x}\text{Sn}_{4-x}\text{S}_{8-x}$) with SnS_6 octahedra are connected with SnS_4 units and the interlayer space is filled with disordered K^+ ions.^[71] KTS-3 has been found as an excellent ion-exchanger for Cs^+ , Sr^{2+} and UO_2^{2+} .^[72]

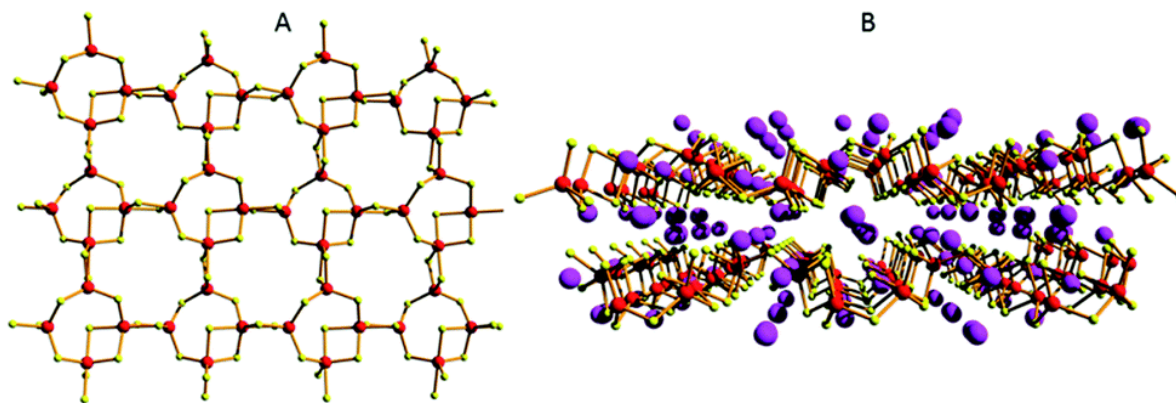


Figure 1.14 (A) Part of the $\text{Sn}_4\text{S}_9^{2-}$ layer (Sn, red; S, yellow). (B) The arrangement of two adjacent layers with the cations (Cs^+ , pink) filling the interlayer space. M. G. Kanatzidis, *Chem. Sci.*, **2016**, 7, 4804 © Royal Society of Chemistry.

1.2.2.6 Layered sulfides with trivalent metal ions in their framework

Layered sulfide materials with trivalent ions like In^{3+} or Ga^{3+} tends to prefer tetrahedral coordination and Sb^{3+} adopts trigonal pyramidal coordination geometry. InSbS ($[(\text{CH}_3\text{CH}_2\text{CH}_2)_2\text{NH}_2]_5\text{In}_5\text{Sb}_6\text{S}_{19} \cdot 1.45\text{H}_2\text{O}$) composed of corner shared InS_4 tetrahedral, bridged by SbS_3 trigonal pyramidal units and Sb_2S_6 dimers with large holes which can accommodate organic counter ions (see figure 1.15). Facile ion-exchange for Cs^+ and Rb^+ have been explored by N. Ding and M. G. Kanatzidis.^[73]

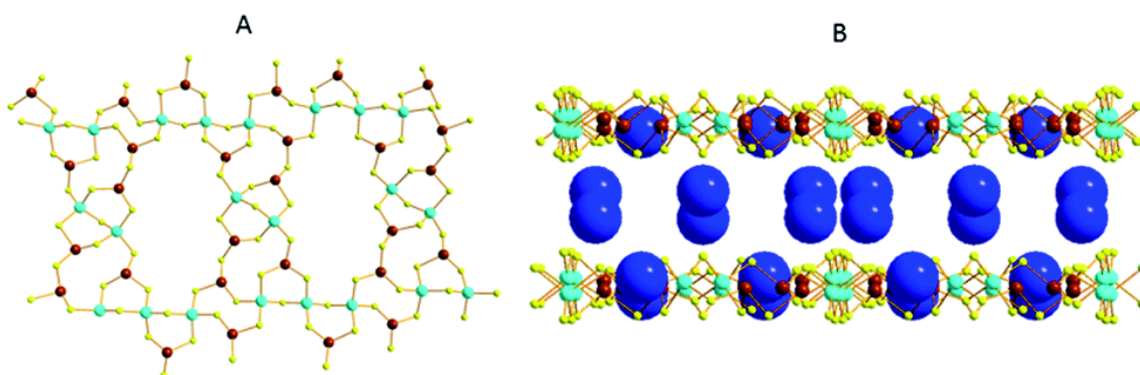


Figure 1.15 (A) Part of the $[\text{In}_5\text{Sb}_6\text{S}_{19}]^{5-}$ layer viewed down the b -axis. (B) Packing of the layers with the N atoms of dipropylammonium cations showing as large balls (C and H atoms were omitted for clarity). In, cyan; Sb, brown; N, blue; S, yellow. M. G. Kanatzidis, *Chem. Sci.*, **2016**, 7, 4804 © Royal Society of Chemistry.

GaSbS-1 ($[\text{CH}_2\text{NH}_2]_2\text{Ga}_2\text{Sb}_2\text{S}_7 \cdot \text{H}_2\text{O}$) comprises of two corner-shared GaS_4 tetrahedra which are bridged by two SbS_3 trigonal pyramidal units forming open window of size $11.36 \times 4.28 \text{ \AA}^2$. Dimethyl ammonium cations, present in the interlayer space by the interaction of N-H with S^{2-} via hydrogen bonding, can be exchanged with Cs^+ leading to the closing of the windows and the size changes to $11.85 \times 3.69 \text{ \AA}^2$. This mechanism is similar to insect capturing by the Venus flytrap plant.^[74]

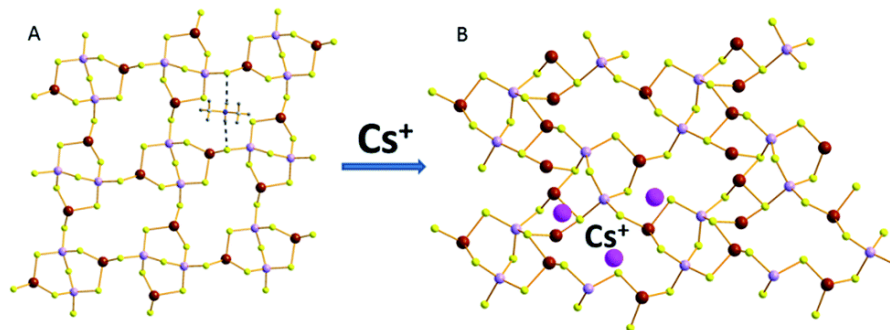


Figure 1.16 (A) Part of the layer of GaSbS-1 . The dashed lines represent hydrogen bonding interactions between the dimethylammonium ions and the layer. (B) Part of the layer of GaSbS-2 and some of the interlayer Cs^+ ions. Ga, purple; Sb, brown; S, yellow; Cs, pink. M. G. Kanatzidis, *Chem. Sci.*, **2016**, 7, 4804 © Royal Society of Chemistry.

1.2.2.7 Polysulfide and MoS_4^{2-} intercalated layered double hydroxides

Recently, S. Ma *et al.* designed a new type of layered double hydroxides (LDHs) intercalated by polysulfide $[\text{S}_x]^{2-}$ groups (Figure 1.17a). They can be ion-exchanged with series of metal ions, such as Ni^{2+} , Co^{2+} , Cu^{2+} , Cd^{2+} , Hg^{2+} , Pb^{2+} , Zn^{2+} , UO_2^{2+} and Ag^+ .^[75-77] The mechanism of metal ion-exchange is dependent on the metal ion:LDH(S_x) molar ratio. The $[\text{S}_x]^{2-}$ groups act as a second host for the incoming ions, shown in Figure 1.17b.

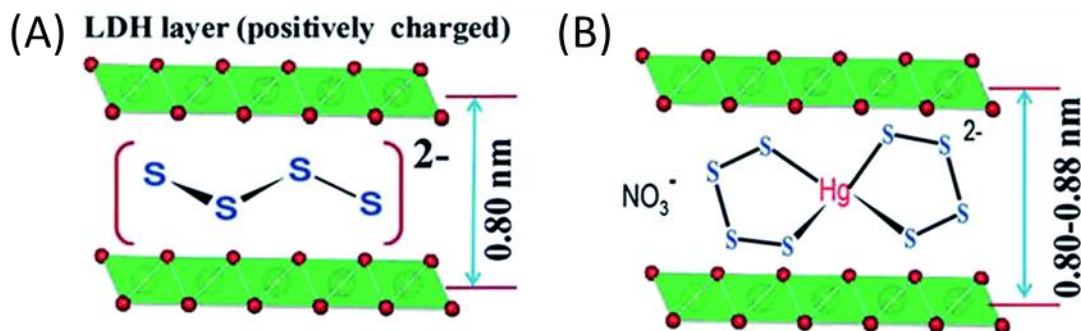


Figure 1.17 (a) Arrangement of $[\text{S}_4]^{2-}$ groups in the interlayer space of the LDH material and (b) Proposed binding of metal ions with the polysulfide unit. Metal, green; O, red. M. J. Manos, M. G. Kanatzidis, *Chem. Sci.*, **2016**, 7, 4804 © Royal Society of Chemistry.

1.3 Metal chalcophosphates

Transition metal chalcophosphate MPX_3 ($\text{M} = \text{Mg}, \text{V}, \text{Mn}, \text{Fe}, \text{Co}, \text{Ni}, \text{Zn}, \text{Pd}$, and Cd ; $\text{X} = \text{S}, \text{Se}$) are semiconducting two-dimensional material. Several phases of MPS_3 were first reported by Friedel.^[78] First transition metal series adopts the FePS_3 structure that is based on cubic close-packed anion array with alternate layers of vacant cationic sites. Within the layer, the cationic sites are occupied by M^{2+} cations and P_2 pairs, as shown in Figure 1.18.

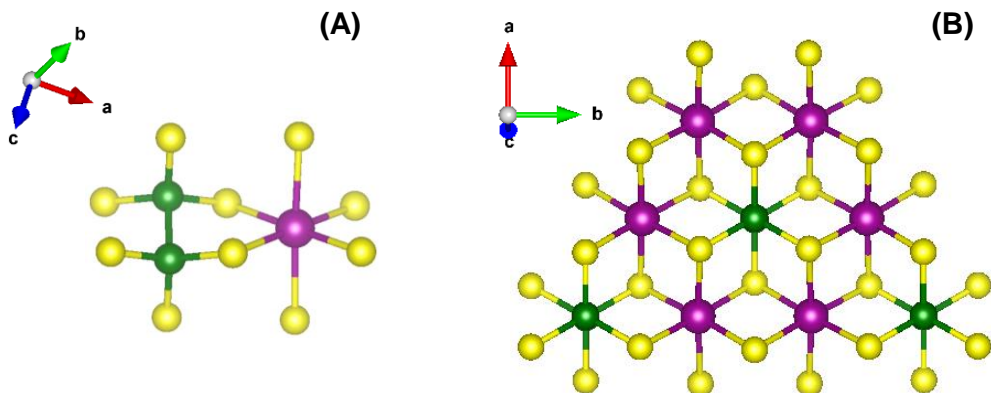


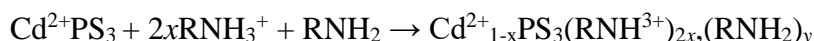
Figure 1.18. MPS_3 structure showing the connection of P_2S_6 and MPS_6 octahedra and (B) ordered arrangement within a single layer. Violet, green and yellow are metal, phosphorous and sulfur atoms.

Each P_2S_6 octahedron is surrounded by six MS_6 octahedra and each MS_6 octahedron has 3 each of MS_6 and P_2S_6 neighbors. The general composition can be written as $M_{2/3}(P_2)_{1/3}S_2$ to emphasize the structural relationship to the dichalcogenides.^[5,8]

The host lattice of MPS_3 is either semiconductor or insulator and the transition metal compounds have magnetic properties characteristic of high-spin octahedral cations. At lower temperatures, the antiferromagnetic order is observed but the susceptibility maxima are broad, indicative of the strong two-dimensional nature of the magnetic interactions.^[79]

1.3.1 Molecular intercalations

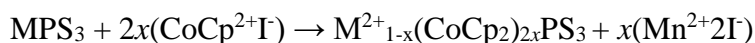
Organic molecules intercalate in transition metal thiophosphates. $MgPS_3$, $MnPS_3$, $CdPS_3$ and $ZnPS_3$ react with n-alkylamines to give rise to intercalation compounds. Pyridine also intercalates in $MnPSe_3$ and expands the layer by 5.9 Å but it fails to intercalate in $FePS_3$:



Intercalation of N-methylated pyridospiropyran cations $SP-R^+$ (R= Me, Ph) into $MnPS_3$ exhibit photochromism due to spiropyran-merocyanin transformation as intercalation stabilizes the merocyanin form.^[80]

1.3.2 Intercalations of organometallic molecules

Clement *et al.* have reported intercalations of organometallic molecules like $Co(\eta-C_5H_5)_2$ and $[Cr(\eta-C_6H_6)_2]$ with lamellar compounds MPS_3 , (M = Mn, Zn, Fe, or Ni) which form intercalates of general stoichiometry $MPS_3[Co(\eta-C_5H_5)_2]^x$ and $MPS_3[Cr(\eta-C_6H_6)_2]^x$ ^[81]. The organometallic molecule transfers its electron to the conduction band of the host lattice and is subsequently intercalated as a cation, causing a substantial lattice expansion. Molecules like bi-pyridine have also been intercalated in $MnPS_3$ to form $Mn_{0.86}PS_3(bipy)_{0.56}$ ^[82]. The general reaction for intercalation by cation transfer with cobaltocene iodide is given as

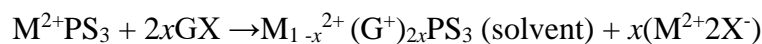


The infrared spectra of the intercalation compounds show the bands expected for the metallocene cation and the absorption of the host lattices is altered. In the pure hosts, the dominant feature is a strong absorption at 560-570 cm^{-1} , which has been assigned to an asymmetric P-S stretching mode. In the cobaltocene intercalates of $MnPS_3$, $CdPS_3$, and $FePS_3$, this band splits into two lines, whereas in $NiPS_3$ it splits into three lines.^[83] This indicates that some distortion of the $P_2S_6^{4-}$ octahedron has taken place.

A cationic iron(III) complex $[\text{Fe}^{3+}(5\text{-OMe-sal}_2\text{trien})^+]$ have been inserted into MnPS_3 host lattice which undergoes spin crossover and shows magnetism.^[84] A family of macrocyclic complexes $[\text{M}_2\text{LnCl}_2]$ where M: Cu^{2+} or Zn^{2+} ; Ln: macrocyclic ligand derived from 2-hydroxy-5-methyl-1,3-benzenedicarbaldehyde and different aliphatic diamines and o-phenylenediamine have also been synthesized by intercalating in the interlamellar space by a microwave assisted cationic exchange reaction.^[85]

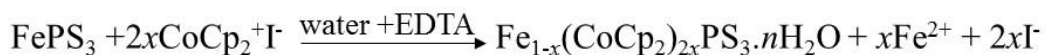
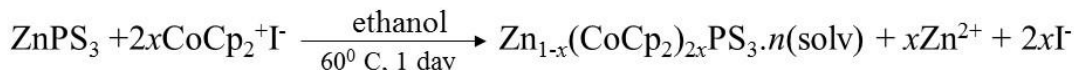
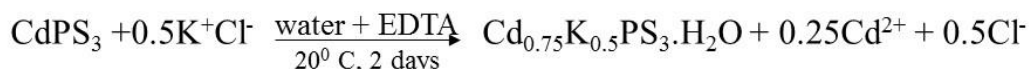
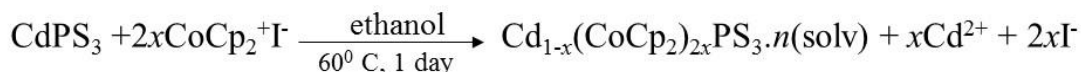
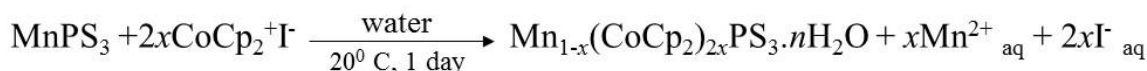
1.3.3 Cationic substitution-intercalation

Clement and Green showed that many ionic salts (G^+X^-) can be intercalated in a polar medium and at room temperature^[78] according to:



with $\text{G} = (\text{C}_2\text{H}_5)_4\text{N}^+$, $\text{Co}(\eta\text{-C}_5\text{H}_5)_2^+$, pyH^+ and $\text{X} = \text{Cl}^-$, I^- .

Substitution is easily achieved in the case of MnPS_3 , CdPS_3 , and ZnPS_3 as M^{2+} ions are not stabilized by ligand field. It is difficult for more stabilized Fe^{2+} ($t^4_2g e^2_g$) to undergo substitution. Hence, basic pH and strong complexing agent (EDTA) are needed to reach sizeable substitution.



1.3.4 Ion-exchange in MPS_3

In the cation-exchange process, the electrical charge of the cationic guest species entering the host lattice is counterbalanced by the loss of intralayer M^{2+} ions. An important feature of the ion exchange chemistry in MPS_3 class is that it yields intercalates which are generally air stable, well crystallized.

The K^+ ions of a $\text{K}_{2x}\text{Mn}_{1-x}\text{PS}_3$ pre-intercalate are exchanged with the tetrafluoroborate salt $(\text{TTF})_3(\text{BF}_4)_2$ in acetonitrile medium. The compound obtained under this conditions was

formulated as $\text{Mn}_{0.83}\text{PS}_3 \cdot (\text{TTF})_{0.42}\text{K}_{0.10}(\text{solv})_y$.^[86] Polyethylene oxide, $(\text{C}_2\text{H}_4\text{O})_n$ [PEO], a polymer has also been intercalated in MnPS_3 .^[87] Intercalation of potentially reactive transition-metal complexes like $\text{Cr}(\text{en})_3\text{Cl}_3$, $\text{Ru}(\text{bpy})_3\text{Cl}_3$ and cyclopentadienylcarbonyl(diphos)iron monocation leads to dramatic modification in magnetic properties.^[88] New hetero-metallic materials, $\text{Cu}_{0.2}\text{Mn}_{0.8}\text{PS}_3 \cdot 0.25\text{H}_2\text{O}$, $\text{Co}_{0.2}\text{Mn}_{0.8}\text{PS}_3 \cdot 0.25\text{H}_2\text{O}$, $\text{Ni}_{0.2}\text{Mn}_{0.8}\text{PS}_3 \cdot 0.25\text{H}_2\text{O}$ and $\text{Zn}_{0.2}\text{Mn}_{0.8}\text{PS}_3 \cdot 0.25\text{H}_2\text{O}$, with an ordered distribution of the secondary metal ions have also been synthesized and shows improved magnetic properties.^[89] Cationic complexes $[\text{M}(\text{salen})]^+$ ($\text{M}=\text{Mn}^{3+}$, Fe^{3+} , Co^{3+} ; salen=N,N-ethylene-bis(salicylal- dimine)) also accommodates themselves in the space between the layers of MPS_3 .^[90] Intercalation compound, $\text{Mn}_{0.84}\text{PS}_3(\text{phen})_{0.64}$ (phen=1,10-phenanthroline) exhibits bulk spontaneous magnetization below 36K.^[91] Polymer- inorganic intercalation nano-composite based on a C_{60} -containing poly-(ethylene oxide) (C_{60} -PEO) into layered MnPS_3 have shown a magnetic phase transition from paramagnetism to ferrimagnetism at about 40 K.^[92] Interestingly, aminoacid intercalates, $\text{Mn}_{0.83}\text{PS}_3(\text{His})_{0.34}$, $\text{Mn}_{0.83}\text{PS}_3(\text{Lys})_{0.35}$ and $\text{Mn}_{0.88}\text{PS}_3(\text{Arg})_{0.25}$ are the first example of a magnetic bioorganic/inorganic material synthesized by inserting a biomolecule into a layered inorganic host.^[93]

1.4 Motivation of the thesis

Intercalated layered inorganic solids are new class of ion-exchangers, which seem highly promising for environmental remediation applications. As the anthropogenic release of heavy metals and radioactive discharges into the environment is becoming a global epidemic, there is a need develop efficient ion-exchange materials to remove the heavy metals and radioactive species from waste waters. Clays, layered double hydroxides, alkali-intercalated metal sulfides like Li_xMoS_2 , KMS-1, KMS-2, KTS-1, protonated acid metal sulfide like LHMS-1, layered sulfides with trivalent metal ions in the framework, etc. have been studied extensively to capture heavy metals like Pb^{2+} , Cd^{2+} , Hg^{2+} , Ni^{2+} , Co^{2+} and radioactive species like Sr^{2+} , Cs^+ , UO_2^{2+} . However, these materials suffer from pH instability as they decompose in extreme pH conditions, low capacity, low distribution coefficients, inability to distinguish between other cations like Na^+ , Mg^{2+} , K^+ , Ca^{2+} , etc and inability to capture heavy metals from low ppb level contamination. So, it is challenging to find a novel stable layered material which can work in

wide pH range with fast kinetics, large ion-removal capacity and is capable of selectively removing heavy metal and radioactive species from water which are present in trace (ppb) amounts. In the following chapters, we will be focusing on selective removal of heavy metals like Pb^{2+} and Cd^{2+} and radioactive species, Cs^+ by using potassium intercalated layered metal chalcophosphate in wide pH range.

References

- [1] C. N. R. Rao, H. S. S. Ramakrishna Matte, U. Maitra, *Angew. Chemie Int. Ed.* **2013**, *52*, 13162–13185.
- [2] P. R. Wallace, *Phys. Rev.* **1947**, *71*, 622.
- [3] R. W. Keyes, *Phys. Rev.* **1953**, *92*, 580.
- [4] M. Chhowalla, H. S. Shin, G. Eda, L.-J. Li, K. P. Loh, H. Zhang, *Nat. Chem.* **2013**, *5*, 263–275.
- [5] M. Stanley Whittingham, A. J. Jacobson, *Intercalation Chemistry*, Academic Press, New York, **1982**.
- [6] C. N. R. Rao, J. Gopalakrishnan, *New Directions in Solid State Chemistry*, Cambridge University Press, **1997**.
- [7] C. N. R. Rao, K. Biswas, *Essentials of Inorganic Materials Synthesis*, John Wiley & Sons, **2015**.
- [8] A. J. Jacobson, L. F. Nazar, *Intercalation Chemistry*, **2006**.
- [9] A. Clearfield, *Chem. Rev.* **1988**, *88*, 125–148.
- [10] N. Dumas, A. Herold, *Comptes Rendus Hebd. Des Seances L Acad. Des Sci. Ser. C* **1969**, *268*, 373.
- [11] R. M. Barrer, *Zeolites and Clay Minerals as Sorbents and Molecular Sieves*, Academic Press, **1978**.
- [12] F. Liebau, *Structural Chemistry of Silicates: Structure, Bonding, and Classification*, Springer Science & Business Media, **2012**.
- [13] A. C. D. Newman, *Chemistry of Clays and Clay Minerals*, Wiley, **1987**.
- [14] A. Usuki, M. Kawasumi, Y. Kojima, A. Okada, T. Kurauchi, O. Kamigaito, *J. Mater. Res.* **1993**, *8*, 1174–1178.
- [15] R. Krishnamoorti, R. A. Vaia, E. P. Giannelis, *Chem. Mater.* **1996**, *8*, 1728–1734.
- [16] T. Lan, T. J. Pinnavaia, *Chem. Mater.* **1994**, *6*, 2216–2219.
- [17] T. J. Pinnavaia, M.-S. Tzou, S. D. Landau, R. H. Raythatha, *J. Mol. Catal.* **1984**, *27*, 195–212.
- [18] A. I. Khan, D. O'Hare, *J. Mater. Chem.* **2002**, *12*, 3191–3198.
- [19] R. Allmann, *Chimia (Aarau)*. **1970**, *24*, 99.
- [20] H. Boehm, J. Steinle, C. Vieweger, *Angew. Chemie Int. Ed. English* **1977**, *16*, 265–266.

- [21] A. Clearfield, G. D. Smith, *Inorg. Chem.* **1969**, *8*, 431–436.
- [22] G. Alberti, U. Costantino, S. Allulli, N. Tomassini, *J. Inorg. Nucl. Chem.* **1978**, *40*, 1113–1117.
- [23] M. Tournoux, R. Marchand, L. Brohan, *Prog. solid state Chem.* **1986**, *17*, 33–52.
- [24] B. Raveau, *Rev. Chim. minérale* **1984**, *21*, 391–406.
- [25] B. Aurivillius, *Ark. kemi* **1950**, *1*, 499–512.
- [26] B. Aurivillius, *Ark. kemi* **1950**, *1*, 463–480.
- [27] S. N. Ruddlesden, P. Popper, *Acta Crystallogr.* **1957**, *10*, 538–539.
- [28] S. N. Ruddlesden, P. Popper, *Acta Crystallogr.* **1958**, *11*, 54–55.
- [29] M. Dion, M. Ganne, M. Tournoux, *Mater. Res. Bull.* **1981**, *16*, 1429–1435.
- [30] A. J. Jacobson, J. W. Johnson, J. T. Lewandowski, *Inorg. Chem.* **1985**, *24*, 3727–3729.
- [31] A. R. Armstrong, P. A. Anderson, *Inorg. Chem.* **1994**, *33*, 4366–4369.
- [32] R. E. Schaak, T. E. Mallouk, *Chem. Mater.* **2000**, *12*, 3427–3434.
- [33] K. Toda, M. Takahashi, T. Teranishi, Z.-G. Ye, M. Sato, Y. Hinatsu, *J. Mater. Chem.* **1999**, *9*, 799–803.
- [34] K. Toda, T. Teranishi, Z.-G. Ye, M. Sato, Y. Hinatsu, *Mater. Res. Bull.* **1999**, *34*, 971–982.
- [35] J.-H. Choy, J.-Y. Kim, I. Chung, *J. Phys. Chem. B* **2001**, *105*, 7908–7912.
- [36] T. A. Kodenkandath, J. N. Lalena, W. L. Zhou, E. E. Carpenter, C. Sangregorio, A. U. Falster, W. B. Simmons, C. J. O'Connor, J. B. Wiley, *J. Am. Chem. Soc.* **1999**, *121*, 10743–10746.
- [37] P. Schaufaütl, *J. Prakt. Chem* **1841**, *21*, 155.
- [38] J. Rouxel, *Rev. Inorg. Chem* **1979**, *1*, 245–279.
- [39] M. S. Whittingham, *Prog. Solid State Chem.* **1978**, *12*, 41–99.
- [40] R. Schöllhorn, *Angew. Chemie Int. Ed. English* **1980**, *19*, 983–1003.
- [41] M. J. McKelvy, W. S. Glaunsinger, *Annu. Rev. Phys. Chem.* **1990**, *41*, 497–523.
- [42] M. B. Dines, *Science (80-.)*. **1975**, *188*, 1210–1211.
- [43] B. A. Averill, S. M. Kauzlarich, *Mol. Cryst. Liq. Cryst.* **1984**, *107*, 55–64.
- [44] A. M. Fogg, V. M. Green, D. O'Hare, *Chem. Mater.* **1999**, *11*, 216–217.
- [45] A. Fogg, V. Green, *J. Mater. Chem.* **1999**, *9*, 1547–1551.
- [46] O. Glemser, G. Lutz, *Zeitschrift für Anorg. und Allg. Chemie* **1951**, *264*, 17–33.

- [47] D. W. Murphy, P. A. Christian, F. J. DiSalvo, J. V Waszczak, *Inorg. Chem.* **1979**, *18*, 2800–2803.
- [48] P. Aldebert, N. Baffier, N. Gharbi, J. Livage, *Mater. Res. Bull.* **1981**, *16*, 949–955.
- [49] J. W. Johnson, A. J. Jacobson, J. F. Brody, S. M. Rich, *Inorg. Chem.* **1982**, *21*, 3820–3825.
- [50] X. D. Xiang, S. McKernan, W. A. Vareka, A. Zettl, J. L. Corkill, *Nature* **1990**, *348*, 145–147.
- [51] J.-H. Choy, S.-J. Kwon, S.-J. Hwang, Y.-I. Kim, W. Lee, *J. Mater. Chem.* **1999**, *9*, 129–135.
- [52] C. Delmas, J. BRACONNIER, A. Maazaz, P. Hagemuller, *Chem. Informationsd.* **1983**, *14*.
- [53] T. Kijima, S. Kimura, Y. Kawahara, K. Ohe, M. Yada, M. Machida, *J. Solid State Chem.* **1999**, *146*, 60–64.
- [54] A. K. Padhi, K. S. Nanjundaswamy, J. B. Goodenough, *J. Electrochem. Soc.* **1997**, *144*, 1188–1194.
- [55] T. A. Kerr, J. Gaubicher, L. F. Nazar, *Electrochem. Solid-State Lett.* **2000**, *3*, 460–462.
- [56] F. G. Helfferich, *Ion Exchange*, Courier Corporation, **1962**.
- [57] W. A. England, J. B. Goodenough, P. J. Wiseman, *J. Solid State Chem.* **1983**, *49*, 289–299.
- [58] M. L. T. Cossio, L. F. Giesen, G. Araya, M. L. S. Pérez-Cotapos, R. L. VERGARA, M. Manca, R. A. Tohme, S. D. Holmberg, T. Bressmann, D. R. Lirio, et al., *Ion Exchange Materials Properties and Application*, **2012**.
- [59] M. J. Manos, M. G. Kanatzidis, **2013**, *0*, 1–3.
- [60] C. O. Oriakhi, M. M. Lerner, *Layer. Mater.* **2004**, 509.
- [61] R. Schöllhorn, W. Roer, K. Wagner, *Monatshefte für Chemie/Chemical Mon.* **1979**, *110*, 1147–1152.
- [62] A. E. Gash, A. L. Spain, L. M. Dysleski, C. J. Flaschenriem, A. Kalaveshi, P. K. Dorhout, S. H. Strauss, *Environ. Sci. Technol.* **1998**, *32*, 1007–1012.
- [63] M. J. Manos, M. G. Kanatzidis, *J. Am. Chem. SOC* **2009**, *131*, 6607.
- [64] M. J. Manos, M. G. Kanatzidis, *Chem. Eur. J.* **2009**, *15*, 4779–4784.
- [65] M. J. Manos, V. G. Petkov, M. G. Kanatzidis, *Adv. Funct. Mater.* **2009**, *19*, 1087–1092.

- [66] M. J. Manos, M. G. Kanatzidis, *J. Am. Chem. Soc.* **2012**, *134*, 16441–16446.
- [67] J. L. Mertz, Z. H. Fard, C. D. Malliakas, M. J. Manos, M. G. Kanatzidis, *Chem. Mater.* **2013**, *25*, 2116–2127.
- [68] J. B. Parise, Y. Ko, J. Rijssenbeek, D. M. Nellis, K. Tan, S. Koch, *J. Chem. Soc. Chem. Commun.* **1994**, 527.
- [69] X.-H. Qi, K.-Z. Du, M.-L. Feng, J.-R. Li, C.-F. Du, B. Zhang, X.-Y. Huang, *J. Mater. Chem. A* **2015**, *3*, 5665–5673.
- [70] G. A. Marking, M. Evain, V. Petricek, M. G. Kanatzidis, *J. Solid State Chem.* **1998**, *141*, 17–28.
- [71] N. (CY) Mercouri G. Kanatzidis, Wilmette, IL (US); Joshua L. Mertz, Evanston, IL (US); Emmanouil Manos, *Chalcogenide Compounds for the Remediation of Nuclear and Heavy Metal wastes, US Patent, US2011290735-A1.*, **2011**.
- [72] D. Sarma, C. D. Malliakas, K. S. Subrahmanyam, S. M. Islam, M. G. Kanatzidis, *Chem. Sci.* **2016**, *7*, 1121–1132.
- [73] N. Ding, M. G. Kanatzidis, *Chem. Mater.* **2007**, *19*, 3867–3869.
- [74] N. Ding, M. G. Kanatzidis, *Nat. Chem.* **2010**, *2*, 187–191.
- [75] S. Ma, Q. Chen, H. Li, P. Wang, S. M. Islam, Q. Gu, X. Yang, M. G. Kanatzidis, *J. Mater. Chem. A* **2014**, *2*, 10280–10289.
- [76] L. Ma, Q. Wang, S. M. Islam, Y. Liu, S. Ma, M. G. Kanatzidis, *J. Am. Chem. Soc.* **2016**, *138*, 2858–2866.
- [77] S. Ma, L. Huang, L. Ma, Y. Shim, S. M. Islam, P. Wang, L.-D. Zhao, S. Wang, G. Sun, X. Yang, *J. Am. Chem. Soc.* **2015**, *137*, 3670–3677.
- [78] R. Brec, *Solid State Ionics* **1986**, *22*, 3–30.
- [79] A. R. Wildest S J Kennedy, T. J. Hickst, *Condens. Matter* **1994**, *6*, 335–341.
- [80] S. Bénard, A. Léaustic, E. Rivière, P. Yu, R. Clément, **2001**, *13*, 3709–3716.
- [81] R. Clement, M. L. H. Green, *J. Chem. Soc., Dalt. Trans.* **1979**, 1566–1568.
- [82] J. Qin, C. Yang, K. Yakushi, Y. Nakazawa, K. Ichimura, *Solid State Commun.* **1996**, *100*, 427–431.
- [83] C. Sourisseau, J. P. Forgerit, Y. Mathey, *J. Solid State Chem.* **1983**, *49*, 134–149.
- [84] S. Floquet, S. Salunke, M. L. Boillot, R. Clément, F. Varret, K. Boukheddaden, E. Rivière, *Chem. Mater.* **2002**, *14*, 4164–4171.

- [85] P. Fuentealba ab, L. Serón ab, C. Sánchez ab, J. Manzur bc, V. Paredes-Garcia bd, N. Pizarro, M. Cepeda, D. Venegas-Yazigi be, E. Spodine ab, P. Fuentealba, et al., *J. Coord. Chem.* **2014**, *67*, 3894–3908.
- [86] A. Lkaustic, J. P. Audibre, P. G. Lacroix, R. Clement, L. Lomas, A. Michalowicz, W. R. Dunham, A. H. Francis, *Chem. Mater* **1996**, *7*, 1103–1111.
- [87] C. O. Oriakhi, M. M. Lerner, *Chem. Mater* **1996**, *8*, 2016–2022.
- [88] R. Clement, *J. Am. Chem. Soc.* **1981**, *103*, 6998–7000.
- [89] P. Fuentealba, C. Cortés, N. Audebrand, E. Le Fur, V. Paredes-García, D. Venegas-Yazigi, J. Manzur, E. Spodine, *Dalt. Trans. Commun. Cite this Dalt. Trans* **2015**, *44*, 12493–12496.
- [90] X. Zhang, H. Zhou, X. Su, X. Chen, C. Yang, J. Qin, M. Inokuchi, *J. Alloys Compd.* **2007**, *432*, 247–252.
- [91] C. Yang, X. Chen, J. Qin, K. Yakushi, Y. Nakazawa, K. Ichimura, *J. Solid State Chem.* **2000**, *150*, 281–285.
- [92] X. Chen, Z. Li, H. Zhou, T. Wang, J. Qin, M. Inokuchi, *Polymer (Guildf)*. **2007**, *48*, 3256–3261.
- [93] H. Zhou, X. Su, X. Zhang, X. Chen, C. Yang, J. Qin, M. Inokuchi, *Mater. Res. Bull.* **2006**, *41*, 2161–2167.

Chapter 2

**Layered Metal Chalcophosphate,
 $K_{0.48}Mn_{0.76}PS_3 \cdot H_2O$, for Efficient
Selective and ppb level
Sequestration of Pb and Cd from
Water***

Layered Metal Chalcophosphate, $K_{0.48}Mn_{0.76}PS_3 \cdot H_2O$, for Efficient, Selective and ppb level Sequestration of Pb and Cd from Water up to ppb Level †

Summary: Sequestration of heavy metal ions from water is an important issue in chemistry. In this chapter, we have discussed the detailed Pb^{2+} adsorption and ion exchange kinetics of a potassium intercalated layered metal thiophosphate, $K_{0.48}Mn_{0.76}PS_3 \cdot H_2O$ (K-MPS-1), which is capable of efficient removal of Pb^{2+} (>99 %) from very dilute concentration (1-100 ppb). K-MPS-1 can selectively capture Pb^{2+} even in presence of other monovalent and divalent cations such as Na^+ , Ca^{2+} , Mg^{2+} with high separation factor. K-MPS-1 can operate within a broad pH range of 2-12 effectively with high distribution co-efficient (K_d^{Pb}) of 5.36×10^5 mL/g, following pseudo second order kinetics. Initially, K^+ intercalation in $MnPS_3$ (MPS-1) increases the interlayer spacing and subsequently creates a Mn^{2+} vacancy to maintain charge neutrality and destroy the center of symmetry of P_2S_6 unit. Finally, Pb^{2+} kicks out K^+ ions from the interlayer and sits into Mn^{2+} vacant sites in MPS-1 which further helps to regain the center of symmetry of the structure. K-MPS-1 has achieved Pb^{2+} removal capacity of 393.5 ± 8 mg/g following Langmuir-Freundlich adsorption model. K-MPS-1 is effective to capture Pb^{2+} far below the mark of tolerance level (15 ppb, USA-EPA) of drinking water. We have extended the overall work to capture Cd^{2+} from water by K-MPS-1 in similar way.

2.1 Introduction

Rapid industrialization has led to discharge of heavy metal ions into water resources. Presence of heavy metal ions such as Pb^{2+} , Hg^{2+} and Cd^{2+} in water is detrimental to human health and environment due to toxicity, non-biodegradability and bioaccumulation.^[1-7] Traditional methods i.e. ion exchange, chemical precipitation, flocculation, membrane separation and evaporation are unable to selectively and effectively remove the heavy metal ions up to the mark of tolerance level (ppb level) of drinking water.^[8] Although, natural hydrophilic adsorbents like clays, zeolites and activated carbon are the promising candidate in this field because of high surface area and low cost, but suffers from weak binding affinity for heavy metal ions, low efficiency and selectivity from dilute solutions.^[9-14] However, intercalated zeolites, layered metal oxides, hydroxides, mesoporous silica, metal organic frameworks and metal chalcogenides have drawn attention with respect to the other materials due to higher removal capacity and selectivity.^[15-24]

Heavy metal ions forms strong covalent bond with sulfides.^[25-27] Specially, in layered metal sulfides, the higher capacity of heavy metal ion absorption arises due to both the open sulfide framework structure and soft Lewis base nature of sulfide anions which has higher affinity towards soft Lewis acidic heavy metal ion center.^[28-36] This strategy is the basis for designing effective adsorbent materials based on inorganic sulfides (e.g. $K_{2x}Mn_xSn_{3-x}S_6$ and $K_{2x}Sn_{4-x}S_{8-x}$) for incarceration of heavy metal ions.^[28-36] Trailing this idea, recently, introduction of polysulfide anions $[S_x]^{2-}$ into layered double hydroxides gallery has proved to be effective in selective capture of heavy metals, but the lack of stability due to oxidation of $[S_x]^{2-}$ species to $[SO_4]^{2-}$ and unsatisfied removal capacity resists the practical utilization.^[37-39] Therefore, it remains a challenge to find a novel stable material which can work in wide pH range with fast kinetics, large adsorption capacity and is capable of removing Pb^{2+} ions selectively from water which is below the drinking water limit (< 15 ppb, USA-EPA).^[40]

In this chapter, we demonstrate an elaborate Pb^{2+} ion adsorption and ion-exchange kinetics studies of a potassium intercalated layered metal chalcophosphate, $K_{0.48}Mn_{0.76}PS_3 \cdot H_2O$ (K-MPS-1). We have determined the nature of sorption by calculating the rate constants. The Pb^{2+} sorption isotherm follows the Langmuir-Freundlich model, which indicates the multilayer adsorption. Further, we have characterized the Pb^{2+} adsorbed K-MPS-1 in detail by IR, Raman

spectroscopy, band gap measurement, X-ray photoelectron spectroscopy and zeta potential analysis to provide mechanistic path of Pb^{2+} adsorption and ion exchange. K-MPS-1 rapidly and efficiently captures Pb^{2+} over 99 % even when the concentration of Pb^{2+} is very low (1-100 ppb). Moreover, K-MPS-1 is stable and captures Pb^{2+} within a broad pH range of 2-12. K-MPS-1 removes Pb^{2+} effectively with a high distribution coefficient of $\sim 10^5$ mL/g, following pseudo second order kinetics. K-MPS-1 has an enormous Pb^{2+} capturing capacity of 393.5 mg/g, which is the respectable compared to the other reported materials.^[29,39,41-54] K-MPS-1 selectively captures Pb^{2+} even in presence of other mono and divalent cations such as Na^+ , Ca^{2+} and Mg^{2+} , which makes it a promising candidate for decontamination of Pb in wide variety of water wastes. Potassium intercalation increases layer spacing and creates Mn^{2+} vacancy in $MnPS_3$. Insertion of Pb^{2+} pulls out K^+ and fills vacancy by forming Pb-S covalent bond, which is generally governed by the strong interaction of soft Lewis acidic sulfide and soft Lewis basic Pb^{2+} . We have extended our work to sequestration of Cd^{2+} from water by K-MPS-1.

2.2 Experimental section

2.2.1 Reagents. Manganese (Mn, Alfa Aesar 99.95 %), red phosphorous (P, Alfa Aesar 98.9 %), sulphur (S, Alfa Aesar 99.999 %), lead nitrate ($Pb(NO_3)_2$, Sigma Aldrich 99.999%), cadmium chloride ($CdCl_2$, Sigma Aldrich 99.999%) and potassium chloride (KCl, Alfa Aesar 99.5 %) were used for synthesis without further purification.

2.2.2 Synthesis. $MnPS_3$ (MPS-1) was prepared by mixing appropriate ratio of elements Mn, P, S followed by sealing under vacuum (10^{-5} Torr) in quartz tube. The tube was slowly heated to 723 K over 12 h, then heated up to 923 K in 2 h, soaked for 144 h, and subsequently cooled to room temperature in 8h. Deep green color reported MPS-1 was obtained.^[55] 1 g MPS-1 was stirred with 50 mL 2M KCl aq. solution for 24 h at room temperature and the light green $K_{0.48}Mn_{0.76}PS_3 \cdot H_2O$ (K-MPS-1) was separated by centrifugation^[56,57], washed with water and ethanol and checked the phase purity by XRD.

2.2.3 Powder X-ray diffraction. Powder X-ray diffraction for all of the samples were recorded using a $Cu K_{\alpha}$ ($\lambda = 1.5406 \text{ \AA}$) radiation on a Bruker D8 diffractometer.

2.2.4 Band gap measurement. To estimate optical band gap of the finely grinded powder samples at room temperature, diffuse reflectance measurements were carried out over the range of 250 nm to 2500 nm using a Perkin Elmer Lambda 900, UV/Vis/NIR spectrometer in reflectance mode. Absorption (α/S) data were calculated from reflectance data using Kubelka-Munk equation: $\alpha/S = (1-R)^2/(2R)$, where R is the reflectance, α and S are the absorption and scattering coefficient, respectively. The energy band gaps were derived from α/S vs E (eV) plot.

2.2.5 Fourier transform infrared spectroscopy. FTIR spectra of powder sample was recorded using a Bruker IFS 66v/S spectrometer.

2.2.6 Raman spectroscopy. Raman spectroscopy measurements of powder sample were carried out with a HORIBA LABRAM HR800 spectrometer. The excitation wavelength of the laser was 514 nm.

2.2.7 Thermogravimetric analysis. TGA was performed using a TGA/DSC 2 STAR instrument in the temperature range of 300–773 K under nitrogen atmosphere with a ramp rate of 5 K min⁻¹.

2.2.8 Fourier transform infrared spectroscopy. FTIR spectra of powder sample was recorded using a Bruker IFS 66v/S spectrometer.

2.2.9 Field emission scanning electron microscopy and energy dispersive spectroscopy analysis. FESEM of the synthesized and lead adsorbed materials were performed using NOVA NANO SEM 600 (FEI, Germany) operated at 15 KV. EDAX compositional analysis was performed during FESEM imaging.

2.2.10 X-ray photoelectron spectroscopy. XPS measurement has been performed with Mg–K α (1253.6 eV) X-ray source with a relative composition detection better than 0.1% on an Omicron Nanotechnology spectrometer.

2.2.11 Zeta potential measurement. The zeta potential measurements were carried out using a NanoZS (Malvern UK) employing a 532 nm laser.

2.2.12 ICP-AES. Actual concentration of the lead containing solutions (1ppm-1000ppm) were measured by ICP-AES. ICP-AES measurements were carried out using Perkin-Elmer Optima 7000DV instrument. Pb standard (1000mg/L, Sigma-Aldrich), Mn standard (1000mg/L, Sigma-Aldrich) and multi-element standard (Ca 2000 mg/L, Na 1000 mg/L, K 200 mg/L and Mg 400 mg/L, Sigma-Aldrich) were used to determine the concentration of various cations.

2.2.13 ICP-MS. Element concentrations in ppb level (1-1000 ppb) were measured using a quadrupole inductively coupled plasma- mass spectrometer (ICP-MS, Thermo Scientific X-Series II) at CEaS, IISc equipped with Nickel sample and skimmer cones. Samples were introduced using a 100 ml/min PFA nebulizer connected to a peristaltic pump running at 30 rpm into an ESI-PC3 Peltier cooled spray chamber. A CETAC ASX-520 auto-sampler was used. Uptake time for samples and standards was 60 seconds while the rinse time (in 2% HNO_3) was 90 seconds.

2.2.14. Pb^{2+} and Cd^{2+} sorption and ion-exchange kinetics. Sorption studies is carried out by batch method at V:m~1000 mL/g. 10 mL of Pb^{2+} aqueous solution (1 ppb-1000 ppm) is taken in a 15 mL centrifuging tube. 10 mg of K-MPS-1 was added and shaken for 24 hrs. The solid material is removed by centrifugation or filtration by Whatman filter paper No. 41 and then measured the initial and final Pb^{2+} concentrations in the supernatant by using ICP-AES and ICP-MS. The obtained data is used for determination of Pb^{2+} sorption isotherm. Similar experiments were performed with Cd^{2+} solutions.

Kinetic studies are carried out to study the rate and path ways of sorption until the equilibrium has reached. Initially, 10 mL of 30 ppm Pb^{2+} aqueous solution and 10 mg of K-MPS-1 is shaken in an individual tube. After a certain time interval, the suspension of each tube is centrifuged and the final concentration is measured by ICP.

2.3 Results and discussion

Layered transition metal thiophosphates MPS_3 , where M is a divalent metal cation, have the similar structural connectivity of $CdCl_2$ structure, where metal ions and P-P pairs occupy the Cd positions and sulphur atoms occupies the chloride positions. [55] Previously, Clement et.al. have reported that layered $MnPS_3$ can intercalate wide range of cations, including organometallic species, ammonium and alkali metal cations. [56, 57]

2.3.1 Sythesis and Characterization

We have synthesized dark green powder of $MnPS_3$ (MPS-1) and light green color K^+ intercalated $MnPS_3$ (K-MPS-1) by stirring a suspension of MPS-1 in 2M KCl solution for 24 h at room temperature (Figure 2.1). [56]



The Pb^{2+} sorption properties are explored by stirring $Pb(NO_3)_2$ solution with the as synthesized K-MPS-1. The synthesized Pb^{2+} sorbed K-MPS-1 (Pb-MPS-1) is distinct in color compared to MPS-1.

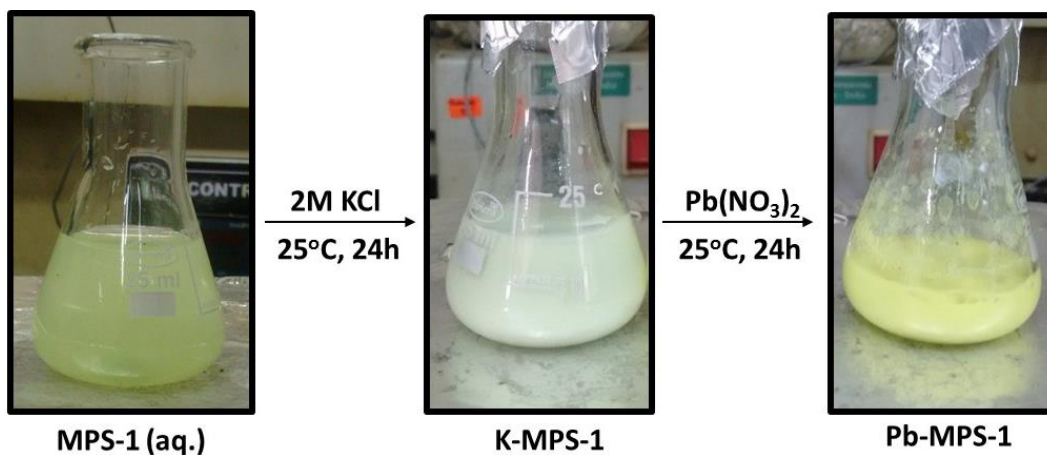


Figure 2.1 Color change during ion-exchange reactions.

Initial elemental analysis by energy-dispersive X-ray analysis (EDAX) of K-MPS-1 and Pb-MPS-1 shows significant amount of Pb^{2+} sorption by K-MPS-1 (see Table 2.1 and Figure 2.2)

Table 2.1 Elemental identification and quantification by EDX spectra analysis

K-MPS-1			Pb-MPS-1		
Element	Wt %	At %	Element	Wt %	At %
P	17.74	20.45	P	11.87	17.88
S	51.82	57.71	S	38.49	56.00
Mn	22.59	14.68	Mn	23.94	20.33
K	7.85	7.17	Pb	25.69	5.78
Total	100	100	Total	100	100

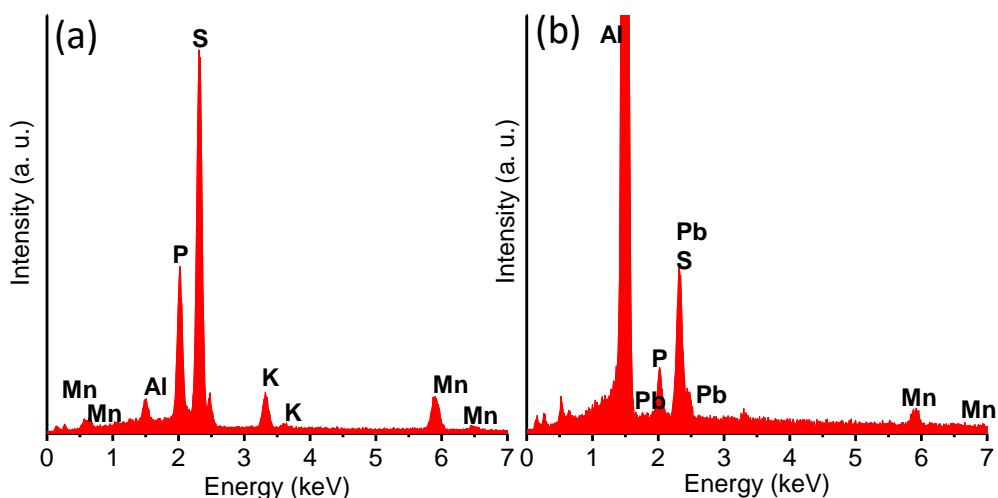


Figure 2.2 EDX spectrum of a) K-MPS-1 and b) Pb-MPS-1

More accurate quantification of the elements in K-MPS-1 and Pb-MPS-1 was carried out by inductively coupled plasma (ICP)-AES and ICP-MS analysis. The chemical formula of K-MPS-1 derived by both ICP and thermogravimetric analysis (TGA, Figure 2.3), which is to be $K_{0.48}Mn_{0.76}PS_3 \cdot H_2O$.

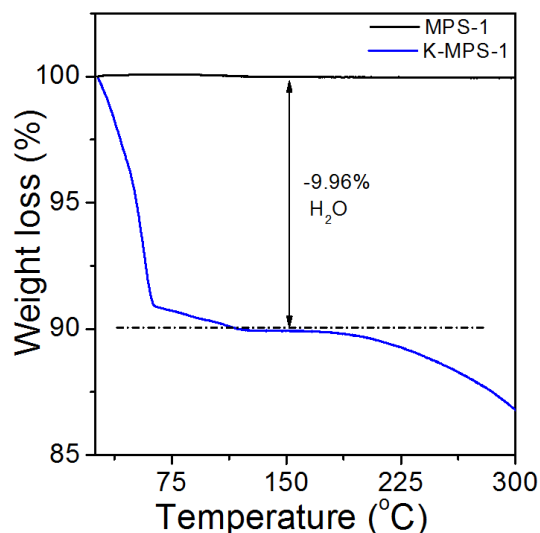


Figure 2.3. TGA analysis of MPS-1 and K-MPS-1

The phase identification and inter layer spacing of K-MPS-1 and Pb^{2+} adsorbed MPS-1 were probed by powder X-ray diffraction (PXRD, see Figure 2.4). K^+ intercalation in MPS-1 increases the inter-layer spacing from 6.45 to 9.40 Å, retaining the monoclinic layered crystal structure. After Pb^{2+} sorption, the inter-layer spacing is decreased back to 6.45 Å, which is similar to pristine MPS-1 (Figure 2.4 and Table 2.2).^[58]

Table 2.2 Interlayer spacing and band gap

Material	Interlayer spacing (Å)	Band gap energy (eV)
MPS-1	6.45	2.39
K-MPS-1	9.40	2.54
Pb-MPS-1	6.45	2.45

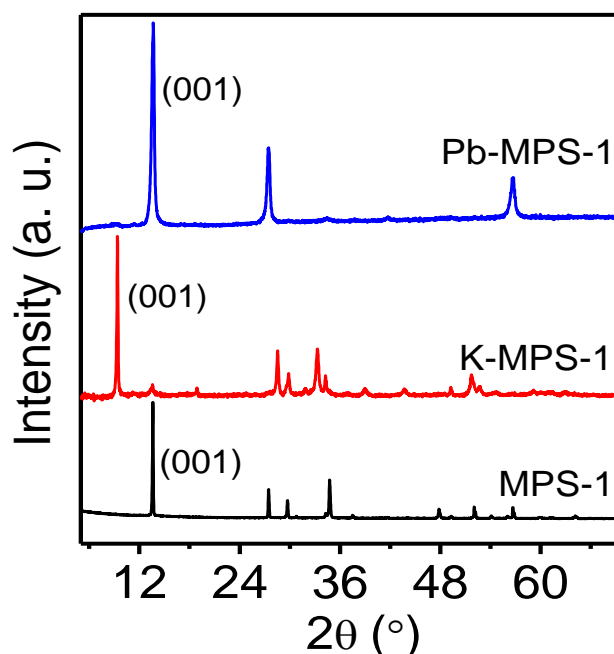


Figure 2.4. PXRD patterns of the MPS-1, K-MPS-1 and Pb-MPS-1.

The binding nature of Pb in K-MPS-1 is derived by infrared (IR) and Raman spectroscopy. In the pristine MPS-1, P-S bond shows single asymmetric P-S stretching at 565 cm^{-1} and P-P bond stretching occurs at 445 cm^{-1} (Figure 2.5a). K^+ ion intercalation in MPS-1 removes few Mn^{2+} from the solid layer for keeping the balance in total charge, which results in intra-layer Mn^{2+} vacancies in K-MPS-1. This destroys the inversion center in structure and the three S atoms do not stay in the same plane. As a result, asymmetric P-S stretching splits into two components (in-plane and out-plane), which are appearing at 604 and 550 cm^{-1} , respectively (Figure. 2.5a).^[59,60] Interestingly, Pb-MPS-1 shows a single P-S stretching at 565 cm^{-1} . Pb^{2+} adsorption removes K^+ ions from interlayer space of $MnPS_3$ and Pb^{2+} occupies the Mn^{2+}

vacancy site, which regenerates the center of symmetry and makes the three S atoms coplanar in the structure. This attributes to merging of two P-S stretching modes in a single peak at 565 cm^{-1} .

The strong Raman band at about 386 cm^{-1} is assigned to the PS_3 stretching mode in MPS-1 (Figure 2.5b).^[59, 60] K^+ intercalation creates an intra-layer Mn^{2+} vacancy and decreases the P-S bond length, which leads to a red shift in the P-S stretching frequency by 2 cm^{-1} K-MPS-1. After Pb^{2+} sorption, this P-S stretching is blue shifted to 384 cm^{-1} due to fill up of Mn^{2+} vacancies (Figure 2.5b). This is attributed to the slight increase in P-S bond length in Pb-MPS-1 with respect to P-S bond length in MPS-1. Another band appearing at 275 cm^{-1} is assigned to degenerate bending modes of the PS_3 unit. Two others bands at 247 and 227 cm^{-1} are assigned to translational, T'_{xy} , and rotational, R'_{xy} , motions of the PS_3 unit, respectively (Figure 2.5b).^[59, 60]

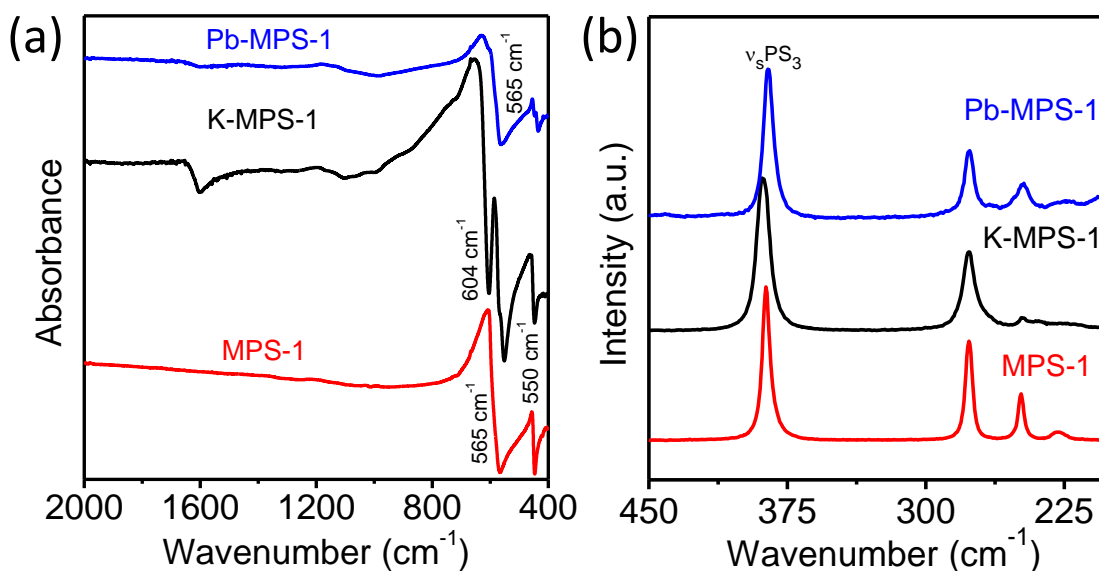


Figure 2.5. a) Infrared spectra and b) Raman spectra of the MPS-1, K-MPS-1 and Pb-MPS-1.

These modes of vibration (275 , 247 and 227 cm^{-1}) are strongly sulfur sensitive. The motions of PS_3 in xy plane (layer plane) are affected due to K-intercalation via loss of symmetry, thus the intensity of the translational (T'_{xy}) and rotational (R'_{xy}) modes decrease in case of KMPS-1 with respect to MPS-1. Pb sorption helps to regain the symmetry in P_2S_6 unit, which further increases the intensity.^[61]

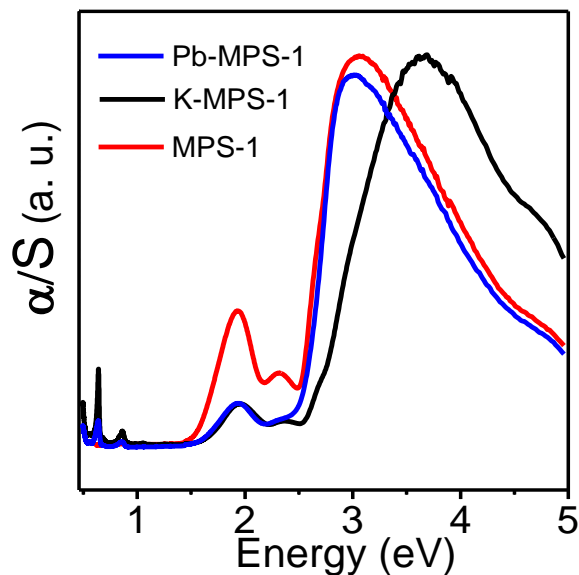


Figure 2.6 Electronic absorption spectra of MPS-1, K-MPS-1 and Pb-MPS-1.

Intercalation of K^+ in $MnPS_3$ increases the band gap from 2.38 eV to 2.54 eV indicating increase the gap between the layers due to K^+ intercalation (Figure 2.6). Sorption of Pb^{2+} in K-MPS-1 leads to removal of K^+ from the interlayer space and Pb^{2+} occupies the Mn^{2+} vacancy in the $MnPS_3$ layer. The larger covalent interaction between Pb and S with respect to K and S destabilizes the valance band resulting to a further reduction in band gap to 2.45 eV. While the covalent character of Pb-S in Pb-MPS-1 is smaller than that of the Mn-S in MPS-1, depicts band gap of Pb-MPS-1 is 0.06 eV higher than that of MPS-1.

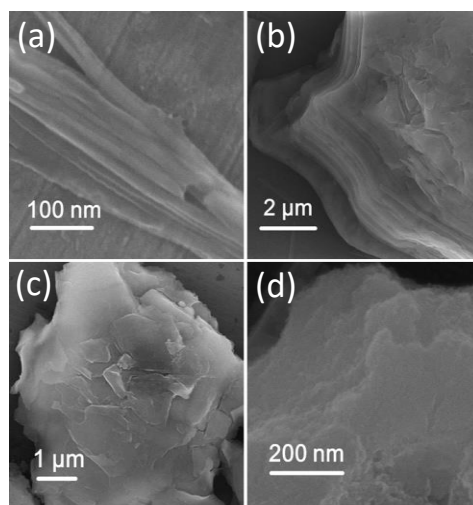


Figure 2.7 FE-SEM images before (a, b) and after (c, d) Pb^{2+} sorption.

The morphology of the materials is studied by field emission scanning electron microscopy (FESEM) analysis (Figure 2.7). The K-intercalated layers are still stacked to each other in K-MPS-1 due to weak van der Waals' force of attraction and the smooth surface are clearly shown in Figure 2.7 (a, b). Pb^{2+} sorption keeps the layer as intact as before, but surface roughness increases in Pb-MPS-1, which might be due to additional surface adsorption. (Figure 2.7. (c, d)).

2.3.2 Mechanism of lead capture by K-MPS-1

We propose a qualitative mechanism of Pb^{2+} sorption in K intercalated MnPS_3 (K-MPS-1) by the above XRD, IR, Raman, electronic absorption spectroscopy and FESEM studies (Figure 2.8 and 2.9). Initially, intercalation of hydrated K^+ in MPS-1 increases the inter-lamellar spacing and creates a Mn^{2+} vacancy for maintaining the overall charge balance.

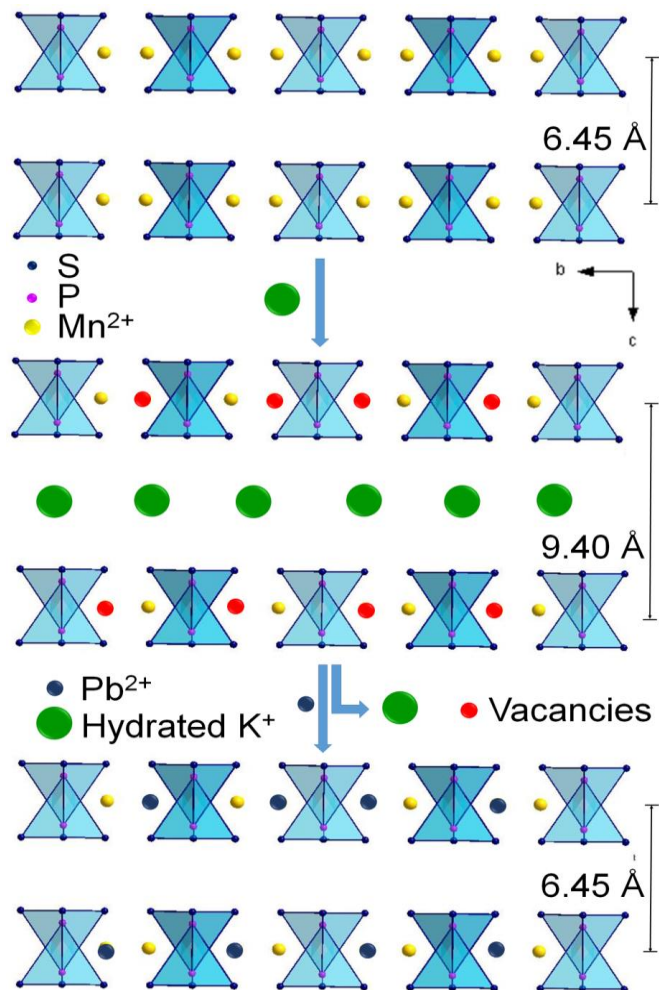


Figure 2.8 Schematic representation displaying the qualitative ion exchange mechanism.

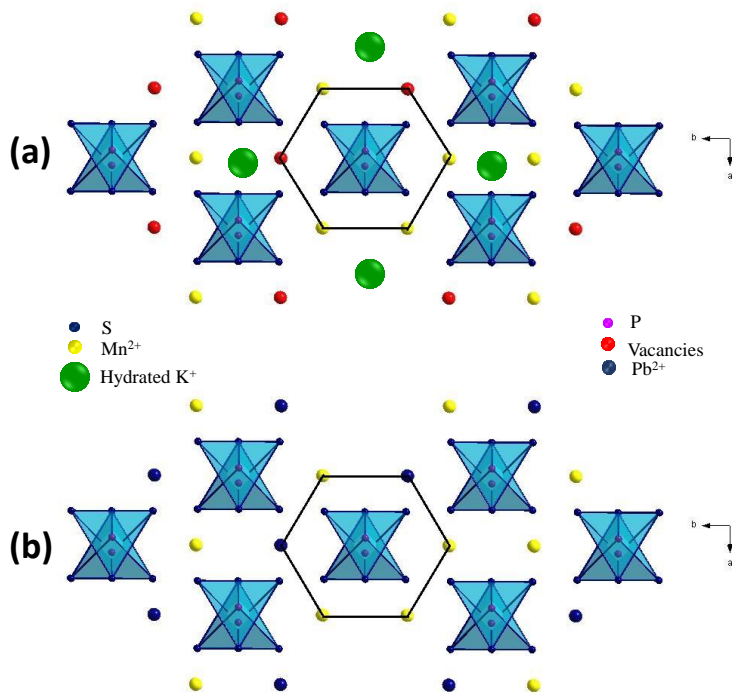


Figure 2.9 Top view of schematic representation displaying the ion exchange mechanism of synthesized and lead adsorbed material.

Additionally, excess Mn^{2+} vacancy formation creates extra negative charges which are balanced by self aerial oxidation of Mn^{2+} to Mn^{3+} in K-MPS-1.^[31] The coexistence of Mn^{2+} and Mn^{3+} in K-MPS-1 is shown in Mn2p X-ray photo electron spectra (XPS) (Figure 2.10a).

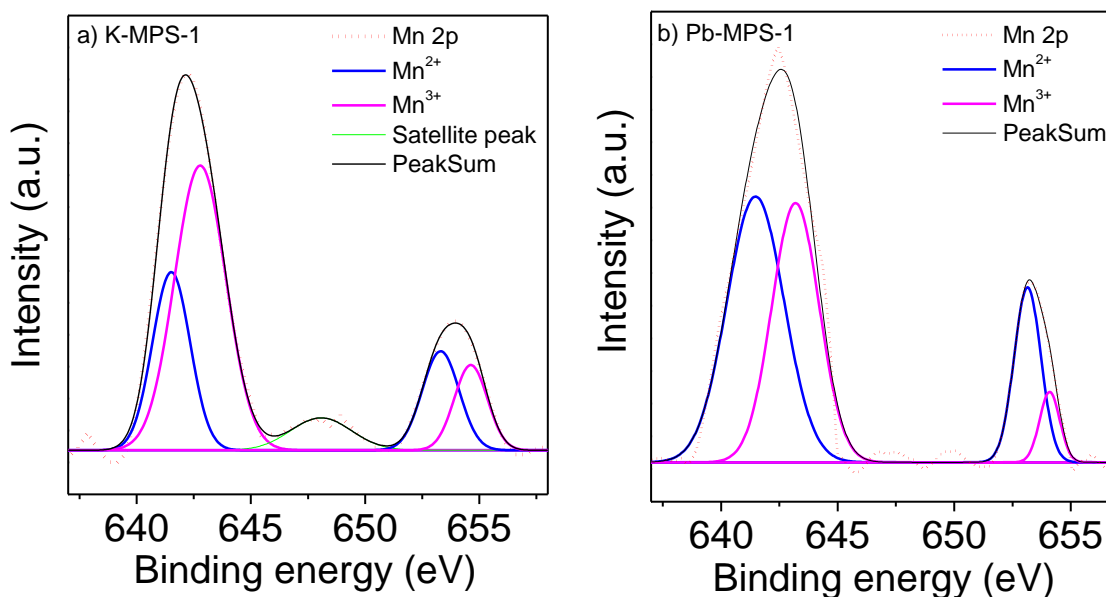


Figure 2.10 Mn2p peak in the XPS spectrum of a) K-MPS-1 and b) Pb-MPS-1

In the Pb^{2+} sorption process, Pb^{2+} goes into the Mn^{2+} vacancy site in the layer and pulls out the intercalated hydrated K^+ ions from interlayer, which decreases the inter-lamellar spacing. Moreover, the formation of an excess Mn^{2+} vacancy during K intercalation creates the excess negative charge on surface S atoms. The additional surface charge on the S atoms promotes the adsorption of extra Pb^{2+} over the surface and makes the surface rough. Surface adsorption of Pb^{2+} diminishes the Mn^{3+} concentration in Pb-MPS-1 which is again confirmed by XPS studies (see Figure 2.10b). Thus, Pb^{2+} adsorbs both in the Mn^{2+} vacancy site and surfaces. The formation excess negative charge on the surface after K-intercalation was further confirmed by the zeta potential measurement. It was found that the negative charge of the MPS-1 increases upon intercalation of K^+ , but it diminishes by sorption of Pb^{2+} into K-MPS-1 (Figure 2.11).

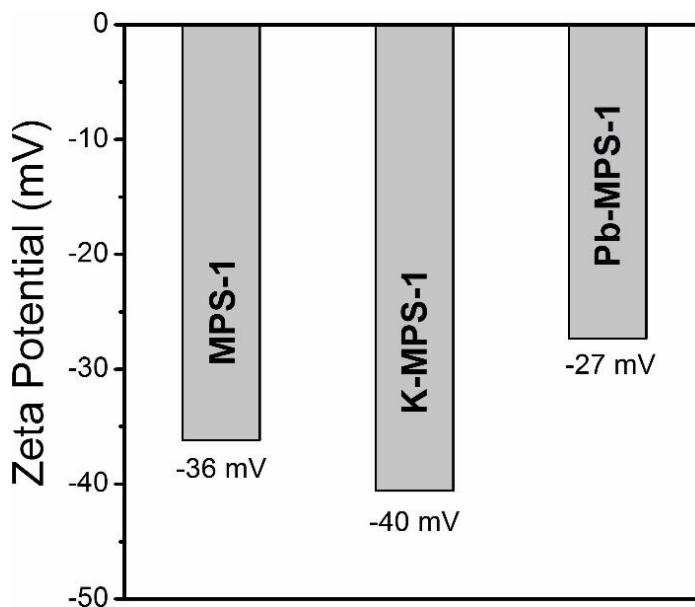


Figure 2.11 Zeta potential of MPS-1, K-MPS-1, Pb-MPS-1 at pH 7 and room temperature.

2.3.3 Sorption studies

To determine the quantitative sorption capacity of K-MPS-1, we performed ion-exchange batch studies at room temperature within a broad range of Pb^{2+} concentrations from ppb to ppm ($V:m = 1000 \text{ mL/g}$, pH ~ 6.5 , Milli-Q water). The initial and final concentration of Pb^{2+} in the aqueous solution are measured by ICP analysis and maximum sorption capacity (q_m) and the distribution co-efficient (K_d) are calculated by using Eq. (1) and (2).

The equilibrium data and K_d are shown in Figure 2.12a and Table 2.3, respectively, which can be fitted using Langmuir and Langmuir-Freundlich adsorption isotherm models.^[31] The equilibrium data were best fitted ($R^2 = 0.991$) with the Langmuir-Freundlich model (see Figure 4a) expressed as below:

$$q = q_m \frac{(bC_e)^{1/n}}{1+(bC_e)^{1/n}} \quad (1)$$

$$K_d = \left(\frac{V}{m}\right) \frac{(C_o - C_e)}{C_e} \quad (2)$$

where q (mg/g) is the amount of the cation sorbed at equilibrium concentration C_e (ppm), q_m is the maximum sorption capacity of the adsorbent, C_o is the initial concentration, b (L/mg) is the Langmuir-Freundlich constant assigned to the affinity of the ions towards the adsorbents. $1/n$ is a measure of the intensity of adsorption where n is a constant.

Table 2.3 Sorption results of K-MPS-1 toward Pb^{2+} .

Initial concentration, C_0 (ppm)	Final concentration, C_f (ppm)	Removal (%)	q (mg/g)	K_d (mL/g)
402.60	1.70	99.6	400.9	2.35×10^5
349.90	1.55	99.5	351.9	2.26×10^5
319.30	1.09	99.6	318.2	2.90×10^5
244.00	0.82	99.7	240.8	2.95×10^5
146.30	0.68	99.5	145.6	2.14×10^5
104.10	0.56	99.4	103.5	1.83×10^5
70.34	0.42	99.4	70.6	1.69×10^5
19.85	0.32	98.4	19.5	6.14×10^4
5.37	0.23	95.6	5.2	2.21×10^4
7.86	0.15	98.0	7.7	5.16×10^4
0.49	0.11	76.7	0.3	3.23×10^3
0.29	0.08	73.2	0.2	2.65×10^3
0.30	0.04	87.7	0.3	6.99×10^3

$m = 0.010$ g, $V = 10$ mL, $V:m = 1000$ mL/g

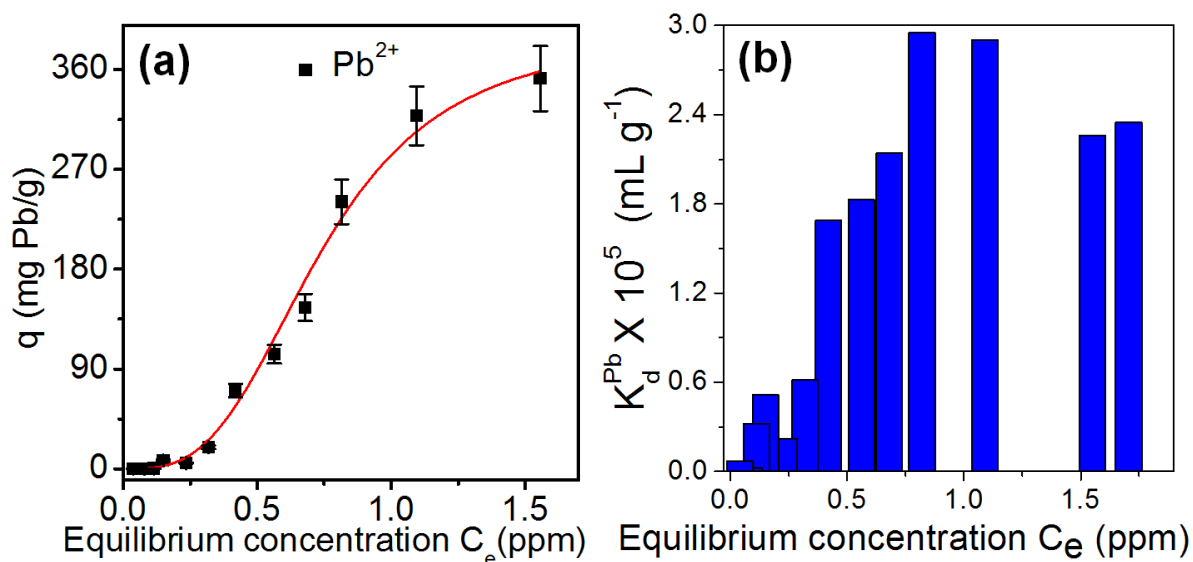


Figure 2.12 a) Sorption isotherm for the sorption of Pb^{2+} in K-MPS-1. (pH ~ 6.5, RT) The solid (red line) represents the fitting of the data with Langmuir- Freundlich model (fitting data for Pb^{2+} : $b = 1.35 \text{ Lmg}^{-1}$, $n = 0.32$, $R^2 = 0.992$) and b) Distribution coefficient (K_d^{Pb}) of Pb^{2+} ion exchange at ppm level concentration of Pb^{2+} .

The K_d is found in a range of 0.4×10^4 to $2.95 \times 10^5 \text{ mL/g}$ (see Figure 2.12b and Table 2.3). The layered material is intact even if the initial concentration of Pb^{2+} (400 ppm) is higher than that of the saturation level of the K-MPS-1 (Figure 2.13).

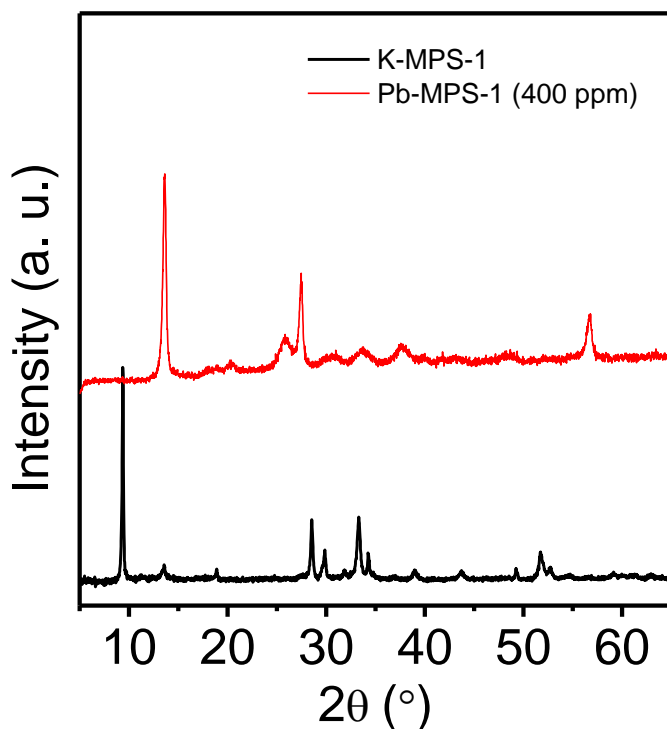


Figure 2.13: XRD of sorbed Pb^{2+} sample at 400 ppm concentration on K-MPS-1.

The sorption data revealed that K-MPS-1 can capture Pb^{2+} rapidly, showing 97% removal within 4.5 h and ≥ 99 % removal within 12 h (see Table 2.4 below).

Table 2.4 Kinetics data of Pb^{2+} sorption using K-MPS-1.

Initial concentration, C_0 (ppm)	Time (min)	Final concentration, C_t (ppm)	Removal (%)	K_d (mL/g)	q_t (mg/g)
28.64	15	17.63	38.4	6.25×10^2	11.0
	180	3.19	88.9	7.98×10^3	25.5
	240	1.04	96.4	2.66×10^4	27.6
	270	0.71	97.5	3.93×10^4	27.9
	1920	0.37	98.7	7.75×10^4	28.3
	3180	0.08	99.7	3.62×10^5	28.6
$m=0.040g, V= 40mL, V:m=1000mL/g$					

We have achieved a maximum Pb sorption capacity q_m of 393.5 ± 8 mg/g for K-MPS-1, which is comparable for Pb sorption capacity for other leading materials (see Table 2.5), with 99.8 % removal within 12h (Figure 2.14a and b). The high value of b (1.35 L/mg) indicates that K-MPS-1 has a strong affinity towards the Pb^{2+} and the rate of removal is rapid with high distribution co-efficient 2.95×10^5 mL/g.^[35] The observed Pb^{2+} exchange capacity (1.91 mmol/g) is almost two times higher than that the theoretical exchange capacity (1.17 mmol/g) of K-MPS-1, which indicates that Pb^{2+} occupies Mn^{2+} vacancy as well as the surface to form multilayer layers.

2.3.4 Kinetics study

Kinetics of the ion exchange of layered K-MPS-1 is also explored. The sorption for Pb^{2+} reaches equilibrium within ~ 8 h (Figure 2.14c) and the rate of Pb^{2+} sorption is calculated by using two different rate equations: pseudo-first-order [Eq. (3)] and pseudo-second-order [Eq. (4)] as stated by the equation below

$$\ln(q_e - q_t) = \ln q_e - k_1 t \quad (3)$$

$$\frac{t}{q_t} = \frac{1}{k_2 q_e^2} + \frac{t}{q_e} \quad (4)$$

where q_e (mg/g) is the amount of Pb^{2+} adsorbed per unit mass of adsorbent at equilibrium, q_t is Pb^{2+} ions adsorbed at time t , k_1 and k_2 ($g/mg \text{ min}^{-1}$) are the rate constants of pseudo-first-order and pseudo-second-order adsorption interactions. The value of k_1 and k_2 are estimated by plotting $\ln(q_e - q_t)$ vs. t and t/q_t vs t plot by using Eq. (3) and (4), respectively (see Table 2.6).

Table 2.5 Comparison of Pb^{2+} sorption capacities between different adsorbents.

Adsorbents	q_m (mg/g)	pH, Temperature	Working pH range	Ref.
K-MPS-1	393.5	6.5, RT	2-12	this work
KMS-1	319	5, RT	2-9	29
MoS₄-LDH	290	RT	2-10	39
Edta-LDH	180	5, RT	3-6	41
DTPA-LDH	170	5.4, RT	3-5.5	42
Cl-LDH	74	5.4, RT	3-5.5	42
LS-LDH	123	5, RT	-	43
LS-GH	1210	5, RT	2-6	44
MNP-CTS	140	6, RT	2-6	45
H100-LDH	128	5, 35° C	-	46
CDpoly-MNPs	65	5.5, RT	2-6	47
Fe₃O₄-GS	158	6-7, RT	2-7.5	48
Titanate-architecture	366	5, RT	-	49
CeO₂ nanowires	642	RT	-	50
EDTA-GO	479	6.8, RT	6.5-7	51
GO-Zr-P	363	6	1-8	52
Graphene oxide	1119	5, RT	3-7	53
NC-FeMg LDH	345	RT	3-7	54

Table 2.6 Kinetic parameters for sorption of Pb^{2+} by K-MPS-1 with two different models.

Order	Adsorbate	R^2	q_e (exp) ($mg\ g^{-1}$)	q_e (cal) ($mg\ g^{-1}$)	k ($g/mg/min$)
Pseudo-2nd	Pb^{2+}	0.9993	28.2	28.9	1.00×10^{-3}
Pseudo-1st	Pb^{2+}	0.2801	28.2	8.1	2.29×10^{-3}

The values of rate constants (k) and correlation coefficient (R^2) revealed the feasibility of kinetic path of Pb^{2+} sorption. [39] Hence, the goodness of fit R^2 (0.991) obtained from the Eq. (4), which very close to unity indicates the sorption of Pb^{2+} on K-MPS-1 follows pseudo-second-order kinetics suggesting the process is chemisorption and irreversible (Figure 2.14d).

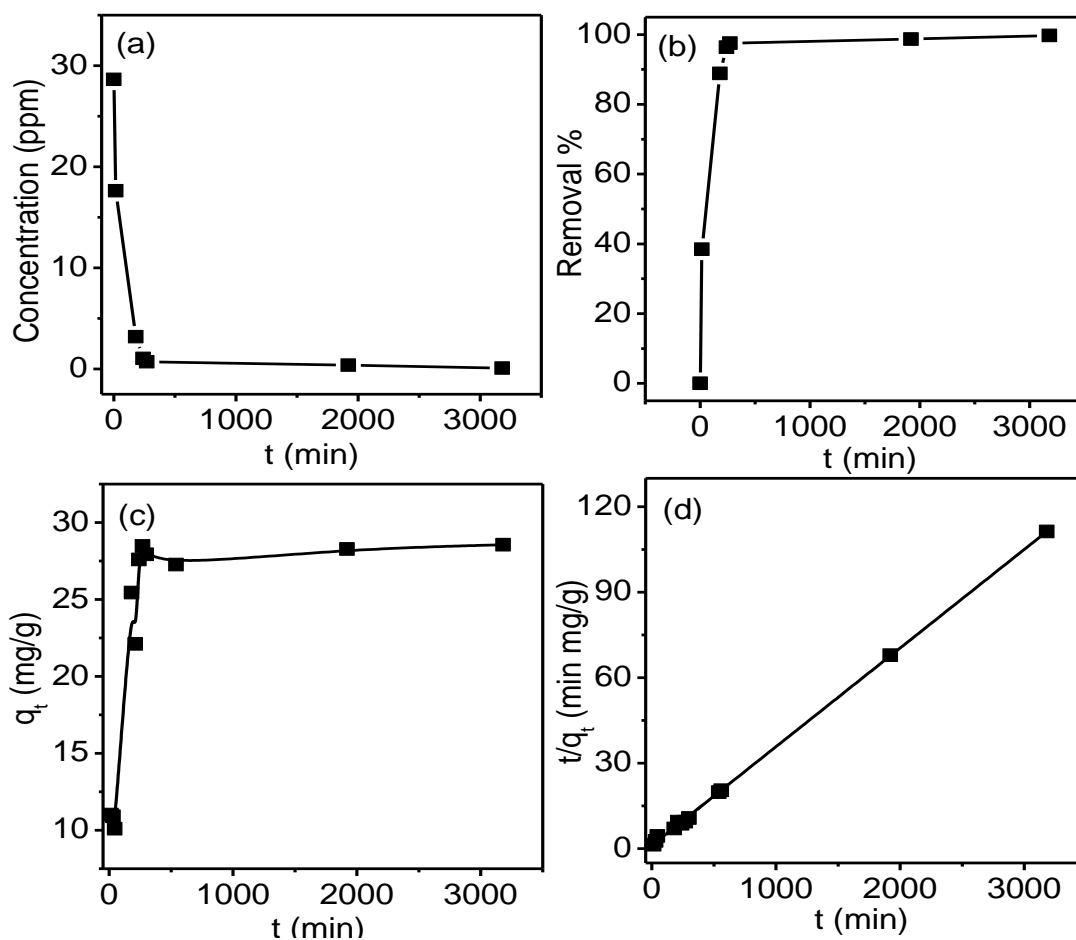


Figure 2.14. Sorption kinetics curve for Pb^{2+} : a) ion concentration change with contact time, b) removal % of Pb^{2+} as a function of contact time, c) sorption capacity (q_t) with contact time and d) pseudo-second-order kinetic plots for Pb^{2+} sorption.

Irreversibility of Pb^{2+} sorption in K-MPS-1 is further proved by the ICP analysis during desorption obtained by stirring Pb-MPS-1 with saturated KCl solution (Table 2.7). Generally, the Pb contamination is in very low concentration level (ppb) in water. At such a low concentration, K-MPS-1 can take an ample amount of Pb ~393.5 mg/g for long time usage.

Table 2.7. Desorption studies of Pb-MPS-1 by using saturated KCl.

C_0 , (ppm)	C_0 , (ppm)	Removed %	Adsorbed on K-MPS-1	Pb^{2+} released, (ppm)	Released %
402.6	1.705	99.6	400.895	0.97	0.2
349.9	1.556	99.6	348.344	0.824	0.2
244	0.815	99.7	243.185	1.005	0.4
146.3	0.679	99.5	145.621	0.579	0.4
70.34	0.419	99.4	69.921	0.044	0.1

m = 0.010 g, V = 10 mL KCl solution, V:m = 1000 mL/g

2.3.5 Competitive ion-exchange and selectivity studies

The affinity and selectivity of the material are expected to be unaffected in presence of other monovalent and divalent cations. Thus, we have performed sorption studies using a solution containing a mixture of Pb^{2+} , Na^+ , Ca^{2+} and Mg^{2+} . K-MPS-1 is capable of discriminating Pb^{2+} ions selectively without a change in K_d^{Pb} value (0.4×10^5 mL/g) and the results are depicted in Table 2.8.

Moreover, the material shows selective sorption of Pb^{2+} even in the presence of high concentration ratio between Ca^{2+} and Pb^{2+} (see Figure 2.15a). This happens due to strong affinity between soft acidic Pb^{2+} and soft basic S^{2-} ligand according to the Hard Soft Acid Base (HSAB) principle^[62], whereas the interaction weakens drastically for the hard Ca^{2+} and Mg^{2+} ions. The ability of an ion-exchange media to separate two ions from one another can be expressed by the separation factor (K_d^a / K_d^b). At lower concentration of Pb such as 30 ppm in presence of Ca (30 ppm) and Mg (20 ppm), the SF (Pb^{2+}/Ca^{2+}) is 4.8×10^3 and SF (Pb^{2+}/Mg^{2+}) is 5.11×10^3 , respectively.^[36] The affinity and selectivity order of cations, determined by comparison of K_d value are to be in the order: $Pb^{2+} \gg Ca^{2+} \approx Mg^{2+} \gg Na^+$.

Table 2.8 Summary of the competitive ion-exchange data of K-MPS-1.

Exchange cations	V:m (mL/g)	Initial concentration (ppm)	Final concentration (ppm)	% Removal	K_d (mL/g)
Pb ²⁺ +		28.16 (Pb)	0.70 (Pb)	97.5 (Pb)	3.90×10^4
Ca ²⁺ +	990	32.82 (Ca)	32.55 (Ca)	0.8 (Ca)	8.21
Mg ²⁺		20.92 (Mg)	20.76 (Mg)	0.8 (Mg)	7.63
Pb ²⁺ +		33.42 (Pb)	0.59 (Pb)	98.2 (Pb)	5.45×10^4
Ca ²⁺ +	980	65.28 (Ca)	63.32 (Ca)	3.0 (Ca)	3.03×10^1
Mg ²⁺		37.78 (Mg)	35.77 (Mg)	5.3 (Mg)	5.51×10^1

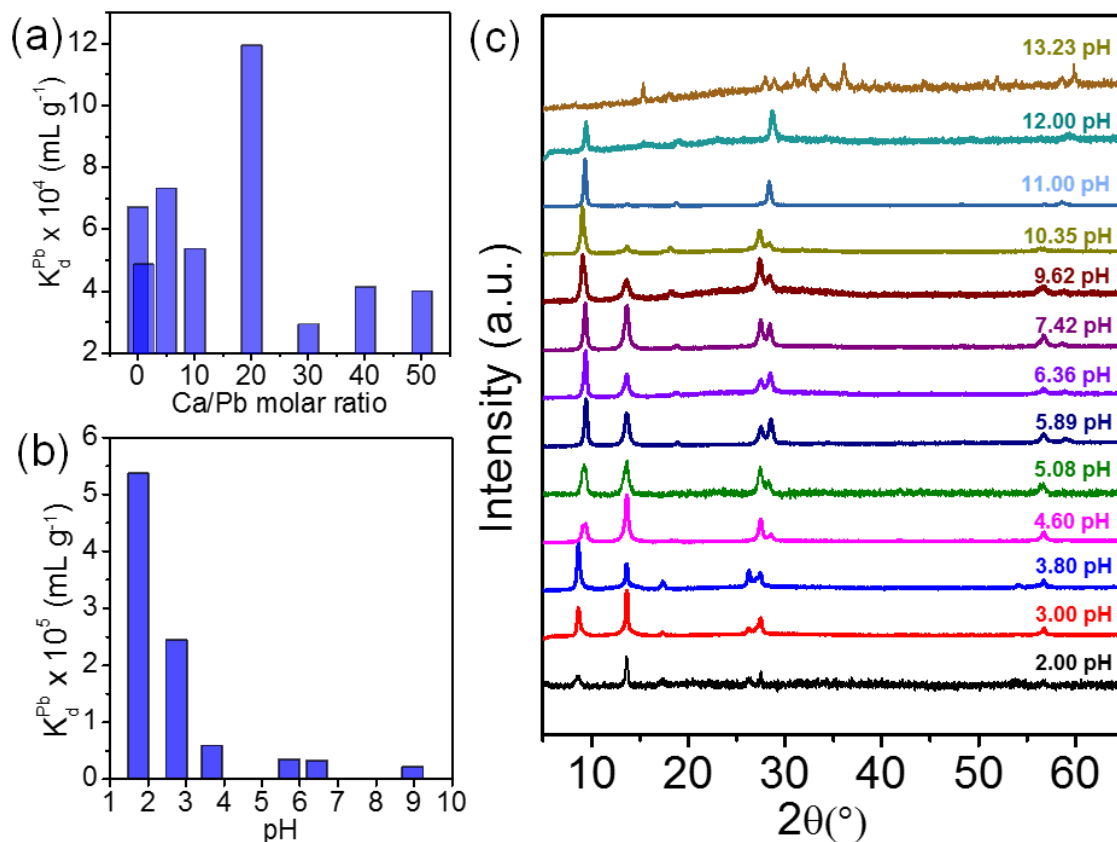


Figure 2.15 a) Variation of distribution coefficient (K_d^{Pb}) with Ca/Pb molar ratios. b) Distribution coefficient (K_d^{Pb}) of Pb²⁺ ion exchange at different pH and c) PXRD patterns of K-MPS-1 in pH range 2-13.2.

2.2.6 pH studies

The interaction between the K-MPS-1 and Pb^{2+} is persistent in a broad pH range 2-12 (Table 2.9) and interaction strength is unaltered with a K_d^{Pb} of the order of $\sim 10^4$ to 10^5 mL g^{-1} in the 2-10 pH range (Figure 2.15b). PXRD analysis shows that the K-MPS-1 is stable within a pH range 2-12 (Figure 2.15c) which indeed indicates the structure and composition is stable in such broad pH range. A maximum K_d^{Pb} value of 5.36×10^5 mL g^{-1} with the highest Pb^{2+} removal capacity of 99.81% is observed at pH 1.75. In acidic condition, hard protons have the lower affinity for soft basic S^{2-} , thus soft acidic Pb^{2+} sorption will be dominant. Thus, Pb^{2+} uptake increases in lower pH. We have performed the Mn leaching experiment at different pH and observed there is the negligible quantity of Mn leaching (Table 2.10), which suffices the stability of the material in different pH.

Table 2.9 Summary of Pb^{2+} sorption by K-MPS-1 in different pH.

pH	Initial concentration, C_o (ppm)	Final concentration, C_f (ppm)	% Removed	q (mg/g)	K_d (mL/g)
1.75	35.62	0.07	99.8	35.9	5.36×10^5
2.75	35.85	0.14	99.6	34.7	2.44×10^5
3.68	35.17	0.58	98.3	34.2	5.88×10^4
5.71	30.46	0.84	97.2	29.0	3.47×10^4
6.44	24.40	0.71	97.1	23.0	3.25×10^4
8.96	13.80	0.60	95.7	12.8	2.14×10^4
10.75	14.00	2.16	84.6	11.7	5.44×10^3
11.39	19.01	3.63	80.9	15.3	4.24×10^3

2.3.7 Low concentration (ppb level) Pb capture and capture of Pb from Bangalore Lake

At lower concentration of Pb^{2+} (1-1000 ppb), the removal capacity and K_d values remain as high as 99 % and $\sim 10^5$ mL/g, respectively (Figure 2.16 and Table 2.11). We have used ICP-MS, Thermo Scientific X-Series II for detecting the ppb level concentration of Pb as it has really low detection limit. Finally, we have tested Pb^{2+} sequestration from the water samples collected from the local Rachenahalli lake in Bangalore, India. The K-MPS-1 is able to

selectively remove 99.2% of Pb^{2+} from the potable water sample containing 68 ppb Pb^{2+} and Pb^{2+} concentration reaches below the tolerance level (15 ppb, USA-EPA) (Table 2.11).

Table 2.10 Mn^{2+} leaching study in different pH showing negligible Mn leaching.

pH	Mn^{2+} Leaching (mmole/mg)
2.2	0.0017
3.0	0.0015
4.9	0.0014
7.1	0.0014
9.3	0.0015
11.9	0.0012

m = 10 mg, V = 10 mL, V:m = 1000 mL/g

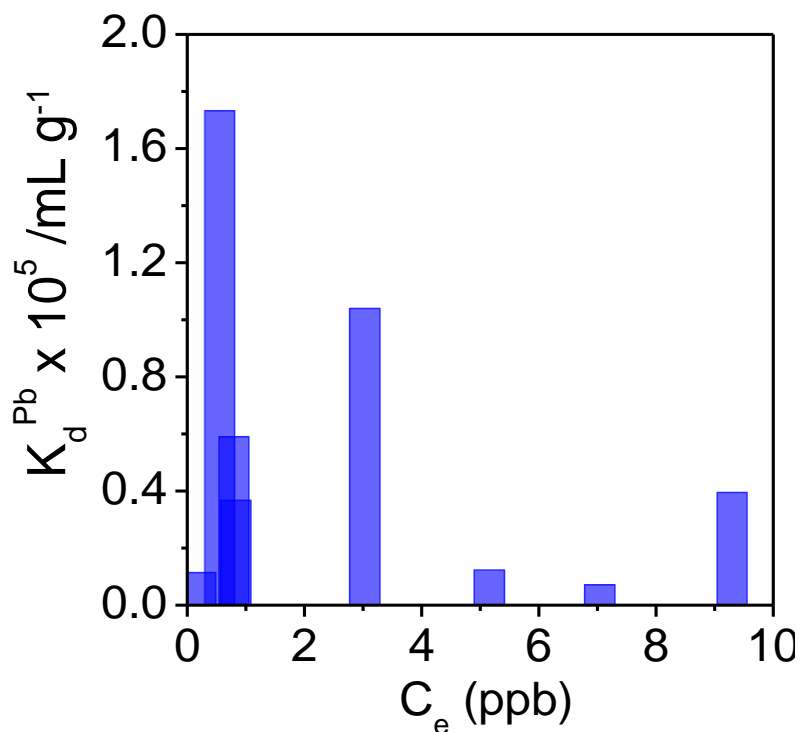


Figure 2.16 Distribution coefficient (K_d^{Pb}) of Pb^{2+} ion exchange at ppb level concentration of Pb^{2+} .

Table 2.11 Removal of Pb^{2+} at lower ppb level.

Initial concentration, C_0 (ppb)	Final concentration, C_f (ppb)	% Removed
0.95	0.10	89.5
2.84	0.23	91.7
11.36	0.40	96.5
31.14	0.83	97.3
47.84	0.80	98.3
68.57	5.16	92.5
56.45	7.05	87.5
96.50	0.55	99.4
375.60	9.30	97.5
318.00	3.03	99.0
834.20	36.52	95.6
68.00 (Rachenahalli lake water)	0.552	99.2
$m = 0.010$ g, $V = 10$ mL, $V:m = 1000$ mL/g		

2.4 Cd sequestration by K-MPS-1

The present study has been extended to capture Cd by K-MPS-1 as Cd^{2+} is also a soft lewis acid like Pb^{2+} . To determine the quantitative sorption capacity of K-MPS-1 for Cd^{2+} ions, we performed similar ion-exchange sorption batch studies (section 2.2.3) at room temperature within a broad range of Cd^{2+} concentrations from 2 ppb to 600 ppm ($V:m = 1000$ mL/g, pH ~ 6.5, Milli-Q water). The initial and final concentration of Cd^{2+} in the aqueous solution are measured by ICP analysis and maximum sorption capacity (q_m) and the distribution coefficient (K_d) are calculated by using Eq. (1) and (2).

Table 2.12 shows the data obtained. The fitting of data was done by Langmuir-Freundlich adsorption isotherm model. K-MPS-1 has very high Cd^{2+} capturing capacity of 401.7 ± 29 mg/g (Figure 2.17.).

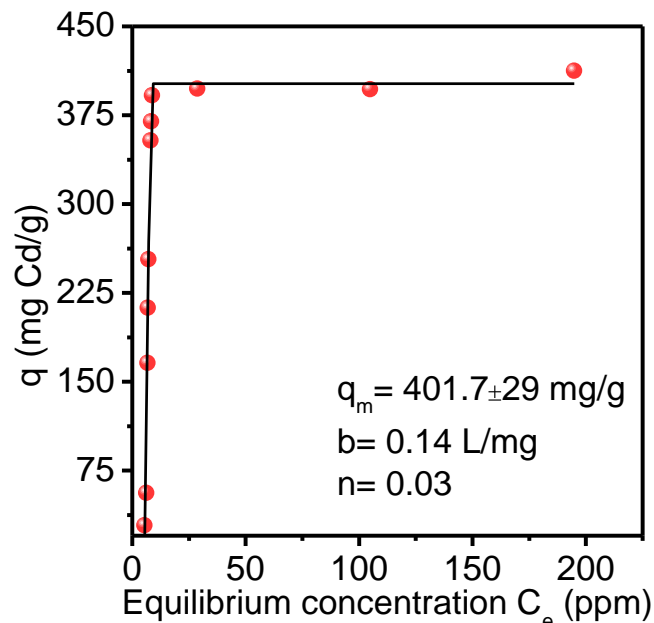


Figure 2.12 Sorption isotherm for the sorption of Cd^{2+} by K-MPS-1(pH ~ 6.5, RT). The solid (black line) represents the fitting of the data with Langmuir- Freundlich model (fitting data for Cd^{2+} : $b = 0.14 \text{ Lmg}^{-1}$, $n = 0.03$)

Table 2.12 Sorption results of K-MPS-1 toward Cd^{2+} .

Initial concentration C_0 , (ppm)	Final concentration C_f , (ppm)	Removal (%)	q (mg/g)	K_d (mL/g)
34.21	5.38	84.2736	28.83	0.54×10^4
63.4	6.16	90.28391	56.11765	0.91×10^4
172.65	6.63	96.15986	166.02	2.50×10^4
222.476	6.826	96.9318	213.5149	3.13×10^4
265.568	7.048	97.34607	253.451	3.60×10^4
368.81	7.99	97.83357	353.7451	4.43×10^4
385.51	8.27	97.85479	369.8431	4.47×10^4
393.72	8.77	97.77253	388.8384	4.43×10^4
438.2	28.71	93.4482	397.5631	1.38×10^4
505.8	104.9	79.26058	396.9307	0.34×10^4
607.5	194.9	67.9177	412.6	0.12×10^4
$m = 0.010 \text{ g}$, $V = 10 \text{ mL}$, $V:m = 1000 \text{ mL/g}$				

The observed Cd^{2+} exchange capacity (3.57 mmol/g) is almost three times higher than that the theoretical exchange capacity (1.17 mmol/g) of K-MPS-1. The K_d , tabulated in Table 2.12, is found in a range of 0.5×10^4 to 4.47×10^4 mL/g.

Cd^{2+} sorption studies were carried out in low ppb range from 1 ppb to 1102 ppb. We have observed 100% removal of cadmium from water in this range. Table 2.13 shows that K-MPS-1 effectively removes Cd from trace level.

Table 2.13 Removal of Cd^{2+} at lower ppb level.

Initial concentration, C_0 (ppb)	Final concentration, C_f (ppb)	% of Cd^{2+} Removed
1	0	100.0
2	0	100.0
7	0	100.0
51	1	98.0
77	1	98.7
143	1	99.3
424	4	99.1
528	3	99.4
788	0	100.0
1102	14	98.7

m = 0.010 g, V = 10 mL, V:m = 1000 mL/g

2.5 Conclusions

In summary, Pb^{2+} and Cd^{2+} sorption and ion-exchange kinetics of K-MPS-1 were studied in detail. K-MPS-1 removes Pb^{2+} and Cd^{2+} with a remarkably high capacity (393.5 mg/g and 401.7 mg/g respectively) following Langmuir-Freundlich model. It has high distribution co-efficient of 5.96×10^5 mL g^{-1} for Pb^{2+} which follows pseudo-second order kinetics, indicates the sorption is chemisorption. K-MPS-1 demonstrates efficient Pb and Cd removal (>99 % and 100 % respectively) from the dilute concentration of aqueous Pb^{2+} and Cd^{2+} solutions (1-1000 ppb). K-MPS-1 exhibits high selectivity towards Pb^{2+} in presence of other hindering hard cations such

as Na^+ , Ca^{2+} , Mg^{2+} due to strong soft acid-soft base Pb-S interactions, according to the HSAB principle. K-MPS-1 can operate even in broad pH range of 2-12. Intercalation of K^+ in $MnPS_3$ creates a Mn^{2+} vacancy, which is occupied by Pb^{2+} and Cd^{2+} during Pb^{2+} and Cd^{2+} sorption in K-MPS-1. Interestingly, K-MPS-1 is effective for removing Pb^{2+} from the potable water collected from the lake in Bangalore and can make the Pb^{2+} concentration below the tolerance level of drinking water. Further, the present study can be extended to capture rare earth elements and radionuclides by using K-MPS-1.

References

- [1] M. J. Manos, M. G. Kanatzidis, *Chem. Sci.* **2016**, 7, 4804-4824.
- [2] T. W. Clarkson in Heavy metals in the environment (Ed.: B. Sarkar), Marcel Dekker, New York, **2002**, pp. 457–502.
- [3] A. P. Carnizello, L. Marcal, P. S. Calefi, E. J. Nassar, K. J. Ciuffi, R. Trujillano, M. A. Vicente, S. A. Korili, A. J. Gil, *Chem. Eng. Data* **2009**, 54, 241-247.
- [4] M. A. Shannon, P. W. Bohn, M. Elimelech, J. G. Georgiadis, B. J. Marinas, A. M. Mayes, *Nature* **2008**, 452, 301-310.
- [5] R. P. Schwarzenbach, B. I. Escher, K. Fenner, T. B. Hofstetter, C. A. Johnson, U. von Gunten and B. Wehrli, *Science* **2006**, 313, 1072-1077.
- [6] S. Majumder, S. Gupta and S. Raghuvanshi in *Heavy Metals In Water: Presence, Removal and Safety* (Eds.: S. Sharma), The Royal Society of Chemistry, Cambridge, **2015**, pp. 44-56.
- [7] M. A. Barakat and R. Kumar in *Heavy Metals In Water: Presence, Removal and Safety* (Eds.: S. Sharma), The Royal Society of Chemistry, Cambridge, 2015, pp. 193-212.
- [8] D. R. Tonini, D. A. Gauvin, R. W. Soffel, W. P. Freeman, *Environ. Prog.* **2003**, 22, 167-173.
- [9] A. Benhammou, A. Yaacoubi, L. Nibou, B. J. Tanouti, *Colloid Interface Sci.* **2005**, 282, 320-326.
- [10] Y. El Mouzdahir, A. Elmchaouri, R. Mahboub, A. ElAnssari, A. Gil, S. A. Korili, M. A. Vicente, *Appl. Clay Sci.* **2007**, 35, 47-58.
- [11] G. Blanchard, M. Maunaye, G. Martin, *Water Res.* **1984**, 18, 1501-1507.
- [12] W. Du, L. B. Yin, Y. Q. Zhuo, Q. S. Xu, L. Zhang, C. H. Chen, *Ind. Eng. Chem. Res.* **2014**, 53, 582-591.
- [13] X. W. Zhao, Q. Jia, N. Z. Song, W. H. Zhou, Y. S. Li, *J. Chem. Eng. Data* **2010**, 55, 4428-4433.
- [14] D. Mohan, K. P. Singh, *Water Res.* **2002**, 36, 2304-2318.
- [15] H.S. Sherry, *J. Phys. Chem.* **1968**, 72, 4086–4094.
- [16] C.-H. Lin, D. S.-H. Wong, S.-Y. Lu, *ACS Appl. Mater. Interfaces* **2014**, 6, 16669–16678.

- [17] Z. Liu, R. Ma, M. Osada, N. Iyi, Y. Ebina, K. Takada, T. Sasaki *J. Am. Chem. Soc.* **2006**, *128*, 4872-4880.
- [18] L. Mercier, T.J. Pinnavaia, *Adv Mater.* **1997**, *9*,500-503.
- [19] X. Feng, G. E. Fryxell, L.-Q. Wang, A. Y. Kim, J. Liu, K. M. Kemner, *Science* **1997**, *276*, 923-926.
- [20] C.W. Abney, J.C. Gilhula, K. Lu, W. Lin, *Adv Mater.* **2014**, *26*, 7993-7997.
- [21] M. J. Manos, C. D. Malliakas, M. G. Kanatzidis, *Chem. Eur. J.* **2007**, *13*, 51-58.
- [22] X.-F. Yu, J.-W. Liu, H.-P. Cong, L. Xue, M. N. Arshad, H. A. Albar, T. R. Sobahi, Q. Gao, S.-H. Yu, *Chem. Sci.* **2015**, *6*, 2511–2515.
- [23] H. Xue, Q. Chen, F. Jiang, D. Yuan, G. Lv, L. Liang, L. Liu, M. A Hong, *Chem. Sci.* **2016**, *7*, 5983–5988.
- [24] A. Chakraborty, S. Bhattacharyya, A. Hazra, A. C. Ghosh, T. K. Maji, *Chem. Commun.* **2016**, *52*, 2831–2834.
- [25] N. Ding, M. G. Kanatzidis, *Nat Chem.* **2010**, *2*,187-191.
- [26] S. Bag, P. N. Trikalitis, P. J. Chupas, G. S. Armatas, M. G. Kanatzidis, *Science* **2007**,*317*, 490-493.
- [27] S. Bag, A.F. Gaudette, M.E. Bussell, M.G. Kanatzidis, *Nat Chem.* **2009**, *1*,217-224.
- [28] M. J. Manos, N. Ding, M. G. Kanatzidis, *Proc. Natl. Acad. Sci. U. S. A.* **2008**, *105*, 3696-3699.
- [29] M. J. Manos, M. G. Kanatzidis, *Chem. Eur. J.* **2009**, *15*, 4779-4784.
- [30] M. J. Manos, M. G. Kanatzidis, *J. Am. Chem. Soc.* **2012**, *134*, 16441-16446.
- [31] M. J. Manos, M. G. Kanatzidis, *J. Am. Chem. Soc.* **2009**, *131*, 6599-6607.
- [32] M. J. Manos, V. G. Petkov, M. G. Kanatzidis, *Adv. Funct. Mater.* **2009**, *19*, 1087-1092.
- [33] Z. H. Fard, C. D. Malliakas, J. L. Mertz, M. G. Kanatzidis, *Chem. Mater.* **2015**, *27*, 1925–1928.
- [34] D. Sarma, C. D. Malliakas, K. S. Subrahmanyam, S. M. Islam, M. G. Kanatzidis, *Chem. Sci.* **2016**, *7*, 1121-1132.
- [35] X. M Zhang, D. Sarma, Y. Q. Wu, L. Wang, Z. X. Ning, F.Q. Zhang, M. G. Kanatzidis, *J. Am. Chem. Soc.* **2016**, *138*, 5543-5546.
- [36] D. Sarma, S. M. Islam, K. S. Subrahmanyam, M. G. Kanatzidis, *J. Mater. Chem. A*, **2016**, *4*, 16597–16605.

- [37] S. L. Ma, Q. M. Chen, H. Li, P. L. Wang, S. M. Islam, Q. Y. Gu, X. J. Yang, Kanatzidis, M. G. J. Mater. Chem. A 2014, 2, 10280-10289.
- [38] S. L. Ma, Y. Shim, S. M. Islam, K. S. Subrahmanyam, P. L. Wang, H. Li, S. C. Wang, X. J. Yang, M. G. Kanatzidis, Chem. Mater. 2014, 26, 5004-5011.
- [39] L. Ma, Q. Wang, S.M. Islam, Y. Liu, S. Ma, M.G. Kanatzidis, J. Am. Chem. Soc. 2016, 138, 2858-2866.
- [40] <https://www.epa.gov/dwreginfo/lead-and-copper-rule>
- [41] M. R. Perez, I. Pavlovic, C. Barriga, J. Cornejo, M. C. Hermosin, M. A. Ulibari, *Appl. Clay Sci.* **2006**, 32, 245-251.
- [42] X. F. Liang, W. G. Hou, Y. M. Xu, G. H. Sun, L. Wang, Y. Sun, X. Qin, *Colloids Surf. A* **2010**, 366, 50-57.
- [43] G. L. Huang, D. Wang, S. L. Ma, J. L. Chen, L. Jiang, P. Y. Wang, *J. Colloid Interface Sci.* **2015**, 445, 294-302.
- [44] F. Li, X. Wang, T. Yuan, R. A. Sun, *J. Mater. Chem. A* **2016**, 4, 11888–11896.
- [45] L. C. Zhou, L. Q. Ji, P. C. Ma, Y. M. Shao, H. Zhang, W. J. Gao, Y. F. Li, *J. Hazard. Mater.* **2014**, 265, 104-114.
- [46] M. A. Gonzalez, I. Pavlovic, C. Barriga, *Chem. Eng. J.* **2015**, 269, 221-228.
- [47] A. M. Badruddoza, Z. B. Shawon, T. W. J. Daniel, K. Hidajat, M. S. Uddin, *Carbohydr. Polym.* **2013**, 91, 322-332.
- [48] X. Y. Guo, B. Du, Q. Wei, J. Yang, L. H. Hu, L. G. Yan, W. Y. Xu, *J. Hazard. Mater.* **2014**, 278, 211-220.
- [49] C.-H. Lin, D. S.-H. Wong, S.-Y. Lu, *ACS Appl. Mater. Interfaces* **2014**, 6, 16669–16678.
- [50] X.-F. Yu, J.-W. Liu, H.-P. Cong, L. Xue, M. N. Arshad, H. A. Albar, T. R. Sobahi, Q. Gao, S.-H. Yu, *Chem. Sci.* **2015**, 6, 2511–2515.
- [51] C. J. Madadrang, H. Y. Kim, G. Gao, N. Wang, J. Zhu, H. Feng, M. Goring, M. L. Kasner, S. Hou, *Appl. Mater. Interfaces* **2012**, 4, 1186–1193.
- [52] S. Pourbeyram, *Ind. Eng. Chem. Res.* **2016**, 55, 5608–5617.
- [53] R. Sitko, E. Turek, B. Zawisza, E. Malicka, E. Talik, J. Heimann, A. Gagor, B. Feist, R. Wrzalik, *Dalt. Trans.* **2013**, 42, 5682–5689.
- [54] L. Ling, W.-J. Liu, S. Zhang, H. Jiang, *J. Mater. Chem. A* **2016**, 4, 10336–10344.

- [55] W. Klingen, R. Ott, H. Hahn, *Z. Anorg. Allg. Chem* **1973**, 396, 271–278.
- [56] R. Clement, *J. Chem. Soc., Chem. Commun.*, 1980, 647-648.
- [57] R. Clement, J. J. Girerd, I. Morgenstern-Badarau, *Inorg. Chem.* **1980**, 19, 2852–2854.
- [58] L.Silipigni, G.D. Marco, G. Salvato, V.Grasso, *Appl. Surf. Sci.* **2005**, 252, 1998-2005.
- [59] Y. Mathey, R. Clement, C. Sourisseau, G. Lucazeau, *Inorg. Chem.* **1980**, 19, 2773-2779.
- [60] P. A. Joy, S. Vasudevan, *J. Am. Chem. Soc.* **1992**, 114, 7792-7801.
- [61] R.; Clement, O. Gamier, J. Jegoudez, *Inorg. Chem* **1986**, 25, 1404–1409.
- [62] R. G. Pearson, *J. Am. Chem. Soc.* **1963**, 85, 3533–3539.

Chapter 3

**Reversible and Efficient
Sequestration of Cs from Water
by Layered Metal
Chalcophosphate, K-MPS-1***

Reversible and Efficient Sequestration of Cs from Water by Layered Metal Chalcophosphate, K-MPS-1

Summary: Environmental pollution with radioactive species is an important issue due to flourishing development in nuclear energy. Cesium (^{137}Cs) radioisotope is non-actinide fission product of the uranium and plutonium and it is long-lived. Hence, selective removal/capture of Cs is essential for management of radioactive waste. In this chapter, we discuss a detailed Cs^+ ion-exchange study of potassium intercalated layered metal chalcophosphate, $\text{K}_{0.48}\text{Mn}_{0.76}\text{PS}_3\cdot\text{H}_2\text{O}$ (K-MPS-1). The sorption of Cs^+ by K-MPS-1 follows Langmuir model with a high capacity of 333.1 ± 17 mg/g and reasonably high distribution coefficients in the order of $\sim 10^4$ mL/g. K-MPS-1 can even sequester Cs^+ efficiently from low concentration (ppb level). K-MPS-1 exhibits high cesium uptake in a broad pH range of 2-12 and the ion exchange process reaches equilibrium within a short time (~ 15 min) following pseudo second order kinetics. K-MPS-1 demonstrates selectivity towards Cs capture in presence of complex solutions containing excess Na^+ , Ca^{2+} and Mg^{2+} ions, which is due to the favorable interaction between Cs^+ (soft acid) and S^{2-} (soft Lewis base). K-MPS-1 reversibly captures Cs^+ and it can be regenerated by treating Cs-MPS-1 by KCl solution.

3.1 Introduction

Nuclear energy has emerged as one of the low cost alternatives for electrical power with no emission of greenhouse gases.^[1] But the management and disposal of radioactive wastes is the key issue with this developing nuclear energy. Radioactive cesium, ^{137}Cs , a non-actinide fission product of the uranium and plutonium, emits harmful gamma radiations, high energy beta particles and has long half-life ($t_{1/2}$) of ~30.17 years.^[2,3] ^{137}Cs accumulates in ecosystems, assimilates in living organisms and plants due to high water solubility and analogous physicochemical properties of K^+ .^[4] In 2013, Castrillejo *et al.* have shown that there is a major increase in radioactive ^{137}Cs levels in the seawater samples taken from the Fukushima Dai-ichi nuclear power plant compared to pre-Fukushima ^{137}Cs levels.^[5,6] Thus, there is a need to design stable materials for treatment of discharged nuclear effluents comprising of inhomogeneous samples with very high salt concentration and extreme pH.

Dissolved inorganic and organic ligands (e.g., EDTA) are generally not capable of binding strongly to Cs^+ .^[7] Biosorption *i.e.* using biopolymers like alginates, isolated from bacteria fungi, yeast, algae have also been used to remove Cs^+ .^[8-10] Methods like coprecipitate flotation, coagulation/sedimentation, evaporation, reverse osmosis, sand filtration, ultrafiltration, microfiltration, electro dialysis and solvent extractions suffers from selectivity in presence of high salt concentrations and can't reduce concentration of Cs^+ below ~50 ppb level.^[3,11-13] Ion-exchange is an inexpensive efficient method, can selectively adsorb Cs^+ and proves to be potential for storage of Cs^+ ions from solidified waste and reductive nuclear discharges.^[14,15] Inorganic ion exchangers are preferred over organic ion exchangers due to superior chemical, thermal and radiation stability.^[16] Tremendous ion-exchange studies of Cs^+ have been done in natural minerals (zeolites and clays)^[7,17], insoluble transition metal ferrocyanides^[18-20], titanium silicates^[21,22], metal oxides (TiO_2 , MnO_2)^[23], MOFs^[24], PAN (polyacrylonitrile) based exchangers,^[25-27] but they lack stability in extreme pH as well selectivity due to presence of other inhibiting cations present in nuclear wastes containing water.

Solid metal chalcogenides have shown improved ion-exchange properties for soft metal ions in comparison to the sulfur-functionalized non-chalcogenide materials.^[28] Recently, researchers have explored layered and three-dimensional open framework metal chalcogenides for ion-exchange applicatios.^[29-34] The soft Lewis base nature of sulfide and selenide anions

provide higher affinity towards soft Lewis acidic metal ion centers^[35,36] Nuclear discharge waste containing high salt concentration of hard ions (H^+ , Na^+ , Ca^{2+} , Mg^{2+}) cannot inhibit the ion-exchange properties of these materials, but some of them suffers from stability due to non-stoichiometry, presence of unbalanced charges^[37] and organic moiety;^[38] and low Cs^+ ion removal capacity^[33,39,40], weak affinity towards Cs^+ in presence of others mono and di-valent cations.^[38] Therefore, there is plenty of room to be explored about the ion-exchange properties of stable inorganic chalcogenides, which can have high capacity and effective distribution coefficient in the broad pH range in presence of high salt concentration. Alkali metal intercalated metal chalcophosphate ($KMPS_3$; $M = Mn, Ni, Fe$ etc) is a layered material which can be easily synthesized and it is stable in broad pH range.^[41] In chapter 2, we have shown that $K_{0.48}Mn_{0.76}PS_3.H_2O$ is capable of selective sequestration of Pb from the water up to low ppb in 2-10 pH range.

In this chapter, we discuss a detailed Cs^+ ion-exchange investigation of potassium intercalated layered metal thiophosphate, $K_{0.48}Mn_{0.76}PS_3.H_2O$ (K-MPS-1). The sorption of Cs^+ by K-MPS-1 follows Langmuir adsorption model with a high capacity of 333.1 ± 17 mg/g (at pH ~7) and distribution coefficients in order of $\sim 10^4$ mL/g. K-MPS-1 exhibits high cesium uptake both under strongly acidic and strongly basic conditions (pH 2-12). Cs uptake reaches equilibrium within 15 min following the pseudo second order kinetics and the distribution coefficients remain unaffected ($\sim 10^4$ mL/g) even in the presence of complex solutions containing excess Na^+ , Ca^{2+} , Mg^{2+} ions. The selectivity over other common cations originates from Cs-S soft Lewis acid-Lewis base interactions rather than size effects. K-MPS-1 can sequester Cs^+ from low ppb level (5-100 ppb). Cs^+ occupies K^+ site and forms a Cs^+ intercalate (Cs-MPS-1). Further, K-MPS-1 reversibly takes Cs^+ and can be regenerated by treating it to 2M KCl solution. The results show that layered K-MPS-1 can be considered as a selective and inexpensive sorbent for ^{137}Cs radioactive isotope which is generally formed during nuclear reactions.

3.2 Experimental section

3.2.1 Reagents. Manganese (Mn, Alfa Aesar 99.95 %), red phosphorous (P, Alfa Aesar 98.9 %), sulphur (S, Alfa Aesar 99.999 %), lead nitrate ($Pb(NO_3)_2$, Sigma Aldrich 99.999%),

cesium chloride (CsCl_2 , Sigma Aldrich 99.999%) and potassium chloride (KCl, Alfa Aesar 99.5 %) were used for synthesis without further purification.

3.2.2 Synthesis. A stoichiometric quantity of Mn, P and S were mixed and heated in vacuum sealed (10^{-5} Torr) quartz tube to synthesize MnPS_3 (MPS-1) which is explained in section 2.2.2.^[42] Potassium intercalated MnPS_3 (K-MPS-1) was synthesized by stirring MnPS_3 powder with saturated KCl solution.^[43,44]

3.2.3 Characterizations. Powder X-ray diffraction of samples were done using a Cu $K\alpha$ ($\lambda = 1.5406 \text{ \AA}$) radiation on a Bruker D8 diffractometer. To estimate optical band gap of the finely grinded powder samples at room temperature, diffuse reflectance measurements were carried out over the range of 250 nm to 2500 nm using a Perkin Elmer Lambda 900, UV/Vis/NIR spectrometer in reflectance mode. Absorption (α/S) data were calculated from reflectance data using Kubelka-Munk equation: $\alpha/S = (1-R)^2/(2R)$, where R is the reflectance, α and S are the absorption and scattering coefficient, respectively. The energy band gaps were derived from α/S vs E (eV) plot. FTIR spectra of powder sample was recorded using a Bruker IFS 66v/S spectrometer. Raman spectroscopy measurements of powder sample were carried out with a HORIBA LABRAM HR800 spectrometer. The excitation wavelength of the laser was 514 nm. TGA was performed using a TGA/DSC 2 STAR instrument in the temperature range of 300–773 K under nitrogen atmosphere with a ramp rate of 5 K min^{-1} . FESEM of the synthesized and lead adsorbed materials were performed using NOVA NANO SEM 600 (FEI, Germany) operated at 15 KV. EDAX compositional analysis was performed during FESEM imaging. XPS measurement has been performed with Mg- $K\alpha$ (1253.6 eV) X-ray source with a relative composition detection better than 0.1% on an Omicron Nanotechnology spectrometer. The zeta potential measurements were carried out using a NanoZS (Malvern UK) employing a 532 nm laser. Actual concentration of the lead containing solutions (1ppm-1000ppm) were measured by ICP-AES. ICP-AES measurements were carried out using Perkin-Elmer Optima 7000DV instrument. Cs standard (1000mg/L, Sigma-Aldrich), Mn standard (1000mg/L, Sigma-Aldrich) and multi-element standard (Ca 2000 mg/L, Na 1000 mg/L, K 200 mg/L and Mg 400 mg/L, Sigma-Aldrich) were used to determine the concentration of various cations. Element concentrations in ppb level (1-1000 ppb) were measured using a quadrupole inductively coupled plasma- mass spectrometer (ICP-MS, Thermo Scientific X-Series II) equipped with Nickel sample and skimmer cones. Samples were introduced using a 100 ml/min PFA

nebulizer connected to a peristaltic pump running at 30 rpm into an ESI-PC3 Peltier cooled spray chamber. A CETAC ASX-520 auto-sampler was used. Uptake time for samples and standards was 60 seconds while the rinse time (in 2% HNO₃) was 90 seconds.

3.2.4 Cs⁺ sorption and ion-exchange kinetics. Typical ion-exchange studies of K-MPS-1 with non-radioactive Cs⁺ (which mimics radioactive ¹³⁷Cs⁺ due to the same size) were carried out using batch method (V:m~1000 mL/g). 10 mg of K-MPS-1 was added to 10 mL of Cs⁺ aqueous solution (5 ppb-1300 ppm) in a 15 mL centrifuging tube and shaken for 15 min in tube rotator. The Cs⁺ ion-exchanged material (Cs-MPS-1) was separated by centrifugation or filtration (through filter paper, Whatman No. 41) and dried in an oven at 60 °C. The filtrate was collected and the concentration of Cs⁺ was measured using ICP-AES and ICP-MS. The obtained concentrations were used to determine the sorption isotherms and calculate maximum sorption capacity.

Kinetic studies of Cs⁺ sorption by K-MPS-1 were carried out until the equilibrium was reached. Ion exchange experiments of various reaction time (5, 10 and 15 min) were performed. For each experiment, 10 mL of ~45 ppm Cs⁺ aqueous solution and 10 mg of K-MPS-1 is taken in a 15mL centrifugation tube and the contents were shaken. After a certain time interval, the suspension of each tube is centrifuged and collected filtrates were analyzed for the final concentration by ICP.

To test the effect of inhibiting ions like Ca²⁺, Mg²⁺ and Na⁺ on Cs⁺ ions, competitive ion exchange studies were carried out with a V/m ratio of 1000 mL/g using solution containing these cations (80ppm Cs⁺, 25ppm Ca²⁺, Mg²⁺, Na⁺) at room temperature with 15 min contact time.

3.3 Results and discussion

3.3.1 Characterization of Cs-MPS-1

The Cs⁺ sorption properties are explored by stirring CsNO₃ solution with the as synthesized K-MPS-1, where V: m is 1000 mL/g. The ion-exchange process is very fast and almost all K⁺ ions were exchanged with Cs⁺ in K-MPS-1 within 15 min which we will discuss in detail later part of the paper. EDAX analysis of cesium exchanged K-MPS-1 (Cs-MPS-1) showed

complete removal of K^+ ions and insertion of Cs has taken place in K-MPS-1. Cs^+ insertion does not change the layered morphology of the K-MPS-1 (Figure 3.1).

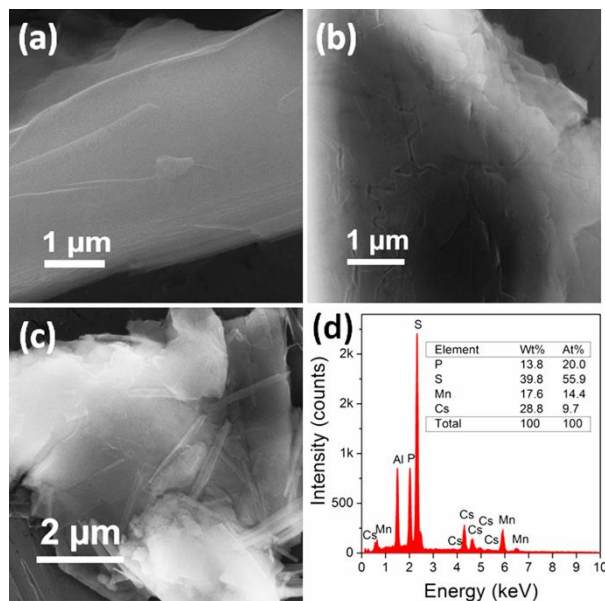


Figure 3.1 (a) FESEM images of K-MPS-1, (b) Cs adsorbed K-MPS-1, (c) Zomed version of Cs-MPS-1 and (d) EDX spectra of Cs-MPS-1

We have characterized MPS-1, K-MPS-1 and Cs-MPS-1 by PXRD to confirm the K^+ intercalation into MPS-1 and Cs^+ ion exchange in K-MPS-1. First, a significant shift of the (001) Bragg peak to the lower 2θ was observed when K^+ intercalated in $MnPS_3$ due to the expansion of the layer in K-MPS-1 (Figure 3.2a).

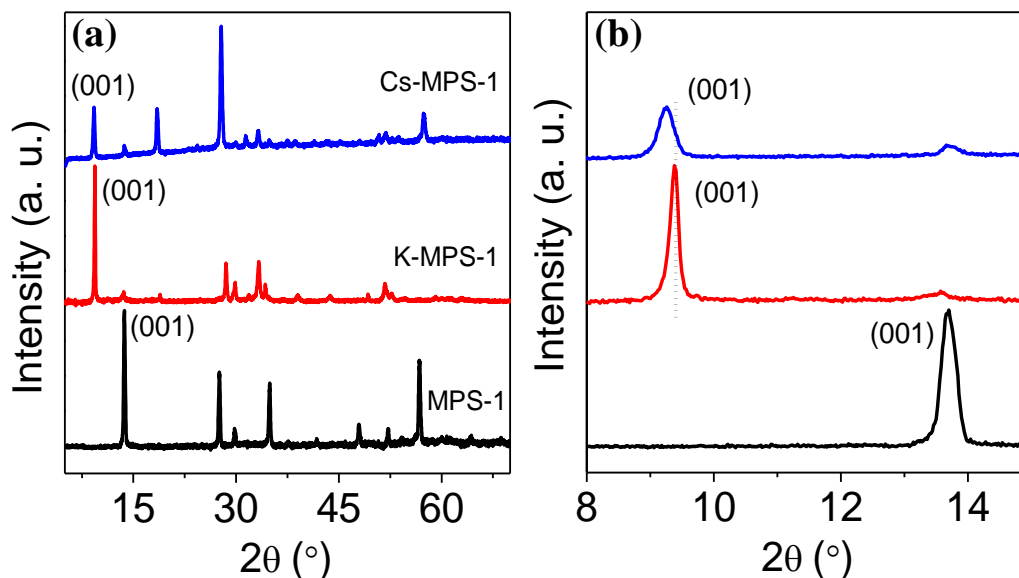


Figure 3.2 (a) PXRD patterns of MPS-1, K-MPS-1 and Cs-MPS-1. (b) Zoomed version of PXRD in the 2θ range of 8-15°.

Cs⁺ ion exchange in K-MPS-1 further shifts the (001) to lower 2θ with respect to K-MPS-1, indicating the increase in inter-lamellar spacing. Cs⁺ insertion into K-MPS-1 increases the interlayer spacing from 9.42 to 9.54 Å which is clearly shown in zoomed version of PXRD (Figure 3.2b). Insertion of larger Cs⁺ ions (3.06 Å) in place of K⁺ (2.80 Å) increases the interlayer spacing by 0.12 Å and shift (001) Bragg peak.

Figure 3.3 shows the schematics of the ion-exchange reaction in K-MPS-1. Chemical equation below describes the ion-exchange process that takes place in K-MPS-1.

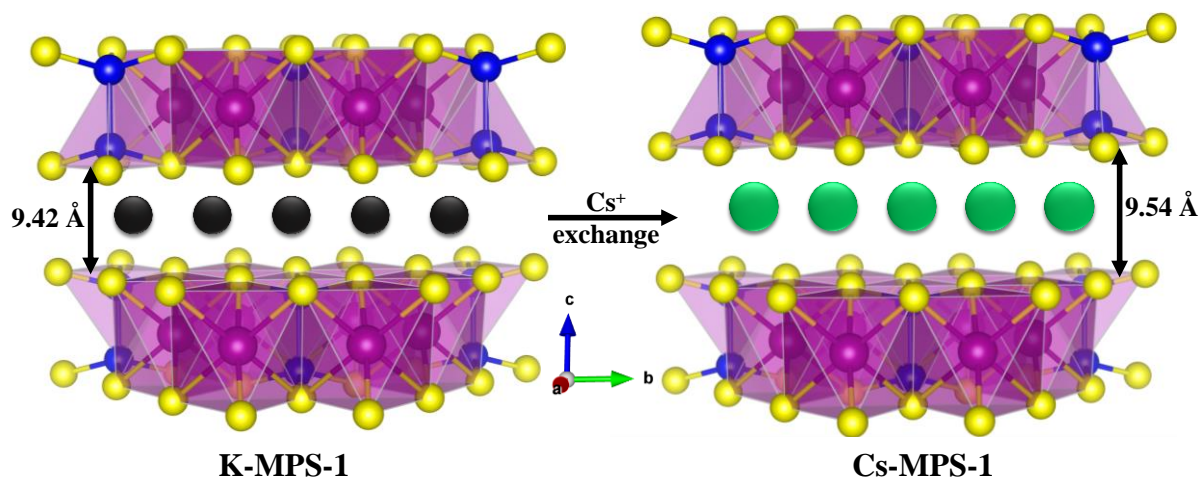


Figure 3.3 Schematic for the mechanism of Cs⁺ capture by K-MPS-1. Mn, purple; P, blue; S, yellow; K, black; Cs, green.



Figure 3.4a and b represents the FT-IR and Raman spectra of MPS-1, K-MPS-1, and Cs sorbed K-MPS-1, respectively. In FT-IR spectra, MPS-1 shows two distinct peaks at 445 and 565 cm⁻¹, arising from P-P and symmetric P-S stretching of the P₂S₆ unit, respectively.^[45] Intercalation of K⁺ doesn't affect the lower energy band (445 cm⁻¹), but splits the higher energy band (565 cm⁻¹) into two bands at 605 and 552 cm⁻¹ including a weak band at 565 cm⁻¹. Intercalation of K⁺ in MPS-1 pulls out Mn²⁺ and creates a Mn²⁺ vacancy in the layer to maintain the charge balance, which leads to distortion of the symmetric P₂S₆ unit.^[46] As a result, asymmetric P-S stretching splits into two components (in-plane and out-plane), which are appearing at 605 and 552 cm⁻¹, respectively. While, sorption of Cs in K-MPS-1 results in the complete disappearance of the weak symmetric P-S band and intensification of two strong

distorted P-S bands. This indicates that Cs^+ replaces K^+ ions in the interlayer space, thereby slightly increasing the extent of distortion due to the large size effect.

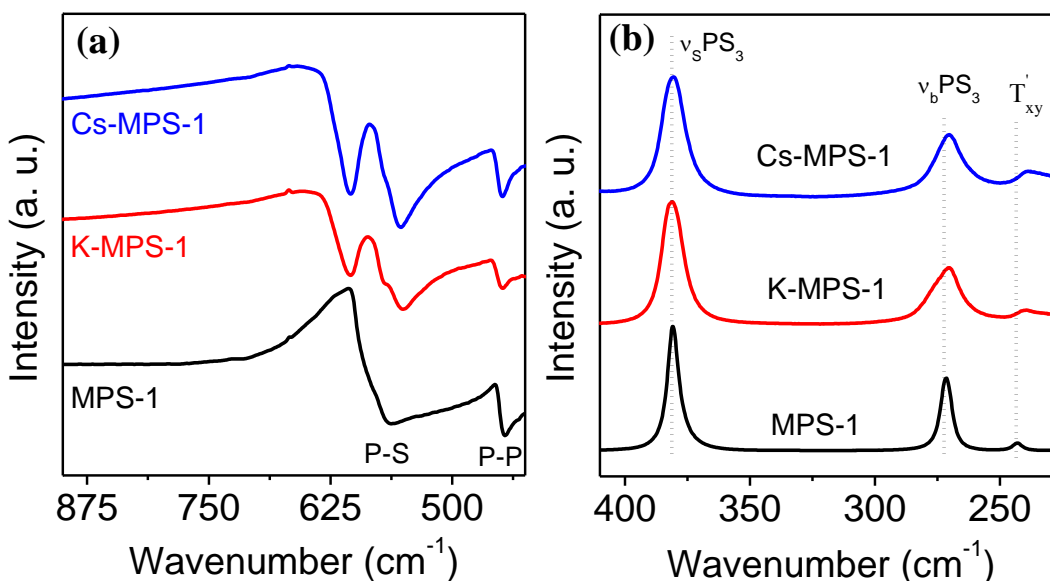


Figure 3.4 (a) IR spectra of MPS-1, potassium intercalated K-MPS-1 and Cs exchanged Cs-MPS-1. (b) Raman spectrum of MPS-1, K-MPS-1 and Cs-MPS-1.

Raman spectra show the higher energy stretching mode of PS_3 unit is unaltered in all cases because it is metal independent (Figure 3.4b). The lower energy vibration modes of K-MPS-1 and Cs-MPS-1 has changed in position and intensity due to less charge density of K and Cs with respect to Mn^{2+} . However, these lower energy bands are highly sulfur and metal ions sensitive.^[45] The $\nu_b(\text{PS}_3)$ and $T_{xy}(\text{PS}_3)$ are red shifted 2 cm^{-1} and 4 cm^{-1} with respect to that of MPS-1, respectively. Metal vacancies formed by intercalation of K^+ ions in MPS-1 distorts the symmetric P_2S_6 units, thereby decreasing the frequency.^[47] In the case of Cs-MPS-1, Cs^+ larger than K^+ ion, which enhances the distortion and reduces the frequency further.

Table 3.1 Interlayer spacing and band gap

Material	Interlayer spacing (\AA)	Band gap energy (eV)
MPS-1	6.45	2.39
K-MPS-1	9.42	2.53
Cs-MPS-1	9.54	2.68

Insertion of K^+ and Cs^+ into MPS-I and K-MPS-1 are further analyzed by UV-Vis study. Figure 3.5 shows the electronic absorption spectra of MPS-1, K-MPS-1 and Cs-MPS-1. Intercalation of K^+ in $MnPS_3$ increases the band gap from 2.38 eV to 2.53 eV indicating increase the gap between the layers due to K^+ intercalation (Table 3.1). Cs exchanged material exhibits a small increase in band gap with respect to K-MPS-1. Cs-MPS-1 shows a band gap 2.68 eV which is 0.15 eV greater than that of the K-MPS-1. This can be attributed to the weak interaction between Cs and S with respect to K and S. The interaction follows in the order of electronegativity ($X_{Cs} < X_K$). The weaker interaction between Cs and S stabilizes the bonding sulfur orbital and increase the band gap in Cs-MPS-1.

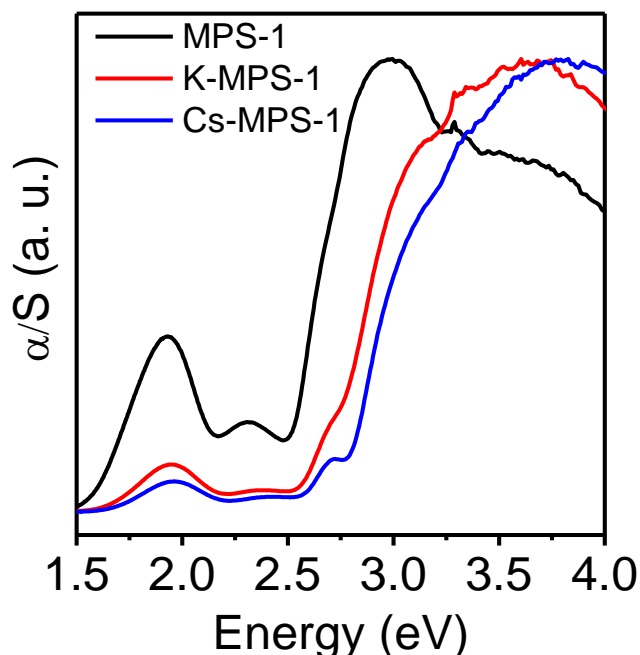


Figure 3.5 Solid state electronic absorption spectra of MPS-1, K-MPS-1 and Cs-MPS-1.

3.3.2 Cs^+ sorption studies

In order to establish a relationship between the amount of cesium ions sorbed in the K-MPS-1 and the concentration of remaining Cs^+ ions in the aqueous phase, the adsorption isotherm studies were performed and ion exchange capacity of K-MPS-1 for Cs^+ was calculated. To determine the quantitative Cs^+ sorption capacity of K-MPS-1, we performed ion-exchange batch studies at room temperature within a broad range of Cs^+ concentrations from ppb to ppm ($V:m = 1000 \text{ mL/g}$, $pH \sim 6.5$, Milli-Q water). The initial and final concentration of Cs^+ in the aqueous solution are measured by ICP analysis. Adsorption isotherm generally provides information about adsorption mechanism, surface properties,

affinity and capacity of adsorbent. The sorbent, K-MPS-1, was contacted with varying concentrations of Cs⁺ until equilibrium was reached and the data is tabulated in Table 3.2 and Table 3.3.

Table 3.2 Sorption results of K-MPS-1 toward Cs⁺

Initial concentration C ₀ , (ppm)	Final concentration C _f , (ppm)	Removal (%)	q (mg/g)	K _a (mL/g)
7.869	0.739	90.6	7.1	9.7 X 10 ³
10.83	3.159	70.8	7.7	2.4 X 10 ³
103.3	45.37	56.1	57.4	1.3 X 10 ³
154.4	49.03	68.2	105.4	2.2 X 10 ³
263	70.77	73.1	188.5	2.7 X 10 ³
389.5	175.4	55.0	212.0	1.2 X 10 ³
827.1	537.8	35.0	286.4	0.53 X 10 ³
1296	989.7	23.6	303.3	0.31 X 10 ³

m = 0.010 g, V = 10 mL, V:m = 1000 mL/g

Figure 3.6a shows the fitting of equilibrium data by two binding models, Langmuir and Langmuir-Freundlich.

$$\text{Langmuir isotherm} \quad q = q_m \frac{(bC_e)}{1+(bC_e)} \quad (1)$$

$$\text{Langmuir-Freundlich isotherm} \quad q = q_m \frac{(bC_e)^{1/n}}{1+(bC_e)^{1/n}} \quad (2)$$

where q (mg g⁻¹) is the amount of Cs⁺ adsorbed at equilibrium concentration, q_m is the maximum Cs⁺ adsorption capacity, b (L mg⁻¹) is the Langmuir constant related to adsorption energy, C_e (ppm) is the equilibrium concentration and $1/n$ is a measure of intensity of adsorption where n is a constant.

Table 3.3 Removal of Cs⁺ at ppb level.

Initial concentration C _o , (ppb)	Final concentration C _f , (ppb)	% Removed	K _d (mL/g)
5.0	0.7	86.0	6.1 X 10 ³
18.5	2.6	85.9	6.1 X 10 ³
72.7	11.0	84.9	5.6 X 10 ³
120.10	17.9	85.1	5.7 X 10 ³
245.8	12.0	95.1	1.95 X 10 ⁴
562.5	36.8	93.5	1.43 X 10 ⁴
693.5	46.9	93.2	1.38 X 10 ⁴
965.9	57.3	94.1	1.59 X 10 ⁴
1420	84.8	94.0	1.57 X 10 ⁴

m = 0.010 g, V = 10 mL, V:m = 1000 mL/g

The affinity of K-MPS-1 towards Cs⁺ is expressed in terms of distribution coefficient (K_d):

$$K_d = \left(\frac{V}{m}\right) \frac{(C_o - C_e)}{C_e} \quad (3)$$

where, V is the volume (mL) of Cs⁺ aqueous solution, m is the amount of K-MPS-1 ion exchanger taken, C_e is equilibrium concentration (ppm) and C_o is the initial concentration (ppm). K_d values in the range of 10³ to 10⁴ which is considered to be good and reversible ion exchange process (see Table 3.2 and Table 3.3). We have observed the maximum K_d value is 1.6 x 10⁴ mL/g (see Table 3.3).

The experimental equilibrium data were well fitted with both Langmuir and Langmuir-Freundlich isotherm with a good agreement of $R^2 \geq 0.95$ and the ion-exchange sorption constants are given in Table 3.4. The value of Langmuir-Freundlich constant $n = 0.9$ was found to be closer to 1 suggesting that the adsorption behavior follows the Langmuir adsorption model. This result indicates that the exchangeable Cs⁺ ions form monolayer assuming that sorption occurs on a structurally homogeneous adsorbent and all the sorption sites are energetically identical. Thus, the adsorption sites for Cs⁺ ions are fixed in between the layers due to weak electrostatic interaction between the S²⁻ ions and interlayer Cs⁺.

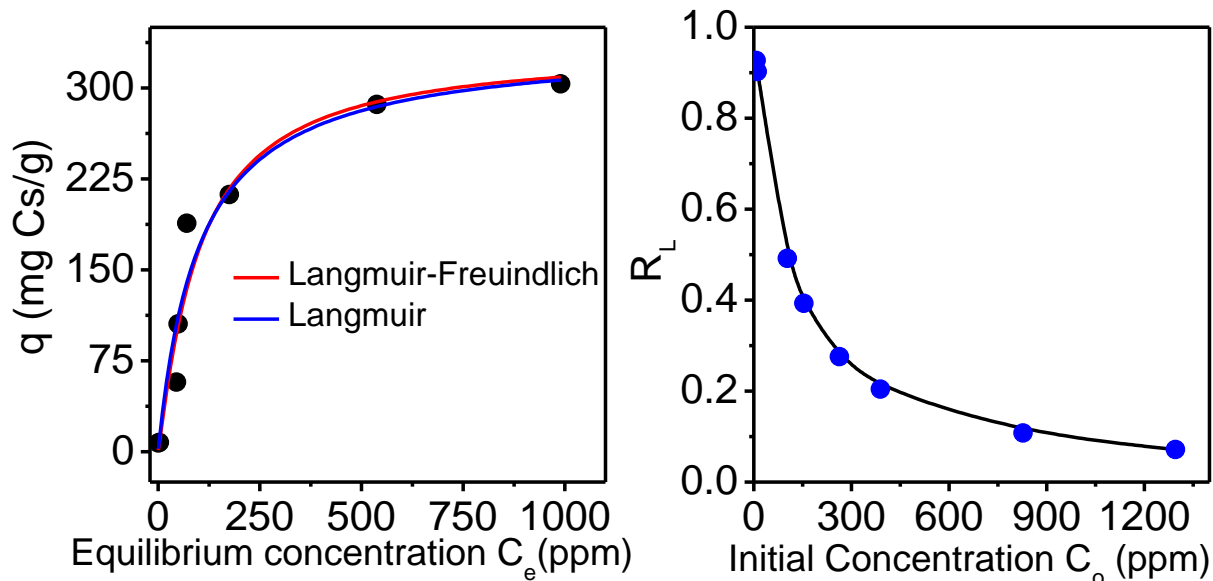


Figure 3.6 (a) Equilibrium data for Cs⁺ ion exchange (pH~ 7, $V:m= 1000$ mL/g). The solid blue and red line represents the fitting with Langmuir and Langmuir-Freundlich model. (b) Variation of R_L with initial cesium concentration of K-MPS-1.

Table 3.4 The ion-exchange sorption constants obtained by fitting the isotherm data with different models.

Parameters	Langmuir	Langmuir-Freundlich
q_m (mg/g)	337.5(17)	333.11(17)
b (L/mg)	0.01	0.01
n	-	0.9
R^2	0.952	0.953

The theoretical capacity of K-MPS-1 for Cs⁺ uptake is calculated to be 310.7 mg/g which is comparable to the maximum ion exchange capacity, q_m , obtained from Langmuir and Langmuir-Freundlich isotherm model (Table 3.4). In the EDAX study of Cs-MPS-1, we have also observed the complete removal of K⁺. Thus, these observation further supports that the Cs⁺ ions occupy the position of K⁺ ions which are intercalated between the MnPS₃ slabs of K-MPS-1. Moreover, Langmuir isotherm model for Cs sorption indicates the homogeneous nature of K-MPS-1, i.e. each Cs⁺ adsorption has equal adsorption activation energy and demonstrates the formation of mono layer coverage of Cs⁺ in between the layers of ion-

exchanger. The observed Cs uptake capacity, q_m , 337.5 ± 17 mg/g obtained from Langmuir model compares well with state of art of materials listed in Table 3.5.

XPS spectra of Cs-MPS-1 shows two distinct peaks at the position 730 and 744 eV for the Cs $3d_{5/2}$ and $3d_{3/2}$ (Figure 3.7a and b) including other elemental peaks as in K-MPS-1. K^+ intercalation creates an excess negative charge on the surface of MPS-1 due to Mn^{2+} vacancy, which further confirmed by Zeta potential measurement. However, Cs^+ insertion in K-MPS-1 does not affect the surface charge (Figure 3.7c). This further supports that Cs exchange takes place only in the position of K^+ in between the layer.

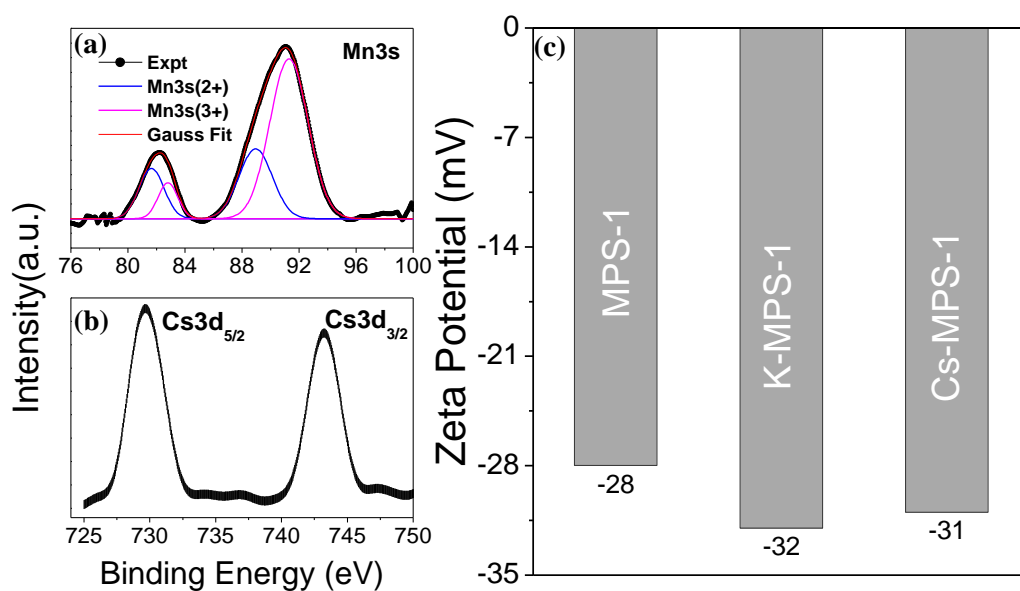


Figure 3.7 (a) XPS spectra for Mn3s; (b) XPS spectra for Cs3d and (c) Surface charge analysis of MPS-1, K-MPS-1 and Cs-MPS-1 by zeta potential measurements.

The nature of Langmuir isotherm was further verified by the analysis of the dimensionless constant separation factor or equilibrium parameter, R_L ,^[48] which is given by

$$R_L = \frac{1}{1+(bC_o)} \quad (3)$$

where b (L/mg) is Langmuir constant and C_o is initial concentration of adsorbate in mg/L. The R_L indicates about the nature of adsorption isotherm accordingly: $R_L > 1$ unfavorable adsorption; $0 < R_L < 1$ favorable adsorption; $R_L = 0$ irreversible adsorption and $R_L = 1$ linear adsorption. From the Langmuir fitting data, the present R_L value ranges from 0.07 to 0.92, (see Figure 3.6b) indicating favorable adsorption of Cs^+ in K-MPS-1.

Table 3.5 Comparison of Cs⁺ ion-exchange characteristics of K-MPS-1 with other materials.

Material	q _m (mg/g) (Langmuir)	K _d (mL/g) (pH~ 7)	Active pH range	Equilibrium study time	Ref.
K-MPS-1	337.48±17	~ 10 ⁴	2-12	15	This work
KMS-1	226±2	≥ 10 ⁴	0.8-12	5	[37]
KMS-2	531±28	≥ 10 ³	3-10	-	[50]
KTS-1	205±6	≥ 10 ⁵	-	-	[40]
KTS-3	280±11	≥ 10 ⁴	2-12	5	[39]
PB/Fe₃O₄/GO	55.56	≥ 10 ³	4-10	720	[20]
Na alginate	80.64	-	2-6	120	[9]
PAN-KNiCF	157.729	≥ 10 ⁴	-	1440	[25]
PATiW	217	≥ 10 ³	2-9	180	[51]
γ-Zr phosphate	180.7	≥ 10 ³		14400	[16]
MnO₂-PAN	321.6	944	1-9	35	[26]
HexaCNFe-Fe	240-380	10 ² -10 ³	-	2880	[52]
K₆MS	66±4	≥ 10 ⁴	2.5-12	-	[33]
K@RWY	310	≥ 10 ⁵	1.6-11.8	5	[53]
Maghemite PVA- Alginate Beads	28.32	≥ 10 ⁴	2-12	330	[8]
Magnetite PB nanocomposites	280.82 (10 °C)	≥ 10 ⁵	2-9	240	[18]
FJSM-SnS	409±29 (65 °C)	≥ 10 ³	0.7-11	5 (65 °C), 30 (RT)	[38]
GeSbS-2	231±15 (65 °C)	≥ 10 ³	2.8-11	2 (65 °C)	[54]
T3NT	200	≥ 10 ³	1-7	10	[55]

The value of Langmuir constant b (L/mg) for Cs⁺ is 0.01 L/mg which indicates the binding affinity of Cs⁺ towards K-MPS-1 is moderate. This weak binding nature of Cs⁺ was proved by the reversibility of the ion-exchange reaction. 89 % of Cs⁺ released from Cs-KMPS-1 in

desorption studies with KCl solutions (Table 3.6). Hence, the material can be regenerated and used repeatedly for Cs⁺ capturing.

Table 3.6. Reversibility studies of Cs-MPS-1 by using saturated KCl.

C ₀ , (ppm)	C ₀ , (ppm)	Cs ⁺ Removed %	Cs ⁺ Adsorbed on K-MPS-1 (ppm)	KCl added (ppm)	Cs ⁺ released, (ppm)	Released %
150.2	40.3	73.2	109.9	634.4	79.2	72.1
				1692		
150.2	26.3	82.5	123.9		109.7	88.5

m = 0.010 g, V = 10 mL KCl solution, V:m = 1000 mL/g

3.3.3 Kinetics study

To understand the dynamics of Cs⁺ sorption, kinetics studies were carried out. Figure 3.8 shows that equilibrium is reached within 15 min, indicating that Cs⁺ exchange takes place rapidly and the data are tabulated in Table 3.7.

Table 3.7. Kinetics data of Cs⁺ sorption using K-MPS-1.

Initial concentration C ₀ , (ppm)	Time (min)	Final concentration C _t , (ppm)	Removal (%)	K _d (mL/g)	q _t (mg/g)
45.97	0	45.97	0	-	-
	5	12.54	72.7	2.69 X 10 ³	33.77
	10	10.75	76.6	3.31 X 10 ³	35.58
	15	10.32	77.6	3.42 X 10 ³	35.30

m=0.010g, V= 10mL, V:m=1000mL/g

The extremely high mobility of K⁺ ions and high affinity of the soft Lewis basic sulfide site for soft Cs Lewis acids sites resulted in the fast ion exchange kinetics in K-MPS-1. To determine the adsorption rate and pathway of Cs⁺ exchange, pseudo first order and pseudo second order model were used.

$$\ln(q_e - q_t) = \ln q_e - k_1 t \quad (4)$$

$$\frac{t}{q_t} = \frac{1}{k_2 q_e^2} + \frac{t}{q_e} \quad (5)$$

where q_e (mg/g) is the amount of Cs⁺ exchanged per unit mass of K-MPS-1 at equilibrium, q_t is Cs⁺ ions adsorbed at time t , k_1 and k_2 (g/mg min⁻¹) are the rate constants of pseudo-first-

order and pseudo-second-order adsorption interactions. k_1 and k_2 are calculated by plotting $\ln(q_e - q_t)$ vs. t and t/q_t vs. t plot by using Eq. (3) and (4), respectively (Table 3.8).^[39]

Table 3.8. Kinetic parameters for sorption of Cs^+ by K-MPS-1 with two different models.

Order	Adsorbate	R^2	q_e (exp) (mg g^{-1})	q_e (cal) (mg g^{-1})	k (g/mg/min)
Pseudo-2 nd	Cs^+	0.999	35.4	36.1	9.82×10^{-2}
Pseudo-1 st	Cs^+	0.933	35.4	21.6	3.75×10^{-1}

The goodness of fit, R^2 , is to be 0.999 for the Eq. (4), which is very close to unity, indicates the sorption of Cs^+ on K-MPS-1 follows pseudo-second-order kinetics (Figure 3.8b).

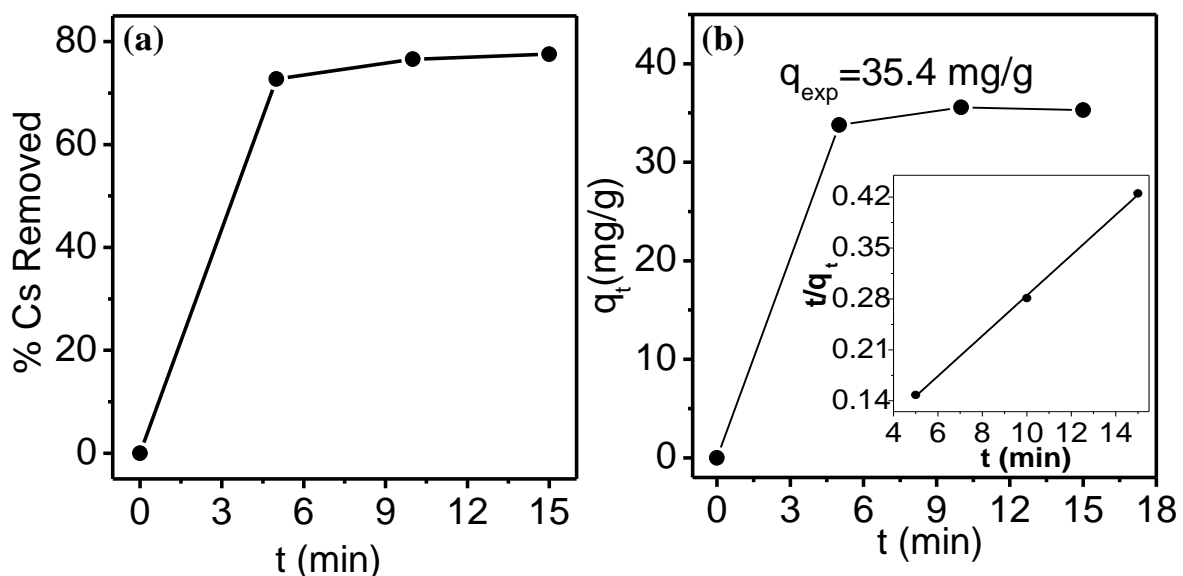


Figure 3.8 Ion-exchange kinetics curve for Cs^+ : (a) removal % of Cs^+ as a function of contact time, (b) ion-exchange capacity (q_t) with contact time and pseudo-second-order kinetic plots (inset) for Cs^+ sorption.

3.3.4 pH and competitive ion-exchange studies

Nuclear discharge containing Cs^+ generally has extreme pH condition, thus it is important to have a material that can withstand within a broad pH range. Therefore, we have carried out ion-exchange studies in the pH range of 2-12 and observed that the K-MPS-1 removes Cs rapidly and effectively. Distribution coefficient, K_d was calculated at various pH (Figure 3.9), which shows that even in extreme pH conditions K_d remains unaffected. Hence, K-MPS-1 proves to retain Cs removal capabilities and it is stable in a wide range of pH compared to other materials in Table 3.5.

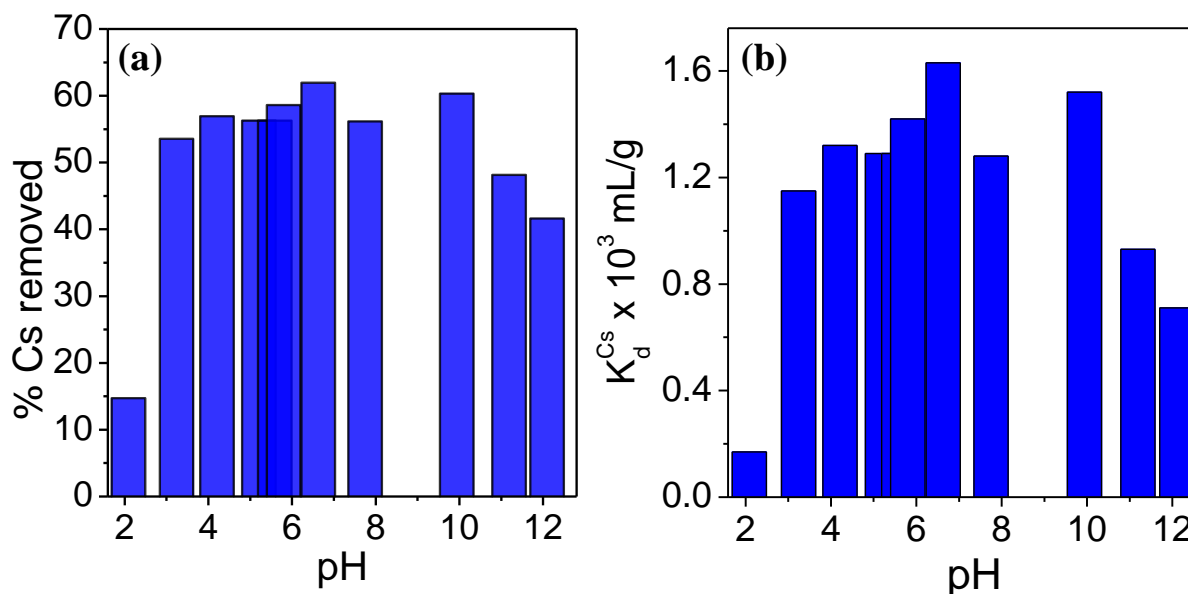


Figure 8: pH Studies: (a) removal % of Cs⁺ ions by K-MPS-1 and (b) distribution coefficient (K_d^{Cs}) of ion exchange.

Further, K_d ($\sim 10^4$ mL/g) remains unaffected even in presence of other hard mono and divalent ions (Na⁺, Ca²⁺ and Mg²⁺), which proves the selectivity of K-MPS-1 for Cs⁺ uptake. The affinity between soft Cs⁺ and soft S²⁻ is the reason for the selective sorption.

3.3.5 Low concentration (ppb level) Cs⁺ capture

Cs⁺ contamination is generally in very low concentration.^[49] We have also carried out experiments in a low concentration ranging from 5-1000 ppb of Cs⁺. Interestingly, we found that K-MPS-1 is able to remove $\sim 85-95$ % of Cs⁺ in low concentration and K_d is unaltered which is tabulated in Table 3.3.

3.4. Conclusions

K-MPS-1 is capable of selective, efficient and reversible sequestration of Cs from the water. The sorption of Cs⁺ by K-MPS-1 follows Langmuir model with a capacity of 333.1 ± 17 mg/g. K-MPS-1 can retain the Cs capturing ability even in extreme pH conditions and reaches ion-exchange equilibrium within a very short period of time (~ 15 min) with high distribution co-efficient. The sorption kinetics follows pseudo second order rate law. The adsorbed Cs⁺ ion occupies the intercalation site of K⁺ ions in K-MPS-1, which is proven by several characterization techniques such as PXRD, Raman, IR, XPS, zeta potential measurement and Langmuir isotherm model. Ion exchange is reversible and the K-MPS-1 can be regenerated by

treating the Cs-MPS-1 with KCl solution. The higher K_d values originate from the favourable interaction between soft acidic Cs and soft Lewis basic S rather than just due to the space filling effects of the layered K-MPS-1. K_d for Cs capture remains unaffected even in presence of mono and di-valent cations (Na^+ , Ca^{2+} and Mg^{2+}), which indicates the selectivity. K-MPS-1 can effectively remove upto 95% of Cs^+ from trace (ppb) concentrations of Cs^+ ions in water samples. Thus, K-MPS-1 can be considered a cost-effective, inexpensive, environmental friendly and reusable ion-exchanger for remediation of radioactive $^{137}\text{Cs}^+$.

References

- [1] World Statistics: Nuclear Energy Around the World, <http://www.nei.org/Knowledge-Center/Nuclear-Statistics/World-Statistics>.
- [2] V. N. Romanovskiy, I. V. Smirnov, V. A. Babain, T. A. Todd, R. S. Herbst, J. D. Law, K. N. Brewer, *Solvent Extr. Ion Exch.* **2001**, *19*, 1–21.
- [3] X. Liu, G. R. Chen, D. J. Lee, T. Kawamoto, H. Tanaka, M. L. Chen, Y. K. Luo, *Bioresour. Technol.* **2014**, *160*, 142–149.
- [4] S. Yoshida, Y. Muramatsu, A. M. Dvornik, T. A. Zhuchenko, I. Linkov, *J. Environ. Radioact.* **2004**, *75*, 301–313.
- [5] et. al. Yasunari T, Stohl A, Hayano R, Burkhart J, Eckhardt S, *Proc. Natl. Acad. Sci.* **2011**, *108*, 19530–19534.
- [6] M. Castrillejo, N. Casacuberta, C. F. Breier, S. M. Pike, P. Masqu, K. O. Buesseler, *Environ. Sci. Technol.* **2016**, *50*, 173–180.
- [7] B. C. Bostick, M. A. Vairavamurthy, K. G. Karthikeyan, J. Chorover, *Environ. Sci. Technol.* **2002**, *36*, 2670–2676.
- [8] Z. Majidnia, A. Idris, *Chem. Eng. J.* **2015**, *262*, 372–382.
- [9] M. Y. Khotimchenko, E. A. Podkorytova, V. V. Kovalev, E. V. Khozhaenko, Y. S. Khotimchenko, *J. Environ. Sci. Technol.* **2013**, *7*, 30–43.
- [10] H. A. Omar, A. S. Abdel-Razek, M. S. Sayed, *Nat. Sci.* **2010**, *8*, 140–147.
- [11] K. Shakir, M. Sohsah, M. Soliman, *Sep. Purif. Technol.* **2007**, *54*, 373–381.
- [12] R. O. Abdel Rahman, H. A. Ibrahim, Y. T. Hung, *Water (Switzerland)* **2011**, *3*, 551–565.
- [13] H. Luo, S. Dai, P. V. Bonnesen, A. C. Buchanan, J. D. Holbrey, N. J. Bridges, R. D. Rogers, *Anal. Chem.* **2004**, *76*, 3078–3083.
- [14] J. Lehto, R. Harjula, *Radiochim. Acta* **1999**, *86*, 65–70.
- [15] D. V. Marinin, G. N. Brown, *Waste Manag.* **2000**, *20*, 545–553.
- [16] S. Komarneni, R. Roy, *Nature* **1982**, *299*, 707–708.
- [17] T. H. Wang, T. Y. Liu, D. C. Wu, M. H. Li, J. R. Chen, S. P. Teng, *J. Hazard. Mater.* **2010**, *173*, 335–342.
- [18] J. Jang, D. S. Lee, *Ind. Eng. Chem. Res.* **2016**, *55*, 3852–3860.

- [19] S.-C. Jang, S.-B. Hong, H.-M. Yang, K.-W. Lee, J.-K. Moon, B.-K. Seo, Y. Huh, C. Roh, *Nanomaterials* **2014**, *4*, 894–901.
- [20] H. Yang, L. Sun, J. Zhai, H. Li, Y. Zhao, H. Yu, *J. Mater. Chem. A*, **2014**, *2*, 326–332.
- [21] M. Ishfaq, H. Karim, M. Khan, *J. Radioanal. Nucl. Chem.* **1993**, *170*, 321–331.
- [22] I. M. Ali, E. S. Zakaria, H. F. Aly, *J. Radioanal. Nucl. Chem.* **2010**, *285*, 483–489.
- [23] A. Dyer, M. Pillinger, J. Newton, R. Harjula, T. Möller, S. Amin, *Chem. Mater.* **2000**, *12*, 3798–3804.
- [24] B. Aguila, D. Banerjee, Z. Nie, Y. Shin, S. Ma, P. K. Thallapally, *Chem. Commun.* **2016**, *52*, 5940–5942.
- [25] Z. Du, M. Jia, X. Wang, *J. Radioanal. Nucl. Chem.* **2013**, *298*, 167–177.
- [26] A. Nilchi, R. Saberi, S. Rasouli Garmarodi, A. Bagheri, *Appl. Radiat. Isot.* **2012**, *70*, 369–374.
- [27] B. J. Riley, D. A. Pierce, J. Chun, J. Matyáš, W. C. Lepry, T. G. Garn, J. D. Law, M. G. Kanatzidis, *Environ. Sci. Technol.* **2014**, *48*, 5832–5839.
- [28] J. Qian, J. Ma, W. He, D. Hua, *Chem. Asian J.* **2015**, *10*, 1738–1744.
- [29] M. J. Manos, M. G. Kanatzidis, *J. Am. Chem. Soc.* **2012**, *134*, 16441–16446.
- [30] N. Ding, M. G. Kanatzidis, *Nat. Chem.* **2010**, *2*, 187–191.
- [31] M. J. Manos, M. G. Kanatzidis, *J. Am. Chem. Soc.* **2009**, *131*, 6599–6607.
- [32] M. J. Manos, N. Ding, M. G. Kanatzidis, *Proc. Natl. Acad. Sci.* **2008**, *105*, 3696–3699.
- [33] M. J. Manos, K. Chrissafis, M. G. Kanatzidis, *J. Am. Chem. Soc.* **2006**, *128*, 8875–8883.
- [34] M. J. Manos, R. G. Iyer, E. Quarez, J. H. Liao, M. G. Kanatzidis, *Angew. Chemie Int. Ed.* **2005**, *44*, 3552–3555.
- [35] M. J. Manos, C. D. Malliakas, M. G. Kanatzidis, *Chem. Eur. J.* **2007**, *13*, 51–58.
- [36] N. Ding, M. G. Kanatzidis, *Chem. Mater.* **2007**, *19*, 3867–3869.
- [37] M. J. Manos, M. G. Kanatzidis, *J. Am. Chem. Soc.* **2009**, *131*, 6607.
- [38] X.-H. Qi, K.-Z. Du, M.-L. Feng, J.-R. Li, C.-F. Du, B. Zhang, X.-Y. Huang, *J. Mater. Chem. A* **2015**, *3*, 5665–5673.
- [39] D. Sarma, C. D. Malliakas, K. S. Subrahmanyam, S. M. Islam, M. G. Kanatzidis, *Chem. Sci.* **2016**, *7*, 1121–1132.
- [40] N. (CY) Mercouri G. Kanatzidis, Wilmette, IL (US); Joshua L. Mertz, Evanston, IL (US); Emmanouil Manos, *Chalcogenide Compounds for the Remediation of Nuclear*

- and Heavy Metal wastes, US Patent, US2011290735-A1., 2011.
- [41] R. Brec, *Solid State Ionics* **1986**, 22, 3–30.
- [42] W. Klingen, R. Ott, H. Hahn, *Zeitschrift für Anorg. und Allg. Chemie* **1973**, 396, 271–278.
- [43] R. Clement, *J. Chem. Soc., Chem. Commun.*, **1980**, 647–648.
- [44] R. Clement, J. J. Girerd, I. Morgenstern-Badarau, *Inorg. Chem.* **1980**, 19, 2852–2854.
- [45] Y. Mathey, R. Clement, C. Sourisseau, G. Lucazeau, *Inorg. Chem.* **1980**, 19, 2773–2779.
- [46] P. Fuentealba, C. Cortés, N. Audebrand, E. Le Fur, V. Paredes-García, D. Venegas-Yazigi, J. Manzur, E. Spodine, *Dalt. Trans. Commun. Cite this Dalt. Trans* **2015**, 44, 12493–12496.
- [47] I. Lagadic, R. Clément, *Microsc. Microanal. Microstruct.* **1993**, 4, 453–460.
- [48] T. W. Weber, R. K. Chakravorti, *AIChE J.* **1974**, 20, 228–238.
- [49] T. Mizuno, H. Kubo, *Sci. Rep.* **2013**, 3, 1742.
- [50] J. L. Mertz, Z. H. Fard, C. D. Malliakas, M. J. Manos, M. G. Kanatzidis, *Chem. Mater.* **2013**, 25, 2116–2127.
- [51] I. M. El-Naggar, *Adv. Chem. Eng. Sci.* **2012**, 2, 166–179.
- [52] T. Vincent, C. Vincent, Y. Barre, Y. Guari, G. Le Saout, E. Guibal, *J. Mater. Chem. A* **2014**, 2, 10007–10021.
- [53] H. Yang, M. Luo, L. Luo, H. Wang, D. Hu, J. Lin, X. Wang, Y. Wang, S. Wang, X. Bu, et al., *Chem. Mater.* **2016**, 28, 8774–8780.
- [54] B. Zhang, M. L. Feng, H. H. Cui, C. F. Du, X. H. Qi, N. N. Shen, X. Y. Huang, *Inorg. Chem.* **2015**, 54, 8474–8481.
- [55] D. Yang, S. Sarina, H. Zhu, H. Liu, Z. Zheng, M. Xie, S. V Smith, S. Komarneni, *Angew. Chemie Int. Ed.* **2011**, 50, 10594–10598.

List of publications

1. **E. Rathore**, P. Pal, K. Biswas, Layered Metal Chalcophosphate (K-MPS-1) for Efficient, Selective and ppb Level Sequestration of Pb from Water, *J. Phys. Chem. C.*, **2017**, DOI: 10.1021/acs.jpcc.7b00908.
2. **E. Rathore**, P. Pal, K. Biswas, Reversible and Efficient Sequestration of Cs from Water by Layered Metal Chalcophosphate, K-MPS-1 (Unpublished).

Biography



Ekashmi Rathore was born on October 5, 1993 in Rawatbhata, Rajasthan (India). She did her B.Sc. Hons. Chemistry (2014) from Hindu College, University of Delhi. She joined as an Int. PhD student (Chemical Sciences) at New Chemistry Unit of Jawaharlal Nehru Centre for Advanced Scientific Research (JNCASR), Bangalore, India in August 2014. She joined Dr. Kanishka Biswas as MS Student in January 2016. Her research work is focused on removal of heavy metals and radionuclide using layered metal chalcogenides.